UNIVERSITÉ DE GRENOBLE

THÈSE

Pour obtenir le grade de

DOCTEUR DE L'UNIVERSITÉ DE GRENOBLE

Spécialité : **Optique et Radiofréquences**

Arrêté ministériel : 7 août 2006

Présentée par

Raji Sasidharan NAIR

Thèse dirigée par **Smail TEDJINI** et
codirigée par **Etienne PERRET**

préparée au sein du **Laboratoire LCIS**
dans **l'École Doctorale EEATS**

Contribution au développement des tags chipless et des capteurs à codage dans le domaine temporel

Thèse soutenue publiquement le **27 Mai 2013**
devant le jury composé de :

Mme Leena UKKONEN
Pr., TUT Finlande, Rapporteur
M. Christian PERSON
Pr., ENST Bretagne, Rapporteur
M. Robert PLANA
Pr., Paul Sabatier, Toulouse, Président
M. Philippe POULIGUEN
Pr., DGA/DS/MRIS, Membre
M. Fréderic GARET
MCF, Université de Savoie, Membre
M. Etienne PERRET
MCF, INP-Grenoble, Membre
M. Smail TEDJINI
Pr., INP-Grenoble, Membre

DECLARATION

DECLARATION

I hereby declare that the work presented in this thesis entitled "CONTRIBUTION TO THE DEVELOPEMENT OF TIME DOMAIN CHIPLESS TAGS AND SENSORS" is a bonafide record of the research work done by me under the supervision of Prof. Smail TEDJINI & Dr. Etienne PERRET, Laboratoire de Conception et d'Intégration des Systèmes, Grenoble Institute of Technology, France and that no part thereof has been presented for the award of any other degree.

Valence,   Raji Sasidharan NAIR

March 2013

DECLARATION

AWARDS & RECOGNITIONS

- ➤ *Best Student Paper Award* from IEEE International Conference on RFID Technologies and Applications held in Barcelona, Spain in September 2011.
- ➤ IEEE MTTS-S *PhD Student Sponsorship* from International Microwave Symposium held in Montréal Canada in June 2012.
- ➤ *Second Prize of the Best Student Paper Award* from IEEE International Conference on RFID Technologies and Applications held in Nice, France in November 2012.

AWARDS & RECOGNITIONS

PUBLICATIONS

International Journals Published

1) Etienne Perret , Smail Tedjini and **Raji Sasidharan Nair**: " Design of Antennas for UHF RFID Tags", Proceedings of the IEEE, Special Issue on Wireless Communication Antenas,Vol.100, Issue,7, 2012, pp.2330-2340.
2) **Raji Sasidharan Nair**, Etienne Perret and Smail Tedjini: "A Novel Temporal Multi-Frequency Encoding Technique for Chipless RFID Based on C-sections", Progress in Electromagnetic Research (PIER) B, vol. 49, pp.107-127, 2013.

International Journals Proposed

1 **Raji Sasidharan Nair,** Etienne Perret and Smail Tedjini **: "**Group Delay Modulation for Pulse Position Coding Based on Periodically Coupled C-sections ", Annals of Telecommunications, Accepted for Publication with minor revisions.
2 **Raji Sasidharan Nair**, Etienne Perret, Smail Tedjini and Thierry Baron, " A Group Delay Based Chipless RFID Humidity Tag Sensor Using Silicon Nanowires", IEEE Antennas and Wireless Propagation Letter, Accepted for Publication with minor revisions.

International Conferences:

1) **Raji Nair**,Etienne Perret, Smail Tedjini and Thierry Barron : "A Humidity Sensor for Passive Chipless RFID Applications", *IEEE International conference on RFID-Technologies and Applications*(RFID-TA), Nice, France, November 5-7, 2012. Got *Second Prize for the Best Student Paper Award*.
2) **Raji Nair**,Etienne Perret and Smail Tedjini : " Temporal Multi-Frequency Encoding Technique for Chipless RFID Applications", *IEEE MTT-S International Microwave Symposium*, IMS 2012, Montreal, Canada, June 17-22,2012
3) **Raji Nair**,Etienne Perret and Smail Tedjini : " Novel encoding in chipless RFID using group delay characteristics", SBMO/IEEE MTT-S *International Microwave and Optoelectronics Conference* (IMOC), Natal, Brazil, October 29-November 1,2011
4) **Raji Nair**,Etienne Perret and Smail Tedjini : " Chipless RFID based on group delay encoding", *IEEE International conference on RFID-Technologies and Applications*(RFID-TA), Sitges, Spain, September 15-16,2011. Got *Best Student Paper Award*.

National Conference

1 **Raji Nair**,Etienne Perret, Smail Tedjini and Thierry Barron, "Vers l'utilisation de tag-capteur RFID sans puce pour la mesure d'humidité", Accepted for oral presentation in 18th Journée National Microondes, 15-17 May, 2013, Paris.

Patent

Etienne Perret, Raji Nair, Smail Tedjini, Guy Eymin Petot Tourtollet, Fréderic Garet, Yann Boutant, « Nouveau procédé de réalisation de dispositifs hyperfréquence », Patent Application filed in Janvier 2013.

Acknowledgement

Apart from the efforts of myself, the success of any project depends largely on the encouragement and guidelines of many others. First and foremost, I would like to thank Prof. Smail Tedjini for providing me an opportunity to do my thesis in LCIS/Grenoble-INP. I would like to gratefully acknowledge Prof. Eduardo Mendes, Director of LCIS, for welcoming me to do a thesis in LCIS.

I would like to express my gratitude to Dr. Etienne Perret for his valuable and constructive suggestions during the planning and development of this research work which helped me in completing my thesis work, in time. His willingness to give his time so generously has been very much appreciated.

I take immense pleasure to thank my reviewers Prof. Leena Ukkonen, Tampere University, Finland, and Pr. Christian Person, ENST Bretagne for accepting to review my thesis.

I express my sincere gratitude to all the project partners in THID project, for their fruitful discussions and valuable time.

With full of my gratitude, I remember my dearest Mohan Sir, Professor Cochin University of Science and Technology, India; who has opened my way to research; for inspiring me to fulfill my thesis. His blessings and willingness to motivate me contributed tremendously to my project.

I also would like to thank to Aanandan Sir, professor, Cochin University of Science and Technology, for his valuable advices and timely care which inspired me to fulfill my thesis.

This research project would not have been possible without the support of many people. I express my gratitude to Carole Seyvet and Jennyfer Duberville for always helping me to float through my administrative papers and Cedric Carlotti for his technical services.

I specially thank to Dr. Arnaud Vena, Dr. Darine Kaddour, Dr. Romain Siragusa, Dr. Yvan Duroc, and Dr. Pierre Lemaitre Auger for their support. Also my special thanks to Florence Galli and Prof. Laurent Lefevre for their timely help with patience. My gratitude to my friends and colleagues Divya, Gianfranco, Mossab, and Tsitoha for their amicable relation and valuable helps.

My heartfelt thanks to my dearest friends, Jitha chechi, Bybi chechi, Prabha chechi, Jijo Chetan, Anu, Shalu and Anju for their constant encouragement and sincere support throughout my research carrier. Also, my special thanks to my house owner Ms. Gleize Françoise & her family for providing me all the support and an excellent stay in France.

I express my deepest gratitude to my dearest Gadhu for his continuous support and patience throughout my research carrier without that, I would have not been able to bring my work to a successful completion.

Last but not the least, my deepest gratitude to my dearest family without whose blessings I would never have been achieve my goal.

Raji Sasidharan Nair

ACKNOWLEDGEMENT

1D	One- Dimensional
2D	Two-Dimensional
3D	Three Dimensional
ASIC	Application Specific Integrated Circuit
cm	centi-meter
CPS	Co-Planar Strips
CRT	Cathode Ray Tube
CW	Continuos Wave
CWT	Continuous Wavelet Transform
dB	decibel
dBi	Gain Expressed in dB with Respect to an Isotropic Radiator
dBm	dB milli Watt
DDS	Dispersive Delay Structure
DSO	Digital Oscilloscope
DUT	Device under Test
EAS	Electronic Surveillance Article
EM	Electro Magnetic
EPC	Electronic product Code
ETSI	European Telecommunications Standard Institute
FBW	Frequency Bandwidth
FCC	Federal Communications Commission
FFT	Fast Fourier Transform
Gd/GD	Group delay
GHz	Giga-Hertz

LIST OF ABBREVIATIONS

GSa/s	Giga Samples per second
IC	Integrated Chip
ID	Identification
IDT	Inter Digital Transducer
IFF	Identify Friend and Foe
ISM	Industrial Scientific and Medical
kHz	Kilo-Hertz
LNA	Low Noise Amplifier
LOS	Line of Sight
LTCC	Low-Temperature Co-fired Ceramic
MHz	Mega-Hertz
mm	milli-meter
mW	milli-Watt
ns	Nano Second
OCR	Optical Character Recognition
OOK	On-Off Keying
PC	Personal Computer
PE	Poly Ethylene
PEC	Perfect Electric Conductor
PET	Poly Ethylene Terephthalate
PNA	Performance Network Analyzer
PSD	Power Spectral Density
PPM	Pulse Position Modulation
ps	pico second
RCS	Radar Cross Section
REP	RF Encoding Particles
RFID	Radio Frequency Identification

LIST OF ABBREVIATIONS

RH   Relative Humidity

Rx   Receiving

SAW   Surface Acoustic Waves

SMA   Sub- Miniature version A

SRR   Split Ring Resonator

TDR   Time Domain Reflectometry

TEM   Transverse Electric and Magnetic

TFTC   Thin Film Transistor Circuits

Tx   Transmitting

UWB   Ultra Wide-Band

VNA   Vector Network Analyzer

LIST OF ABBREVIATIONS

LIST OF MAJOR SYMBOLS

LIST OF MAJOR SYMBOLS

E	Electric Field density
H	Magnetic Field density
J	Current Density
$\tan\delta$	Tangent Loss
Ω	Ohm: SI unit of resistance
ε_r	Relative Dielectric Constant
ε_{re}/ ε_{reff}	Effective Dielectric Constant
h	Height of the substrate
w	width of the transmission line
l	length of the line
g	gap between coupled lines
V	Voltage
I	Current
Z	Impedance
η	Wave Impedance in free space
c	Velocity of light in free space
V_p	Phase Velocity
λ	wavelength
λ_g	Guided Wavelength
T,t	Time
μ	Permeability
Φ	Phase
τ	Delay
F_C	Cut-off Frequency

LIST OF MAJOR SYMBOLS

ω   Angular Frequency

R   Far-field Distance

Δt   Time Difference

CONTENTS

Chapter Four

MICROSTRIP MULTI- GROUP OF C-SECTIONS AND DELAY BASED ID GENERATION

CONTENTS

CONTENTS

CHAPTER ONE
INTRODUCTION

Automatic Identification procedures (Auto-ID) have become very popular in recent years. They are used to provide information about people, animals, goods, and products in transit or in storage. Barcodes and RFID (Radio Frequency IDentification) are the two widely used identification systems. Chipless RFID owing to its low cost has opened a new era for the identification world. There are not a lot of chipless RFID tags available in the market. However, due to the low cost, these tags started to conquer a part of the market. Several constraints such as coding capacity, miniaturization, cost per tag, printable designs etc. need to be considered while developing chipless tags. Thus, it became a challenging research area for many groups worldwide. There are number of chipless tags available in the literature. This thesis reviews the existing chipless tags and also proposes novel chipless tags that respect the existing regulations with a significant coding capacity.

INTRODUCTION

1.1 RADIO FREQUENCY IDENTIFICATION

Automatic identification system refers to the process of identifying and tagging objects which mainly involves technologies such as barcodes, Optical Character Recognition (OCR), biometric procedures, voice identification, fingerprint, smart cards, RFID systems etc. [1]. Among these, barcodes and RFID are the most widely used identification techniques. RFID is a technology firstly introduced during the 2nd World War to Identify Friend and Foe (IFF) aircrafts. Further, Stockman introduced the term RFID in his paper 'Communication by Means of Reflected Power' in 1948 [2]. However, the first real tag was the Electronic Surveillance Article (EAS) device that is the ancestor of modern tags, developed in 1960s [3]. RFID uses radio frequency communications to label and identify objects and stores/retrieves data wirelessly. A typical RFID system includes transponders (also called as tags) attached to objects and interrogators (also called as readers) which communicate wirelessly. Each tag carries information such as a serial number, a model number, location of assembly, and other data as in the case of Electronic Product Code (EPC) which is designed as a universal identifier that provides a unique identity for every physical object anywhere in the world. When tags pass in the vicinity of a reader, they communicate with the reader wirelessly and identify themselves [4]. Fig.1. 1 shows a typical RFID system.
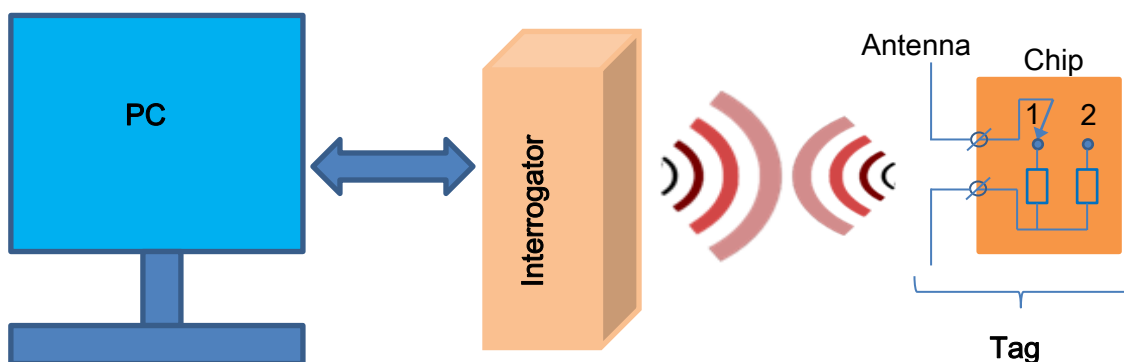
Fig.1. 1 : Passive RFID system.

Usually the RFID tag consists of an antenna and an Application Specific Integrated Circuit (ASIC) chip, both with complex impedances. The chip receives power from the RF signal transmitted by the reader. The tag sends data back by switching its input impedance between two states and thus modulating the backscattered signal. At each impedance state, the RFID tag presents a certain radar cross section (RCS). Both impedance states must be sufficiently distinct to be able to achieve a coding type with a modulation in amplitude or phase [5].

RFID tags are broadly classified as; active, passive, and semi-passive. Active tags contain a small power source. Active tags have a larger radio range. For instance, they can be read from a long distance more than 30 meters [4].On the other hand, passive tags do not include an on-tag power source. Passive tags are powered by the electromagnetic field generated by a reader and retrieve or transmit data back to a reader by modulating energy through a transducer. In the case of tags which operate in high frequency (in HF), they are energized by means of electromagnetic induction, namely by inductive coupling between the coil in the reader and the tiny coil in the tag. For the tags operating at higher frequencies (typically UHF), a portion of the power of the emitted signal by the reader will be collected by the tag antenna and permits the activation of the tag. Passive tags can be either Low Frequency (LF), HF or Ultra High Frequency (UHF). Usually the systems operating at LF and HF are known as inductively-coupled systems and are limited to short ranges comparable to the size of the antenna. In practice, inductive RFID systems usually use coil size of a few cm, and frequencies of 125/134 KHz (LF) or 13.56 MHz (HF). Thus the wavelength (respectively about 2000 or 20 meters) is much longer than the size of the "antenna". These kinds of passive tags are smaller, have comparatively good life span, lighter, less expensive than active tags, and can only be read from a short-range distance of less than one meter. When the antennas have a comparable size (of the order of credit card size) to that of wavelength, the RFID usually employ radioactive systems (systems which emits radiation); normally in the UHF frequency range (868-928 frequency range; 868-870 MHz in Europe, 902-928 MHz in USA, and 950-956 MHz in Japan). These systems use wave propagation, and read range is not limited by reader antenna size but by the tag or reader sensitivity [5]. The read range for UHF passive tags are of the order of 10 m. Semi-passive RFID uses an internal power source to power the chip, but works on the principle of retro modulation, i.e. contrary to the active tags; the backscattered wave is not generated by the battery of the tag.

Semi-passive tags differ from passive in the sense that semi passive tags possess an internal power source for the tag's circuitry which allows the tag to complete other functions such as monitoring of environmental conditions (temperature, shock) and which may extend the tag signal range. They also have a small life time (smaller than passive tags but larger than active tags) and a cost that lies in between the two.

1.2 LIMITATION OF BARCODES AND EVOLUTION OF RFID

The most widely adopted method for product identification is barcodes. The barcode is a vertically stripped identification tag printed on products, allowing retailers to identify billions of products. There are two types of barcodes that are widely used; one-dimensional (1D), which represent data in the widths (lines) and the spacing of parallel lines, and two-dimensional (2D), which come in patterns of squares, dots, hexagons and other geometric patterns within images [6]. The former one is common in most household products while 2D barcode is common in industrial products where more information is needed to be stored in the label. 2D barcodes have maximum capacity of 128 bits and hence can be comparable with EPC. They are increasingly being used and also appear more on consumer goods. In the case of 1D barcodes, the maximum capacity is 41 bits (ex: EAN 13 barcodes). Barcode, either 1D or 2D, has been proven to effectively optimize business processes and reduce operational cost. Although appropriate in many instances, there are cases where barcodes cannot meet the need. Even though RFID and barcodes are two techniques of auto-identifications, they are different in many ways. There are numerous comparison charts that qualify the advantages and disadvantages of RFID and barcoding technology. Table 1.1 explains the main advantages of RFID compared to barcode [4], [7].

Table 1. 1*: Difference Between RFID and Barcodes*

RFID	Barcode
Can read without Line of Sight (LOS)	It requires LOS
Can read through obstacles like paper, fabric, wood etc. through which EM wave can propagate.	It cannot
Multiple tags can be read simultaneously	Can only be read individually
Can cope with harsh or dirty environments	Cannot read if damaged or dirty
Can store hundreds or thousands of bytes of information	Limited to 13 digits of information or a few hundred digits in the case of two-dimensional barcodes
New information can be over-written	Cannot be updated
Small size of the tags allows to add them to most objects unobtrusively	Require plain surface to be read; However their size is usually smaller than that of RFID tags.
Can be automatically tracked removing human error	Require manual tracking and therefore are susceptible to human error
Has uniqueness of article	Uniqueness is possible by 2D barcodes
Can directly integrated to the products	Cannot
Volumetric reading is possible	Cannot

Thus, the retailers were looking for a solution to overcome the limitations of barcodes. Fortunately, RFID could become a promising solution for this. RFID could eventually replace barcodes in some applications where bulk counting is routinely performed. However, the cost

of the RFID tags still makes it inappropriate for low-cost applications such as market unit product for mass production. Thus, almost 70% of the articles are still tagged using barcodes. Approximately 15000 billion of units are fabricated each year for this purpose. Following are the main inconveniences of RFID technology.

Cost: Tag price is one critical issue; chip tags are not normally available below $0.3 if ordering less than one million tags [8]. Currently, RFID tags are more expensive than barcodes. This is one of the most important factors that limit the usage of RFID technology. The marginal cost of a barcode is approximately less than one tenth of a cent. It has been estimated that if the cost as low as $0.09 per tag is achieved, RFID tags will have a cost-benefit advantage over barcodes and will replace barcodes altogether.

Privacy Issues: Allowing remote access and data sharing implies abuse usage of private information. Tags could be read without a person's knowledge because humans cannot sense radio signals; tags could be read by unauthorized parties; it is possible to create a database to track associations between tags and owners of tagged items over a long period of time; information exchange between a tag and tag reader could be secretly monitored.

Security Issues: Compared to other networks, RFID system is relatively secure as an authentication technology and an identification technology. Counterfeiting radio frequency identification chips is difficult. However, a hacker having specialized knowledge of wireless engineering, encoding algorithms, and encryption techniques, still can hack the system.

Technical Performance: RFID tags cannot be used to identify all categories of products. The tags are divided into number of groups and each group can be used to tag the corresponding products. As an example, there exist seven different categories of tags which can be used to tag seven different product groups [9]. Retailers use ARC (Arkansas Radio Compliance) benchmark data to create lists of approved tags for their RFID use cases. These approved tag lists are made available to the Retail Suppliers. This number is too large and which dramatically slow down the deployment of RFID tags.

Cross Reading : Cross reading is a major problem in practice. The tag or very distant shot of the tag (not supposed to be read) can be read according to the configuration (objects but also tags) present in reading area.

1.3 RFID APPLICATIONS

RFID devices are generally deployed in four main communication bands, as allowed by the FCC and its global counterparts [10]. These bands are: 1) the low-frequency (up to 135 kHz); 2) High Frequency, at 13.56 MHz; 3) Ultra High Frequency, 868-870 MHz in Europe and 902-928 MHz in USA; and 4) Microwave Frequency, at 2.4 GHz. Each band has its own advantages and disadvantages. As an example of application, for item-level tagging, typical read-range requirements are expected to be in the order of few meters [10]. Both HF and UHF RFID are used for item level tagging and pallet tracking applications. HF offers a smaller read range. However, it offer a better performance in terms of reading since it is based on near field coupling. In contrast, UHF RFID offers a better read range in comparison to HF RFID. However, since the reading is based on propagation of radio waves, the performance is limited in this case.

RFID systems have various applications where automatic identification of objects, people, or locations is needed. Asset Management, warehouse, supply chain management; authentication, counterfeit protection, security, mining human activities, automatic toll collection etc. are some of the applications [4, 11]. Other widespread applications of RFID systems include contactless payment, access control, or stored-value systems, Wal-Mart, aircraft maintenance, tagging people, livestock, libraries etc. The fashion industry has also been an early RFID-adopter. Clothing is particularly suited for RFID, since it does not contain metals or liquids that interfere with some types of RFID systems [12].

Even though RFID has numerous applications, the tagging of documents and large volumes of paper/plastic based items such as, postage stamps, tickets, banknotes, and envelopes is a problem due to the relatively high price of the RFID tag. As far as the mass market is considered, the cost of the entire RFID system is strongly dependent on the cost of the IC (Integrated Chip). This is the reason why RFID couldn't replace barcodes even though the barcodes have numerous disadvantages compared to RFID, such as the need for line of sight and short reading range. Chipless RFID tags offer a promising solution for this. Chipless tags, as their name implies do not contain any silicon chip. It can operate under the vicinity of a reader through electromagnetic waves. The chipless tags can offer a price of $0.005 per tag which is a comparable price as in the case of barcodes [13-14]. There are chipless tags that can be printed on paper and plastic using conductive ink and thus proves to be a viable and

economical solution. Thus, the main objectives are to develop low cost chipless RFIDs which have a price comparable to that of barcodes and also to develop tags where classical RFID tags cannot be employed. As an example, the SAW chipless RFID has been used as a temperature sensor in a steel plant which has a harsh production environment [15]. The sensor was designed to monitor temperatures in the range of $400°C$, where the conventional semiconductor based RFID tags cannot be used. A special packaging and assembly was used for the SAW tags in order to utilize it for such a harsh environment. The titanium/aluminum based metallization was used for the SAW delay lines. Instead of soldering, laser welding was used. The packaging was with a metallic housing with two glasses- to- metal seals. Due to the elevated temperatures of up to 300°C, no conventional design was applicable for the reader antenna. Therefore a custom-built dipole wire antenna was developed. In this case the dipole was attached onto a coaxial cable with a steel mantle and SiO2 dielectric, which can be used up to 1000°C. The reflected pulses from the SAW tags were used for the identification and sensing purpose. Thus, chipless RFID tags can be used in harsh environment which is not the case for conventional RFID tags. However, SAW tags cannot be categorized under low cost tags (they are even more expensive than passive RFID tags). Still they come under the category of chipless as they do not contain any chip. The next section of this thesis explains the principle of chipless tags.

The chipless RFID owing to its low cost has opened a new era for low cost and robust identification system [16]. Chipless RFID transponder consists of some planar, potentially multi-layer labels which will re-radiate the electromagnetic wave in the vicinity of a reader. The principle of information encoding in chipless tags is based on the generation of a specific electromagnetic signature. Depending on the shape of the particular label, the nature of the electromagnetic signature can change from tag to tag. In the measurement where the identification is directly contained in the temporal signal, we call the tag as a temporal tag. In the succeeding section, we'll see another approach to encode the information directly on the frequency representation of the signal, in this case, we call the tag as frequency domain tag. Hence we define two main families of chipless tag. Fig.1.2 shows the example of a time domain chipless RFID system which contains a transmitting/receiving antenna and a delay line.
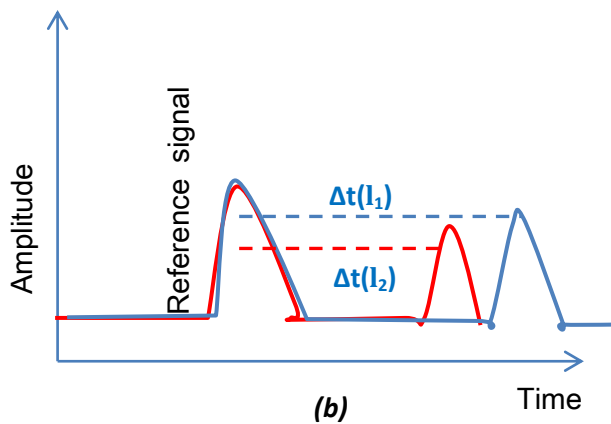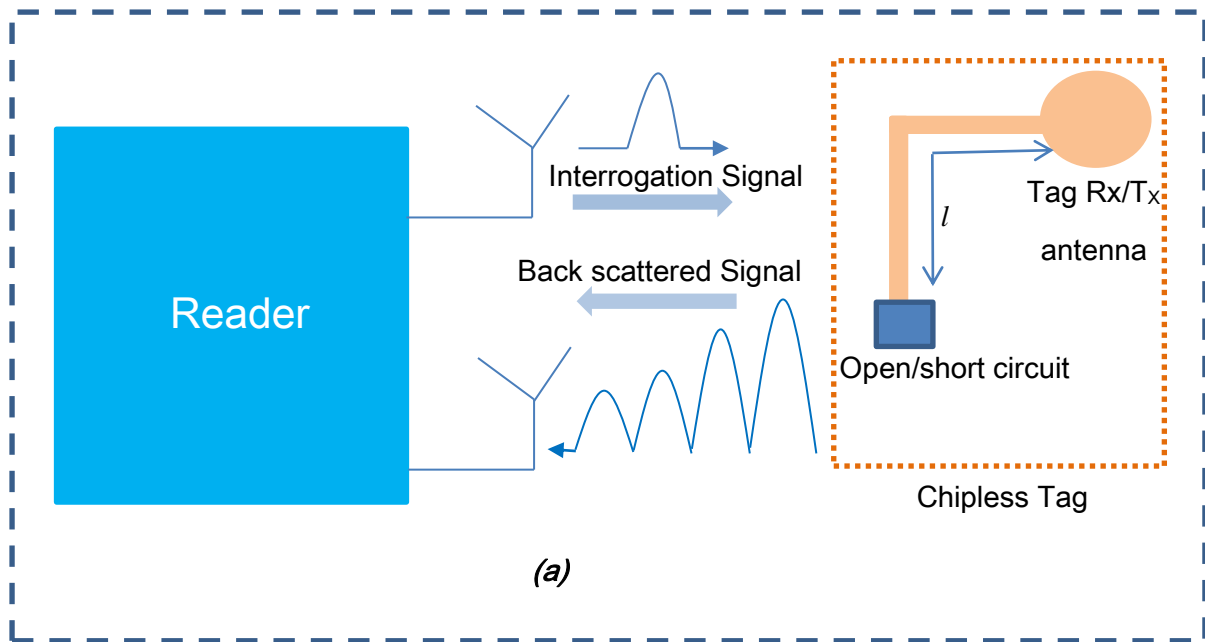
Fig.1. 2 : Principle of operation of time domain chipless RFID system and time domain encoding. a) Chipless RFID system. b) Principle of encoding.

Let us consider a chipless tag contains an antenna and a delay line with length l, terminated with open or short circuit. As shown in Fig.1. 2 (a), the tag Rx antenna receives the interrogation signal send by the reader. This signal passes through the delay line. When the signal reaches open or short circuit, the signal will reflect back with a time delay which will be a function of length l. Tx antenna can re-transmit this signal reflections with different delays for encoding. Fig.1.2 (b) shows the reflected signal for two different lengths l_1 and l_2, where l_1 is the longer line and l_2 is the shorter line. Thus the time difference between the reflected signals and reference signal will be a function of these lengths. The longer line will produce more Δt than shorter line.

The first commercially successful chiplesss RFID is the SAW tag developed by RFSAW Inc. [17]. SAW tags follows Time Domain Reflectometry (TDR) (time domain) based encoding scheme which will be explained in the succeeding chapter. As already explained, mainly there are two kinds of coding schemes available in the literature; TDR based coding (time domain) and spectral signature (frequency domain) based coding. Chipless tags based on these coding techniques will be explained in the succeeding chapter. The SAW tags use a piezoelectric material in which different reflectors are placed and signal reflections occur from these reflectors are used for the encoding. 256 bits can be encoded in this way. However, the cost of the tag is significant and also due to the piezoelectric properties, electrostatic discharges can damage the tag. Moreover, they do not provide a fully printable solution due to their piezoelectric nature, which cannot be printed on banknotes, postage stamps or other paper/plastic based items. In the case of low cost non-piezoelectric substrate, a longer transmission line is needed to produce a measurable delay [18-21]. Moreover, the coding capacity is also limited in this case. The highest reported coding capacity under this category is 8 bits [18].

The second method of information encoding is the amplitude/phase/group delay-frequency approach or spectral signature approach [22-25]. Most of the tags found in the literature come under this category since it allows more capacity of coding. The highest capacity of coding reported under this category is 49 [25]. The frequency signature approach uses quite wide band of frequencies, because more the band more the number of bits that can be encoded. The problem with this technique arises when we take the Federal Communications Commission (FCC) or European Telecommunications Standard Institute (ETSI) frequency regulation into account; they cannot be used for the applications where power level is important. More emission power level will lead to a high read range. Frequency signature based tags can only be used for low read range applications. In the succeeding chapter, these two techniques will be introduced in detail.

1.4 MOTIVATION OF THE THESIS

As already explained above, chipless RFID systems must be compatible with the existing FCC standards or ETSI standards in terms of allocation frequency and emission power. According to ETSI EN 300 440 [26], UHF RFID bands can use a maximum E.R.P.

(effective radiated power) of 33 dBm (2 W). However, in the case of ISM bands, at 2.45 GHz, the RFID applications can use an E.I.R.P. (effective isotropic radiated power) of 27 dBm (500 mW) in outdoor and 36 dBm (4 W) in indoor applications. 5.8 GHz is a rarely used RFID band. However, it allows an E.I.R.P. of 14 dBm (25 mW). Fig.1. 3 (a) & (b) shows the power spectral mask for UHF band (at 865-868 MHz) and Microwave band (at 2.45) GHz respectively. The absolute levels of RF power at any frequency shall not exceed the limits defined in the spectrum mask envelope. For Fig.1. 3, the X axis shall be in linear frequency and the Y axis shall be scaled in dBm E.R.P. for Fig.1. 3 (a) and in dBm E.I.R.P. for Fig.1. 3. (b). fc is the center frequency of the carrier transmitted by the interrogator. However, the RFID application at 2.45 GHz which respect these above explained power levels should also use FHSS (Frequency Hopping Spread Spectrum) or un-modulated carrier (Continuous Wave) in the case of outdoor application, and FHSS only in the case of indoor application, as the emission signal. FHSS is spread spectrum technique in which the transmitter signal occupies a number of frequencies in time, each for some period of time, referred to as the dwell time. Transmitter and receiver follow the same frequency hop pattern. The number of hop positions and the bandwidth per hop position determine the occupied bandwidth. The commercially successful SAW tags limited their power limit as 10 mW, which corresponds to


(a)   (b)
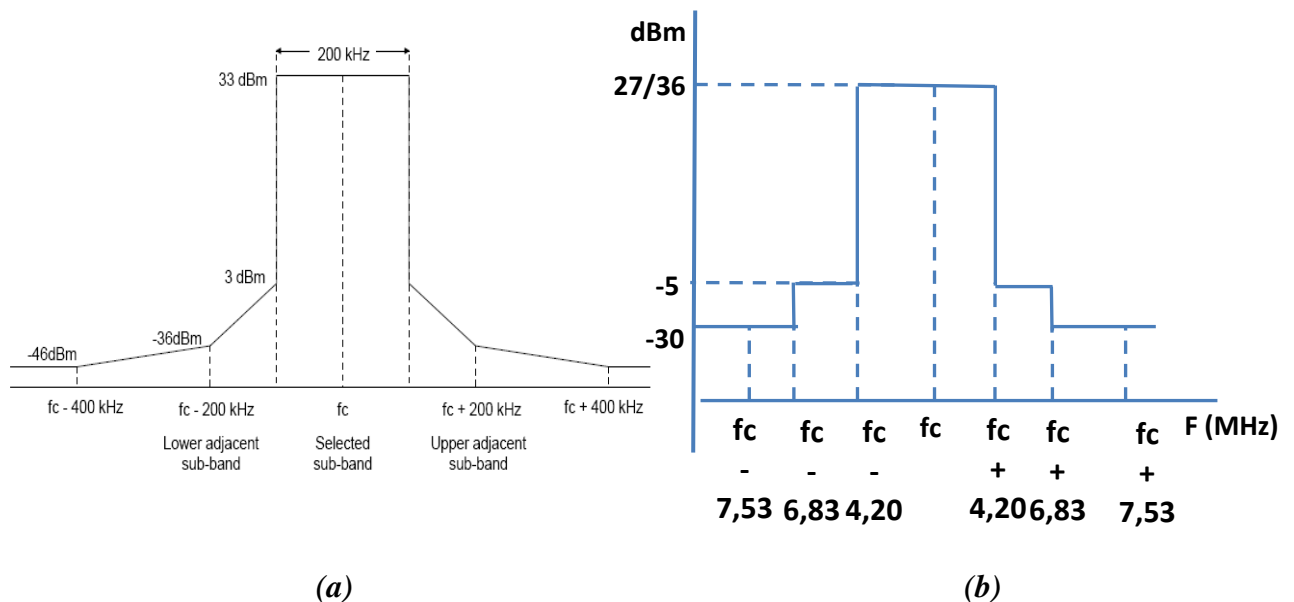
Fig.1. 3 : The proposed ETSI stair case spectral mask given in [23] for a) UHF band at 865-868 MHz b) Microwave band at fc=2.45 GHz.

the power approved by ETSI for "generic use". However, SAW tags were able to produce a read range greater than 5 m with this power limit [16]. At 5.8 GHz, an E.I.R.P. of 25 mW can be used for "generic use" within a band of 5.725 - 5.875 GHz. Thus, the ISM bands allow the use of two bands having bandwidth of 100 MHz and 150 MHz with a power of the order of tens of mW.

In frequency domain (spectral signature tags) the only solution to respect these standards while having a broad frequency band is to emit short pulses, i.e. using UWB standard (like in UWB radar) [27]. However, the allowed power level is very low in this case which leads to a low reading range of the order of 50 cm. However, 2 m is also theoretically attainable. ([28] presents a theoretical study of the reading distance as a function of RCS of the tag. In measurement, a reading distance of 50 cm is also reported [29]). UWB regulation allows only a Power Spectral Density (PSD) of -41.3 dBm/MHz (0.07 µW/MHz). Hence, for the applications where the power level is more important, the only solution is to use ISM bands. Since ISM bands can use more power, it can increase the reading range as in the case of SAW tags. However, in this case the frequency band is very limited, but it remains compatible with the use of a temporal approach. The time domain tags (TDR based tags) have a significant importance while dealing with the practical measurement techniques, as in the case of SAW tags, where a mono pulse (at 2.45 GHz) has been used as the interrogation signal [17]. In frequency domain approach, the Radar Cross Section (RCS) of the structure has to be determined using specific, and sometimes complex, calibration process in order to extract the tag information contained in the electromagnetic signature (presence/absence of peaks). Contrary to this, in temporal encoding, the information detection is simply based on the time position of the reflected pulse. It is easy to isolate the tag from its external environment by performing a time domain windowing and hence be less affected by it [30]. Thus by combing the two preceding observations; the use of ISM bands and the robust communication; it was found that the reading range of temporal tags is two to three times larger than that of the frequency domain tags. Moreover, the easiness in detecting the tag information is also predominant.

As already explained in the preceding paragraphs, the frequency signature tags allow a better coding capacity and TDR based tags offer better reading range. Thus this thesis, for the first time, combines certain advantage of time domain tags and frequency domain tags. As a result, a novel temporal multi-frequency tag has been developed. Time domain tags were less

studied in the literature since it can produce only few bits in terms of coding capacity. This problem is solved in this thesis by allowing multi-frequency bands in time domain. In the case of TDR based tags, the delay is produced by using a linear or meandered transmission line which allows information encoding at a single frequency. In contrast, the proposed tag uses transmission line sections coupled at alternative ends; which is also known as C-sections; which is able to produce group delay peaks at a particular frequency as a function of the length. Thus, the C-sections with different lengths will be able to produce different peaks at frequency and which will be independent on each other also. The dispersive character of the C-sections is exploited for this purpose. Dispersive character allows different spectral components to be arranged in different time (see Fig.1.4). All these aspects will be explained in details in the succeeding chapters. The use of C-sections in RFID can be seen [31-32]. However, the use of temporal multi-frequency is not yet been reported anywhere. Information can be encoded at different frequencies. Thus it allows the augmentation of coding capacity compared to the existing TDR based tags.
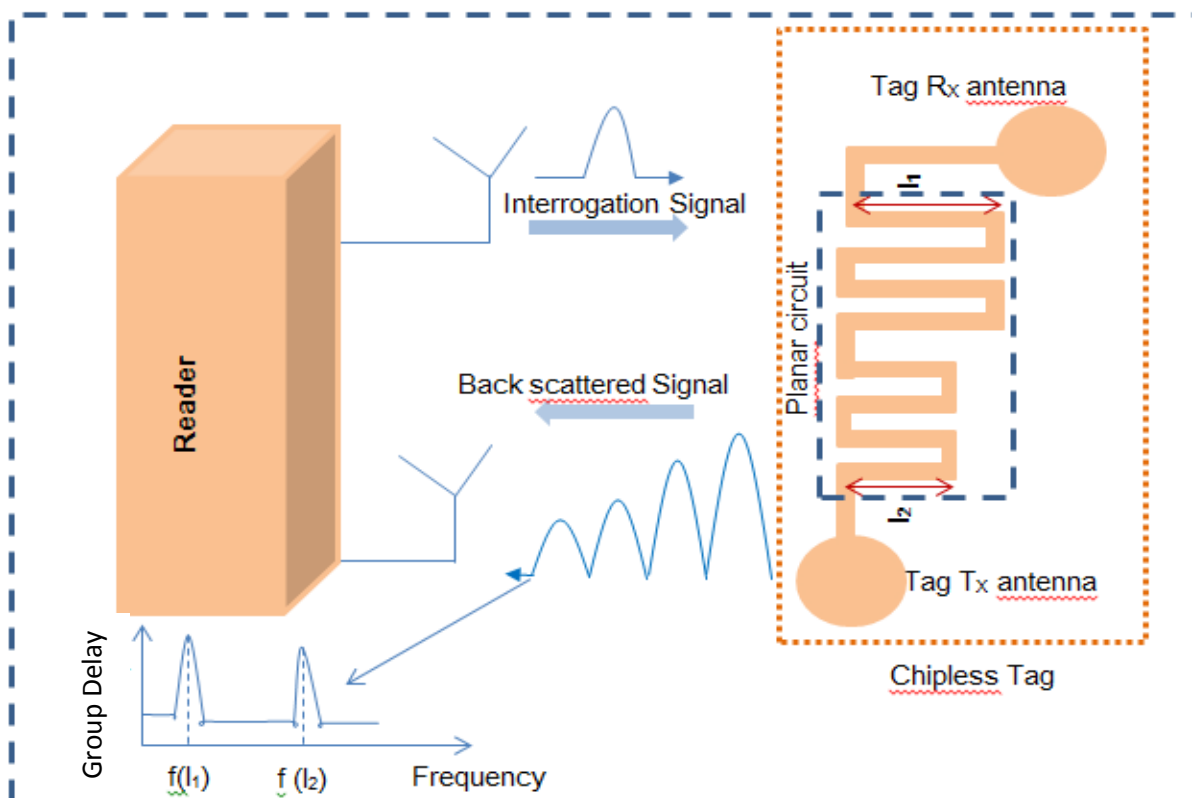
Fig.1.4: Proposed temporal multi-frequency chipless RFID tag consists of two different groups of C-sections and hence two operating frequencies f(l$_1$) and f(l$_2$).

Fig.1.4 shows the proposed temporal multi-frequency chipless RFID system. As shown in Fig.1.4, the chipless tag introduced here consists of cross polarized Ultra Wide Band (UWB) tag antennas and cascaded multi-group of C-sections. The UWB antennas are used to receive the interrogation signal from the reader and also to re-transmit the backscattered signal from the tag which contains the tag information. The proposed chipless tag is based on microstrip design and it is potentially printable also. Contrary to the linear and meandered transmission line, C-sections makes use of the coupling effect and hence can produce a significant amount of group delay with a reduced size. The C-section shown in Fig.1.4 uses edge coupling.

The thesis also proposes the use of a multi-layer design. Contrary to the linear arrangement of C-sections as explained in Fig.1.4, in this case the C-sections are arranged as one on the top of another with a thin dielectric layer in between. Thus it makes use of the broadside coupling which in turn increases the group delay significantly and makes the delay peaks highly narrowband allowing augmentation of coding capacity. As we will see in the succeeding chapters, a coding capacity of 5.78 bits is obtained using single group of C-sections and 12.05 bits is obtained using multi-group of C-section, in the allowed unlicensed ISM band. It can also offer 43.27 bits with UWB regulations. This is a significant amount in comparison to the existing TDR based tags where the highest coding capacity is 8 bits [19] (except SAW tag).

The proposed multi-layer C-section offers chipless tags with higher coding capacity, compatible with ISM bands; thus allowing more reading range and potentially printable also (the proposed tags are also fabricated on paper). This is the first time, all these characteristics are studied. The thesis also proposes an application of the proposed tag as a sensor tag to monitor humidity. For this, silicon nanowires are used. The nanowires are manually deposited on strips of the C-sections. The nanowires can change their permittivity upon humidity absorption and thus can change the backscattering response. The change in S21 magnitude, phase, and group delay is studied.

1.5 ORGANIZATION OF THE THESIS

The thesis is organized as follows;

Chapter 2 Literature Review

This chapter gives a thorough review of the existing chipless tags. Tags have been categorized as time domain reflectometry tags and spectral signature tags and each tag is explained thoroughly. An attempt has been made to cover different existing encoding technique and hence to arrive at the motivation of the thesis.

Chapter 3 Microstrip Single Group of C-sections and Delay Based ID Generation

This chapter deals with the design of tag using single group of C-sections. The first section deals with the different delays produced by linear transmission line, meandered transmission line, and C-sections. Thereafter, the design of tag prototype using single C-section group is explained along with the ID generation technique. Various experimental results using Digital Oscilloscope and commercially available UWB radar are also incorporated.

Chapter 4 Microstrip Multi- Group of C-sections and Delay Based ID Generation

This chapter deals with the design of tag using multi- group of C-sections. The design of a tag which can operate in the two ISM bands, at 2.45 GHz and 5.8 GHz respectively, is explained along with the ID generation. Different measurements using Digital Oscilloscope and UWB radar can be seen in this chapter also.

Chapter 5 Multi-Layer C-sections and Delay based ID generation using Flexible Substrates

This chapter explains folded multi-layer C-sections fabricated on flexible substrates. In contrast to the previously reported C-sections which were planar, this chapter explains folded multi-layer C-sections with broad-side coupling. Full-wave simulation has been done and the results are validated experimentally. It is assumed that instead of 3 bits as in the case of linear C-sections, a coding capacity of 5.78 bits using single group of folded C-section and 12.05 bits using multi-group of C-section can be obtained in the allowed unlicensed ISM band. It can also offer 43.27 bits with UWB regulations.

Chapter 6 Chipless RFID Humidity Sensor Using Silicon Nanowires

This chapter explains a novel temporal chipless RFID sensor tag for humidity sensing application. It proves the candidature of silicon nanowires in the humidity sensor measurements. Firstly, a prototype of the sensor tag is tested. Further, measurement of a chipless tag in a real environment is incorporated.

Conclusion

It serves the conclusions drawn from the studies with directions for future work. It describes the important findings of the thesis and salient features of the proposed temporal multi-frequency tag.

Appendix Methodology

In this section, the methodology adopted for characterizing the chipless tag is described. It deals with the various techniques employed for the design, fabrication, and measurement of tags. Simulation analysis using commercial EM simulation package such as CST is also outlined.

REFERENCES

1   G.R.T. White, G. Gardiner, G. Prabhakar, and A. A. Razak, "A Comparison of Barcoding and RFID Technologies in Practice," Journal of Information, Information Technology, and Organizations, Volume 2, 2007.

2   H. Stockman, "Communication by Means of Reflected Power", Proceedings of the IRE, pp. 1196-1204, October 1948.

3   K. Finkenzeller, "RFID Hand Book, Fundamentals and Applications in Contactless Smart Cards and Identification," Second Edition, John Wiley & Sons, Ltd., 2003.

4   Y. Xiao, S. Yu, K. Wu, Q. Ni, C. Janecek and J. Nordstad, "Radio Frequency Identification: Technologies, Applications, and Research Issues", WIRELESS COMMUNICATIONS AND MOBILE COMPUTING Wirel. Commun. Mob.

Comput. 2007; 7:457–472 published online in Wiley InterScience (www.interscience.wiley.com). DOI: 10.1002/wcm.36.pp. 457-472, 24 July 2006

5 E. Perret, S. Tedjini and R.S. Nair, "Design of Antennas for UHF RFID Tags", Proceeding of the IEEE, Vol.100, Issue 7, pp.2330-2340.

6 M.R. H. Khandokar, G. Tangim, M. K. Islam, M. N. I. Maruf, "Simultaneously Multiple 3D Barcodes Identification Using Radio Frequency", 2nd International Conference on Signal Processing Systems (ICSPS), 2010, pp.633-636.

7 G. R.T. White, G. Gardiner, G. Prabhakar, and A. A. Razak, "A Comparison of Barcoding and RFID Technologies in Practice," Journal of Information, Information Technology, and Organizations, Volume 2, 2007, pp.119-132.

8 IDTechEx. An Introduction to RFID and Tagging Technologies, 2002.

9 Arkansas Radio Compliance Retail Suppliers : Available online http://rfid.uark.edu/2060.asp

10 T. Scharfeld, "An analysis of the fundamental constraints on low-cost passive radio-frequency identification system design," M.S. thesis, Massachusetts Inst. Technol., Cambridge, 2001.

11 V. Subramanian, J. M. J. Fréchet, P. C. Chang, D. C. Huang, J.B. Lee, S. E. Molesa, A. R. Murphy, D. R. Redinger, And S. K. Volkman, "Progress Toward Development of All-Printed RFID Tags: Materials, Processes, and Devices", Invited Paper, Proceedings of the IEEE, Vol. 93, No. 7, July 2005, pp. 1330-1338.

12 G. M. Gaukler, "Application of RFID in supply chains", [online] Available at: http://ise.tamu.edu/people/faculty/gaukler/Applications%20of%20RFID%20in%20Supply%20Chains%20-%20Gaukler%20and%20Seifert.pdf, Accessed on January 2013.

13 A. Vena, E. Perret, S. Tedjini, G. Eymin-Petot-Tourtollet, A. Delattre, F. Garet, and Y. Boutant, "Conception de tags RFID sans puce imprimés sur papier par Flexographie " acepted for presentation at the 18èmes Journées Nationales Microondes, Paris, France, 2013.

14 A. Vena, E. Perret, S. Tedjini, G. E. P. Tourtollet, A. Delattre, F. Garet, and Y. Boutant, "Design of Chipless RFID Tags Printed on Paper by Flexography," *submitted to IEEE Transactions on Antennas and Propagation,* Jan. 2013.

15 R. Fachberger, A. Binder, "SAW RFID and Temperature Monitoring of Slide Gate Plates", Sensors, IEEE 2009, pp. 1514-1517.

16   S.Tedjini , E. Perret , A. Vena, D. Kaddour " Mastering the electromagnetic signature of chipless RFId system", In: Chipless and Conventional Radio Frequency Identification: Systems for Ubiquitous Tagging: Karmakar NC, editor , IGI global; 2012.

17   C. S. Hartmann, "A global SAW ID tag with large data capacity," *Proc. IEEE UltrasonicsSymp.*, Munich, Germany, October 2002, pp.65–69.

18   L. Zhang, S. Rodriguez, H. Tenhunen, and L. Zheng, "An innovative fully printable RFID technology based on high speed time-domain reflections", Proc. of International conference on High Density Microsystems Design and Packaging and Component Failure Analysis, HDP'06, Shanghai, China, June 27-30, 2006.

19   L. Zhang, S. Rodriguez, H. Tenhunen, and L. Zheng , "Design and implementation of a fully reconfigurable chipless RFID tag using Inkjet printing technology", IEEE International Symposium on Circuits and Systems, May 2008, pp. 1524 - 1527.

20   Chamarti and K. Varahramyan, "Transmission Delay Line Based ID Generation Circuit for RFID Applications", IEEE Microwave and Wireless Components Letters, Vol. 16, No. 11, November 2006, pp. 588-590.

21   J. Xu, R. S. Chen, "Meandered Microstrip Transmission Line Based ID Generation Circuit for Chipless RFID Tag", 2011 IEEE International Conference on Electrical Design of Advanced Packaging and Systems Symposium (EDAPS), Taiwan, December, 2011, pp.1-4.

22   I. Jalaly and I.D. Robertson, "RF barcodes using multiple frequency bands", in IEEE MTT-S Microwave Symp. Dig. Long Beach CA, June 2005, pp.139-141.

23   S. Preradovic, I. Balbin, N. C. Karmakar, "Multiresonator based chipless RFID system for low-cost item tracking", IEEE Transactions on Microwave Theory and Techniques, vol. 57, no. 5, pp:1411-1419, May 2009.

24   T. Kim, U. Kim, J. Kwon, and J. Choi, "Design of a Novel Chipless RFID Tag Using a Simple Bandstop Resonator", Proceedings of Asia-Pacific Microwave Conference, Yokohama, Japan, December 2010, pp.2264-2267.

25 A. Vena, E. Perret, and S. Tedjini, "A Fully Printable Chipless RFID Tag With Detuning Correction Technique," IEEE Microwave and Wireless Components Letters, vol. 22, pp. 209 – 211, March 2012.

26 European Standard Telecommunication Series, ETSI EN 300 440-1, V1.6.1 (2010-08).

27 European Standard Telecommunication Series,UWB, ETSI EN 300 440-1, (2010-08).

28 A. Vena, "Contribution au developpement de la technologie RFID sans puce a haute capacite de codage", PhD Dissertation, LCIS, Grenoble-INP, June 2012.

29 A. Vena, E. Perret, and S. Tedjini, "High Capacity Chipless RFID Tag Insensitive to the Polarization", IEEE Transactions on Antennas and Propagation, vol. 60, No 10, 2012.

30 A. Ramos, A. Lazaro, D. Girbau, and R. Villarino, "Time domain measurement of time-coded UWB chipless RFID tags", Progress In Electromagnetic Research, vol. 116, pp. 313-331, (2011)

31 S. Gupta, B. Nikfal, C. Caloz: "RFID System based on Pulse-Position Modulation using Group Delay Engineered Microwave C-Sections," Asia Pacific Microwave Conference, December, 2010, Yokohama, Japan pp. 203-206.

32 S. Gupta, B. Nikfal, C. Caloz "Chipless RFID System Based on Group Delay Engineered Dispersive Delay Structures", Antennas and Wireless Propagation Letters, IEEE. 2011;10:1366-8.

CHAPTER TWO
REVIEW OF LITERATURE

This chapter serves to review the important developments in chipless RFID tags. Different types of chipless RFID tags based on different encoding techniques are reviewed with illustrations. Different generations of chipless tags have been categorized and explained thoroughly. This state of the art will clearly highlight the solution developed in this thesis.

REVIEW OF LITERATURE

2.1 REVIEW OF CHIPLESS RFID TAGS

As already explained in the introduction, chipless RFID has opened a new era for low cost and robust identification system [1]. The tags which are exhibiting extremely low cost will be explained in the succeeding part of this thesis. Chipless RFID transponder consists of some passive circuits which will re-radiate the electromagnetic wave in the vicinity of a reader. The principle of information encoding in chipless tags is based on the generation of a specific electromagnetic signature. Depending on the shape of the particular passsive circuit, the nature of the electromagnetic signature can change from tag to tag. This is closely related to the principle of radar.

An introduction to RFID and the difference between RFID and barcode are already explained in the preceding chapter. It also explains the principle of chipless RFID. However, in this chapter, the recent developments of chipless RFID are reported. While designing chipless tags, the major challenge faced by the researchers is the information encoding without silicon chip. Literatures provide various encoding techniques mainly based on time domain reflectometry (time domain tags) [2-21, 25] or amplitude/phase frequency signature (frequency domain tags) [26-56]. This classification is not based on the measurement technique used; i.e. whether time domain or frequency domain. Instead, this classification is based on how the information is encoded. In time domain tags the information will be directly contained in the reflected signal from the tag. In contrast, in the case of frequency domain tag, the information will be contained in the signal frequency. We have to perform a Fourier analysis in order to separate the tag information. It is not an easy task to categorize these tags in a tree diagram. However, Fig.2.1 shows a general classification of chipless tags based on different kind of encoding. As already explained in the preceding chapter, time domain tags are used for the applications where a significant read range is needed (of the order of few meters). This is because, time domain tags can operate at narrow band frequencies (preferably ISM bands) using the more allowed emission power. On the other hand, frequency domain tags use mostly UWB band where the emission power is quite low and hence can only be used for short reading range applications (of the order of 50 cm). In frequency domain tags, if more
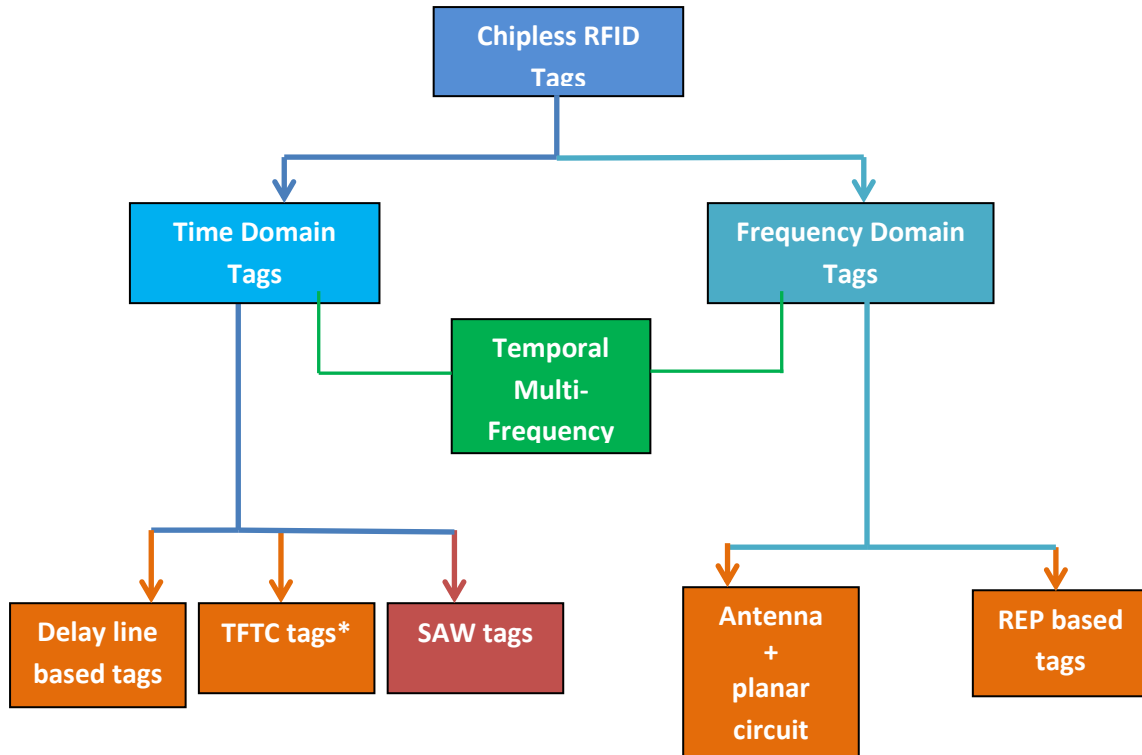
Fig.2. 1 : Classification of Chipless RFID tags based on encoding available in the literature; SAW-Surface Acoustic Wave, TFTC- Thin Film transistor circuits, REP-RF Encoding Particles.* TFTC tags are inappropriate in this category since it follows the transmission protocol. However, since an electronic format of the IC chip is printed in this tag, making it completely printed and potentially low cost as in the case of chipless tag, it is categorized here.

coding capacity is needed, more number of bands has to be used. In the succeeding section, different categories of time domain tags are explained.

2.1.1 TIME DOMAIN REFLECTOMETRIC TAGS

The evolution of time domain chipless RFID tag starts with *SAW tag* developed by RFSAW Inc., which is an apt example that takes into account of the frequency regulation [2-3]. In the SAW tag, signal reflections occurred from reflectors placed at particular distances in a piezoelectric material and therefore at different times are used for the encoding. SAW tag operates at 2.45 GHz [4-7]. It permits coding of 256 bits which is comparable with the Electronic Product Code (EPC) standard and thus the conventional RFID using an IC chip. It uses a power of 10 mW (compliant with the ETSI regulation as explained in the introduction) which is very low compared to the conventional RFID tags. The conventional IC tags require

continuous radiation of few watts in order to have the same reading distance as in the case of SAW tags. Also the tags have achieved a reading range of the order of few meters. The encoding is based on PPM (pulse position modulation) [8-12]. However, the cost of the tag is
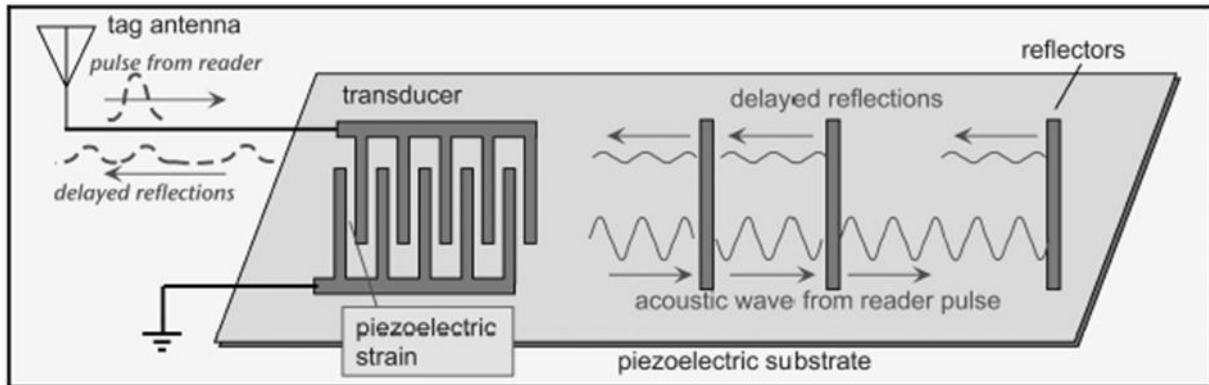

Fig.2. 2: Principle of SAW tags explained in [2-12].Dimension of the tag : 10X10 mm^2.

significant and due to the piezoelectric properties, the tags are *non-printable* on paper like materials.

Fig.2. 2 shows the principle of operation of SAW tags. The interrogation pulse is converted to a surface acoustic wave using an inter digital transducer (IDT). The surface acoustic wave propagates across the piezoelectric crystal and is reflected by a number of reflectors which create a train of pulses with time delays. The train of pulses is converted back to an EM wave using the IDT and detected at the reader end where the tag's ID is decoded. Thus, the SAW tags use a unique nature of piezoelectric materials which allow a transformation of electromagnetic waves into 100 000 slower surface acoustic waves. SAW tags can hence act as delay lines which provide sufficient amount of delay with a relatively small substrate length (10X10 mm^2, without antennas). In case of low cost non-piezoelectric substrate, a longer transmission line is needed to produce a measurable delay. These kinds of tags are explained in the succeeding paragraphs.

As an example, ***delay line based tags*** are explained in [13-14] in which each transmission line sections used has a length of 180 mm and hence to produce a 4 bit code. Thus, the total transmission line length needed is 4*180=720 mm. Eight segments of such transmission lines are needed to produce an 8-bit data [14]. Data encoding is done using the impedance mismatches along the transmission line. The tag in turn re-transmits the reflections

at each point of impedance mismatches which is created by passive capacitors. All the above techniques are potentially printable also. Fig.2. 3 explains the 4 bit data encoding of such a tag.

(a)

(b)

(c)
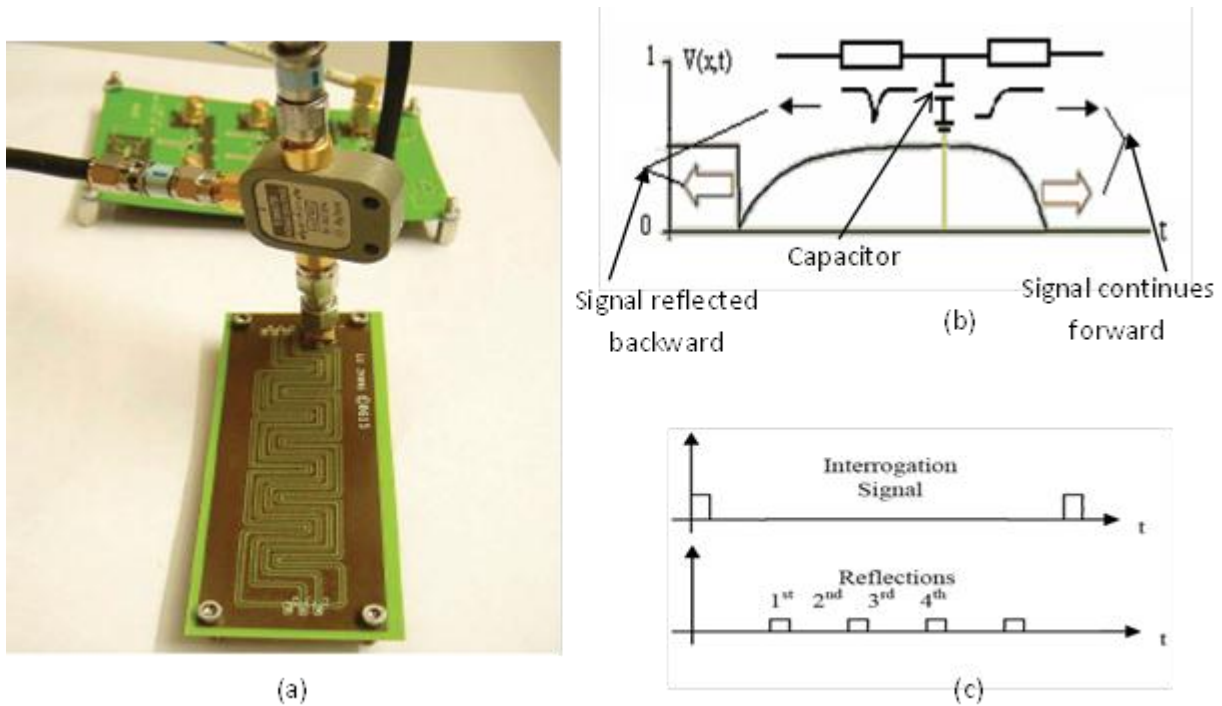
Fig.2. 3:Delay based tags illustrated in [13]. a) Prototype of such a tag with test environment, b) signal propagation after a capacitive impedance discontinuity, c) wave received by reader. The dimension of the tag is 8.2X3.1 cm^2.

Fig. 2.3 (a) shows the prototype (without tag antennas) of delay based tag with test environment developed to produce 4-bit code. Fig.2.3 (b) shows a simple example of a capacitive discontinuity in which part of the signal is reflected back and part continues its forward path. Reflections are generally considered as undesirable effects in microwave circuits. However, in this paper the authors take the advantage of these reflections by controlling the placement and characteristics of the impedance mismatches which gives the image of a SAW tag. These reflections have been used to represent the data information that is embedded in the tag. The interrogation wave consists of a train of Gaussian pulses with a 2 ns pulse width and a period of 20ns. In order to avoid the overlap between the interrogation wave and the reflection waves in the reader, the reflection waves should appear after 2 ns. The

value of capacitance is calculated in such a way that each reflected signal has the same amplitude. Fig. 2. 3 (c) shows such a wave received by the reader.

The same idea can be seen in [15] also, where an interrogation pulse has been transmitted to the *delay line* through tag transmitting antenna. At periodic discontinuities, (discontinuities may be resistive, inductive, or capacitive) a part of the signal is reflected back. Here the difference with the preceding tag is that the information encoding has been done using the signal phase of the reflected signal with respect to the reference phase. The reflection of the pulse at the antenna terminals when entering the delay line is used as a reference.

Later appears another common technique of time domain encoding using *transmission lines and antennas* [16-21]. Usually a longer transmission line is connected at the end of an antenna and the transmission line is terminated with different kinds of load conditions like open, short and matched [16-17].

Here encoding is done using the reflected signal at these loads using PPM (Pulse Position Modulation) technique. Different categories of tags are realized by changing the length of the transmission line and hence the time delay. Fig. 2. 4 (a) shows the prototype of balloon shaped UWB antenna tag. One key feature in these kinds of tags is the two different backscattering modes produced by the antenna. The backscattering is the phenomenon by which the antenna re-radiates some of the electromagnetic energy into the space. Such a re-radiating signal will have two modes. One is the structural mode, which is the inherent property of the antenna and will not change due to any load conditions. On the other hand the other mode, i.e. antenna mode is a load dependent property and varies along with variation in the impedance of the load [22]. Antenna mode scattering is assumed to be the core of the chip based RFID system, where the impedance of the tag is switched to different impedance states to vary the amount of reflected power and hence to convey the information [23]. The time difference between these two modes can be varied by changing the length of the transmission line and can be used for coding. In addition to the time domain coding, the phase difference between different antenna modes can also be used for coding. Such modes can be seen in Fig.2. 4 (b) for the backscattered time domain response of the balloon shaped UWB antenna. The early time pulse is known as the structural mode of the antenna and it is constant

irrespective of the load conditions. The late time pulse is known as the antenna mode, which varies upon different loads as shown in Fig.2. 4(b).

<p align="center">*(a)*   *(b)*</p>
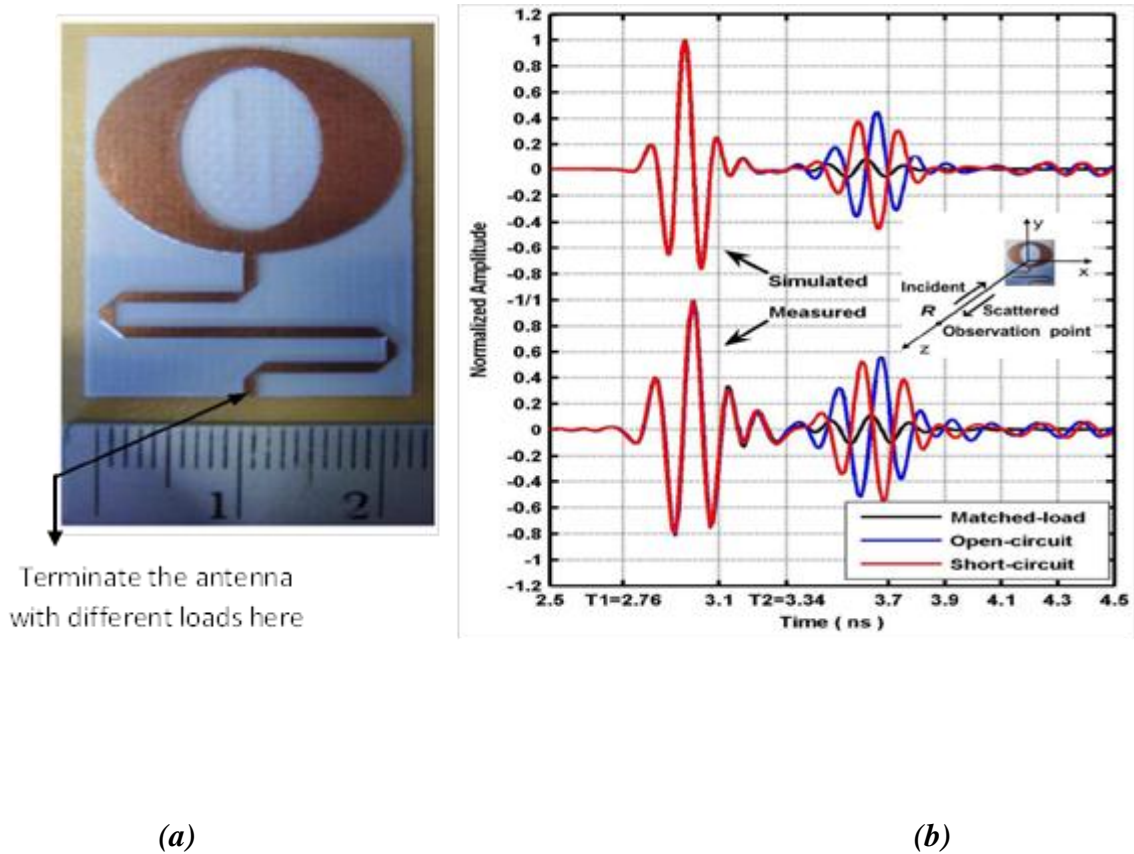
Fig.2. 4: Prototype and results of balloon shaped UWB antenna tag proposed in [16]. a) Prototype of the tag, b) backscattered time domain signal at various load conditions. The dimension of the tag is 23X 31 mm^2. The meandered line is with length of 48 mm.

Another kind of ***transmission delay line*** based ID circuit can be seen in [19-20]. Here, the ID generating circuit is designed based on the transmission delay line concept. A compact, inset-fed triangular patch antenna is developed for integration with the tag application. An OOK (On-Off Keying) modulation technique is employed for characterization of the tag. The received output consists of delayed signal from the tag added to the direct signal from the transmitter. All these tags are potentially printable also.

In [19], the ID generation circuit consists of two transmission line branches as shown in Fig.2. 5 (a). One of the branches is short and straight while the other branch is long but

meandered. The signal tapped at different lengths of the meandered branch of the ID generation circuit has different delays. The tapping of the signal can be done using isolators. Binary code is generated using the superimposition of these tapped signals as shown in Fig.2. 5 (b). However, realization of circulator or isolator at low cost is still challenging and hence it is not realistic. Moreover, the presence of these active components makes the tag differ from passive chipless RFID tag category. It is not printable also. In addition to this, the structural mode can be used as the reference as explained earlier and hence there is no need to use the transmission line as a reference. Even though, the time domain tags has the advantages such as long read range and compliance with the regulation, fabrication of long delays within acceptable loss is a challenge

(a)   *(b)*
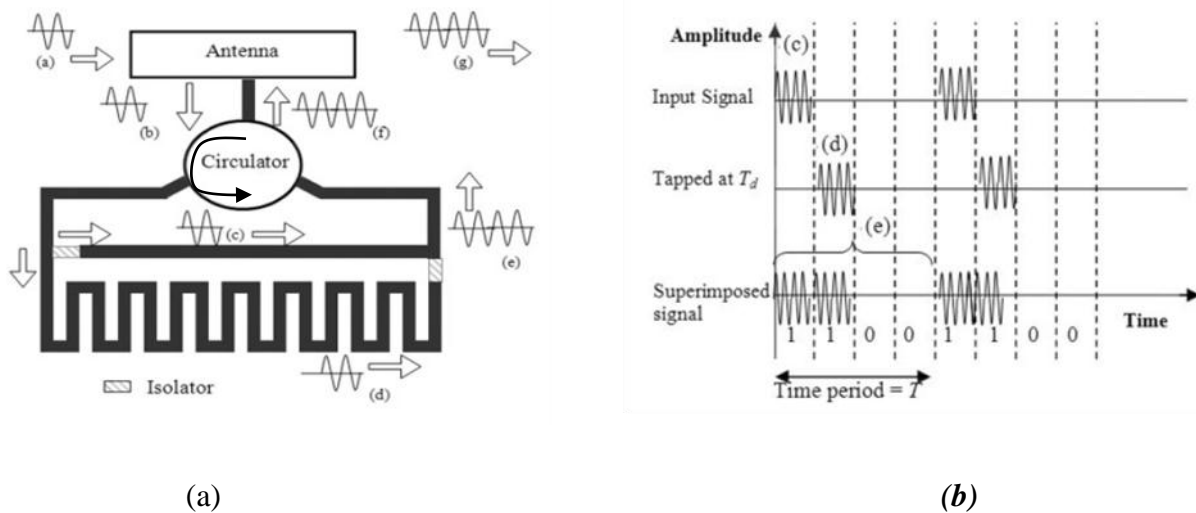
Fig.2. 5: Schematic diagram of the RFID tag and its code generation given in [19]. a) Proposed RFID tag, b) binary code generation using the superimposition of delayed signals.

Another example of time domain tag based on transmission line is depicted in [24]. It uses *left handed artificial delay lines* and in order to increase the information density, a higher order modulation scheme is also envisaged. This method could avoid the problems while porting the surface acoustic wave approach of building passive radio-frequency identification and measurement systems to the electromagnetic domain, without the need of mechanical (acoustic) delay lines of SAW tag while implementing it in the electromagnetic

domain. It could reduce the transmission line length considerably (transmission line used here has a length of 26 mm). 20 different left handed unit cells are used here. With this technique, a coding capacity of 5 bits is obtained. However, these tags are not directly printable and hence cannot be easily used for labeling. Moreover, these tags are neither realistic nor potentially low cost since they have used the discrete components and via. As already said, it is the cost which gives meaning to the chipless RFID tags. Hence this tag cannot be considered in the practical chipless RFID system.

Even though time domain tags have number of advantages, researchers are mostly interested in the frequency domain approach because of the higher number of bits that can be encoded. Frequency domain approaches have reached a maximum of 49 bits [25]. On the other hand, the maximum number of bits that are encoded with time domain approach is still 8 (except the case of SAW tag) [14].This is why the time domain approach needs more attention in increasing the coding capacity. The next section describes the chipless tags based on amplitude/phase –frequency encoding. i.e. these tags are mostly based on the electromagnetic spectral signature of the tag.

2.1.2   SPECTRAL SIGNATURE BASED TAGS

These kinds of tags encode data mainly based on the amplitude/phase of the spectral signature. Contrary to the time domain tags, the information in the frequency domain tags is directly accessible from the spectral signature. Usually they exhibit high capacity of coding with a reduced size compared to the time domain tags. This is because, some of the frequency domain tags do not use antennas (as we will see in the succeeding sections) and hence offer a reduced size because it is the antennas which consumes most of the tag surface. However, in practice we observe that they are mainly less robust than time domain tags in terms of reading range and also they need a reference tag to extract the tag information. This will be explained in the succeeding sections of this thesis. They most often require a high complexity calibration process in order to recover the information. In time domain tags the information lie directly in the reflected pulse. In contrast, in the case of frequency domain tags, the information lie in the amplitude or phase of the backscattered signature and hence it demands a calibration to separate this information. However, this approach does not always need tag antennas which are not possible in the case of time domain tags, where they most often possess the tag antennas.

In 2005, *Jalaly et al.* introduced the RF barcodes with encoding using presence or absence of the null [26]. The basic idea was to optically reproduce the barcodes by translating the optical barcodes to the RF and hence producing an equivalent RF barcode. Five **microstrip dipoles** were utilized to produce a 5 bit code. Each dipole has a ground plane and hence it produces a trough at a particular frequency and which was assigned by the binary code 1. The absence of the trough was assigned as logic 0 which is the On OFF Keying (OOK) coding technique in frequency. This principle can be seen in Fig. 2. 6 (a) along with the dipole structure as in Fig. 2.6 (b). 13 dipoles can be seen in the figure which corresponds to the dipoles operating at two ISM bands (2.45 GHz and 5.8 GHz).
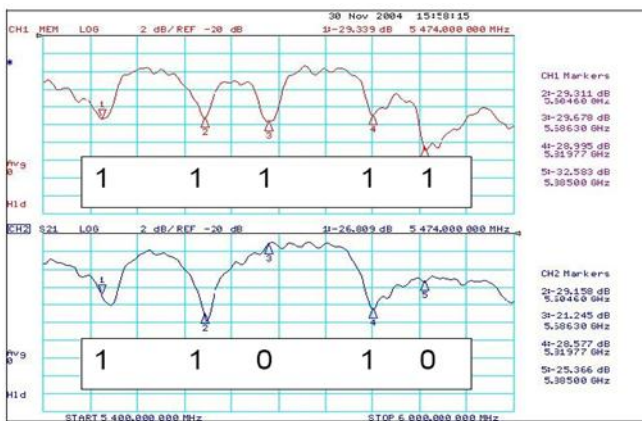
(a)   *(b)*

Fig.2. 6: Coding principle along with the 5 bit resonator structure given in [26]. a) Principle of encoding of 5 bits, b) the dipole designs with near field measurement probes.

Further the same author has also investigated the use of capacitively tuned array of microstrip dipoles to produce the RF barcodes [27]. Each dipole can resonate at different frequencies within the desired unlicensed ISM bands with each peak associated with a binary code. Thus *'n'* dipoles can produce 2^n-1 identifier. Here comes a new era of identification using OOK in frequency.

From here, different spectral signature tags based on **spiral resonators** appeared [28-34]. These chipless tags use the amplitude and phase of the spectral signature of a multi-resonator circuit and provide 1: 1 correspondence of data bits. Each planar circuit in the tag will be able to produce a peak or trough where we can also observe a phase jump. Thus,

amplitude or phase can be used for data encoding. Later it will be seen that despite of these, group delay has also been used to encode the information. The tag comprises of a microstrip spiral multi-resonators and cross-polarized transmitting and receiving microstrip ultra-wideband disc loaded monopole antennas (Fig.2. 7 (b)). Here, the reader antenna used is a log periodic dipole antenna. The tag was able to code up to 35-bit. Most of the amplitude/phase-frequency signature encoding follows the same kind of strategy; i.e. 1:1 bit correspondence (OOK coding). Presence of one resonator gives one bit. The presence of the resonator means a resonant trough and can be assigned as logic 0 and the absence of the resonator and hence the absence of trough can be assigned as logic 1. In this particular example logic zero is created by shorting the spiral edge and hence the corresponding trough will be absent.

By shorting the turns of the spiral, the resonance frequency of the spiral will be shifted up where it will be of no significance. The shift of the resonant frequency with the shorting of the turns is shown in Fig.2. 7 (a). The advantage of shorting turns in regards to removing the entire spiral from the layout is the fact that it enables future printing techniques to preserve the layout with all of the spirals shorted and when encoding data the shorting can be removed via a laser or other etching technique. Fig.2. 7 (b) shows the 35-bit chipless RFID transponder developed with this way of encoding.
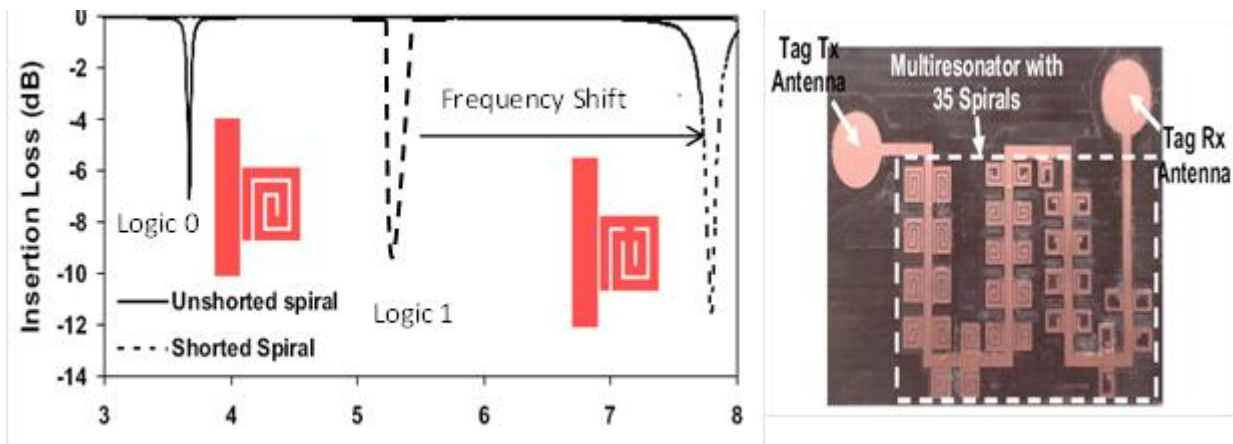

(a)   (b)

Fig.2. 7: Principle of encoding of the spiral resonator along with the 35-bit RFID transponder proposed in [28]. a)1 :1 correspondance of bits, b) 35 bit RFID transponder. Tag dimension is 88X65 mm^2.

Following the above explained method, several designs have been developed by the researchers based on amplitude/phase encoding [28, 35-36, 38-40]. In all these designs, the encoding concept remains the same; only the resonating structure differs. However, [28] experimentally proves that the phase information is more resilient to noise and can be read from a greater distance when compared to the amplitude information of the frequency signature. The robustness of phase is also explained in [37]. Hereafter, some investigations focused on phase/frequency signature have been occurred [39].

A chipless tag composed of simple **microstrip patch antennas** which are used as the planar radiating circuits are shown in Fig.2. 8 (a). These antennas will re-radiate the backscattered signals when they excite with their resonant frequency signals. This re-radiated signal will have distinct phase characteristics which have been encoded for the chipless tags as shown in Fig.2. 8 (b). The stubs are printed on the antennas for controlling the phase. Three or four states of the phases are used for the encoding (see Fig.2. 8 (b)). The orthogonally polarized backscattered signal (H plane, see Fig.2. 8 (b)) has been used as the reference. The recovered phase corresponds to one patch antenna may be also a function of other patches and

(a)   *(b)*
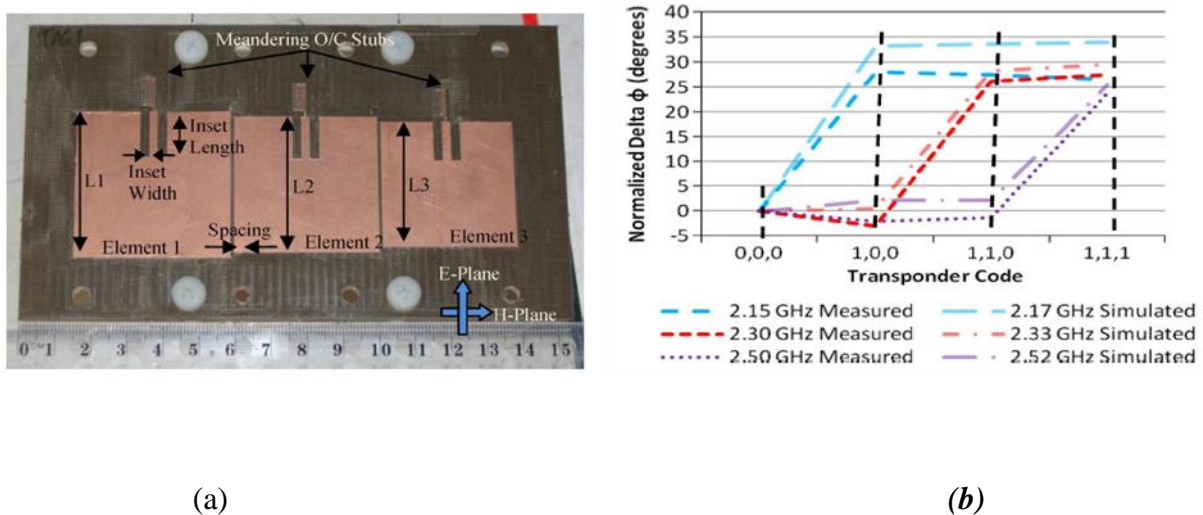
Fig.2. 8: Proposed chipless RFID system and its phase response given in [38]. a) The chipless RFID tag contains three stub loaded microstrip patch antennas. b) Corresponding phase response. The tag has 15 cm length.

hence limits this approach considerably. Hereafter, there are lot of investigations can be seen in phase-frequency signature along with amplitude encoding.

Thus, due to the robustness of phase, some designs were developed using this concept. Further, in addition to phase, researchers were interested to use group delay also, where group delay is negative derivative of the transmission phase. Such investigations can be seen in [39-40]. As an example, Chipless RFID using multiple *microstrip open stubs* can be seen in [40]. The tag contains microstrip open resonators and cross polarized disc monopole antennas. Each resonator was capable of producing a resonant peak and hence a group delay peak at the corresponding frequency. Magnitude and group delay of the tag are used for the data encoding.   1:1 correspondence can also be seen here. Compared to the existing tags in the literature, this tag offers a difference of 5 dB in magnitude and 6 ns in group delay and hence can be easily decoded. Like all other existing frequency domain techniques, this tag also uses a reference tag and calibration process making the whole system complex. Fig.2. 9 (a) and (b) respectively, shows the proposed tag and the magnitude & group delay.

(a)   *(b)*
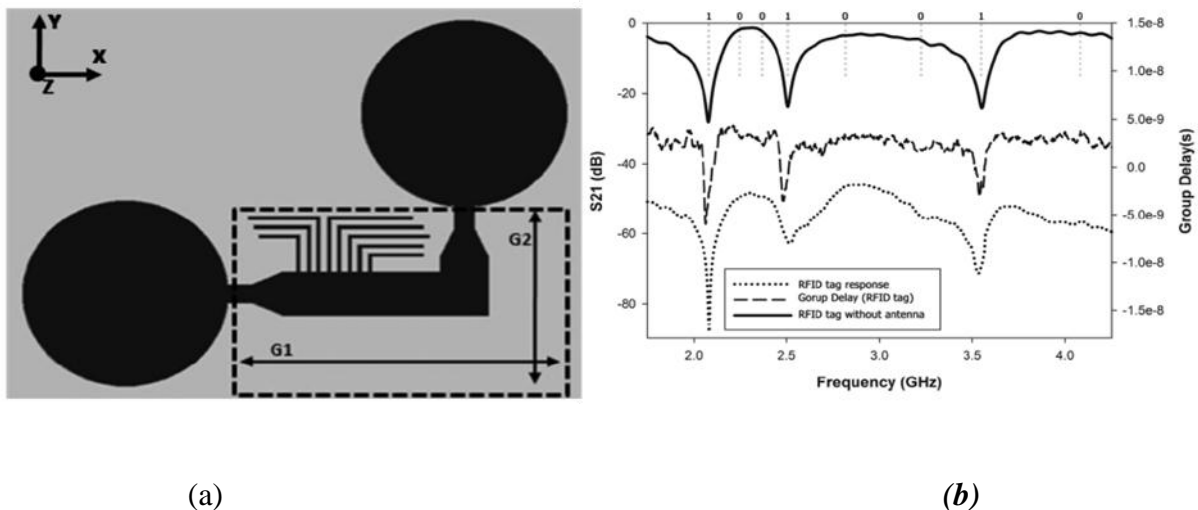
Fig.2. 9: Chipless tag design with principle of encoding proposed in [40]. a) Proposed design b) 1 :1 bit correspondance for the S21 response.

Thus all the above explained tags use amplitude/phase-frequency approach of encoding. They also exhibit 1:1 bit correspondence (OOK coding). Each time there will be a resonant peak associated with each frequency band. More the frequency band more the number of bits that can be encoded. Moreover, the higher order resonance peaks of the lower order resonance limits coding of more information. These tags often uses UWB band of frequencies to have a high capacity of coding (35 is the highest capacity of bits produced in these category [28]).

Recently, a group delay modulated metamaterial based chipless RFID has emerged in [41]. The tag prototype is based on a frequency domain on-off keying backscatter modulation scheme with small patch antenna resonators. The tag dimension is 40X40X4.5 mm^3 (three substrates with 1.5 mm of height has been stacked here). It also incorporates the approach of using group delay modulation proposed in [42]. Fig.2. 10 (b) shows the constellation diagram used for the group delay encoding. As shown in the figure, there will be always a reference delay, τ_g. Any variation from this delay (τ_g- τ_{g0}) can be used for the encoding.

(a)

(b)   *(c)*
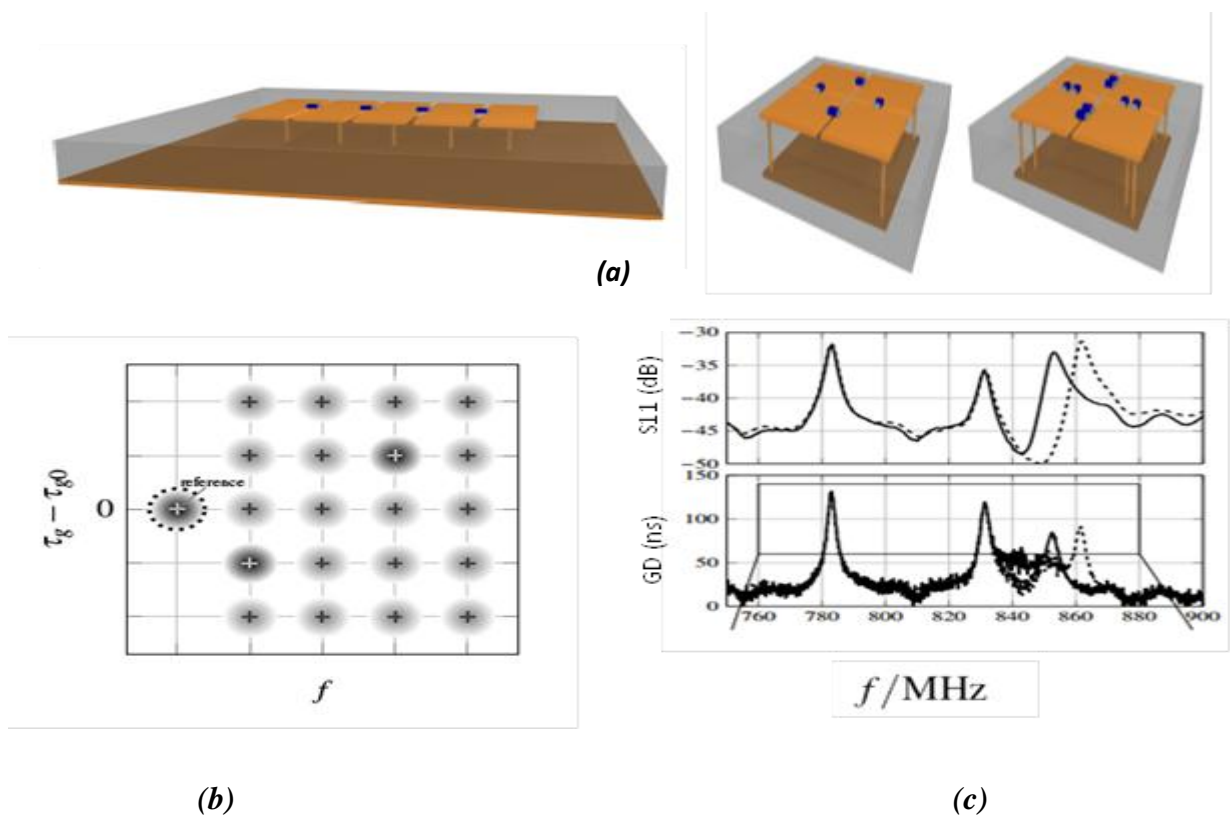
Fig.2. 10: *The chipless RFID and the encoding techniques proposed in [41]. a) Proposed tag ; blue color indicates the discrete capacitors and the long stubs indicates the inductance via. b) Proposed group delay modulation constellation diagram. c) Measured results for resonance frequency and group delay.*

In order to make compact resonators with higher delay/phase change, metamaterials are used here. Fig.2. 10 (a) shows the structure used. The resonance frequency is determined by the lumped element capacitor traversing the gap of the patch and the inductance of the via and the group delay is determined by the loaded quality factor.Fig.2. 10 (c) shows the measured results. However, the use of via and discrete components make the entire system complex and therefore inadequate for passive chipless RFID applications.

In chipless RFID, use of some planar circuit instead of the chip is still challenging. However, researchers are trying to add *more advanced features* to the existing planar circuits. Hereafter comes the era of chipless tags which use REP (RF Encoding Particles) technology and possess lot of features such as polarization diversity, use of single layer, high capacity coding, structure without tag antennas, miniaturized dimension compatible with the size of credit card etc. [43-50]. We will see these features in the following sections. Here, functionalities such as signal receptions, signal processing and signal transmission are no longer separated from each other geometrically and conceptually speaking. In this case, these REP act at the same time as a transmitting antenna, a receiving antenna, and a filtering circuit [43, 47]. It has already been proved that a better surface coding efficiency can be achieved with the REP approach. Moreover, these tags are smaller and a ground plane is not always needed which eases the realization. At that time, the REP approach is only compatible with a frequency encoding, whereas, the circuit approach can use the frequency [47] and temporal encoding [25, 49].

''**C' like metallic** structures which utilizes amplitude/phase/group delay-frequency signature can be seen in [42]. This tag uses CPS design and it does not possess any tag antennas which reduces its dimension to the size of a credit card as shown in Fig.2. 11 (a). Moreover, it does not have a ground plane makes it easy for printing. The proposed tag is based on twenty 'C' like metallic strip resonators having resonance frequency within the band of 2.5 GHz to 7.5 GHz. The tag is potentially low cost since only one conductive layer is needed for the fabrication. Moreover, the tag has also been realized with paper substrate which leads to a production cost of 0.4 cents per tag. The tag possess 20 scattering structure and hence it obtains a coding capacity of 20 bits (1:1 correspondence).

Fig.2. 11 (b) shows the corresponding group delay response obtained. In this proposed tag, the author was able to end a conclusion that group delay appears to be reliable and promising way to retrieve the coding information. As the tag has no ground plane, the resonance frequency and the global level of RCS are strongly dependent on the carrier's permittivity and thickness. In order to rectify this, a simple compensation technique is also introduced. To do so, two resonators having extreme frequency were reserved for sensing the frequency shift due to the permittivity of the container item. The same kind of structure can also be seen in [47], where a hybrid coding technique is proposed in order to increase the coding capacity. The proposed tag has a dimension of 2X4 cm^2. It is based on 5 'C' like metallic strip resonators. The proposed hybrid coding technique combines the PPM coding in frequency and utilization of phase variation which is independent of amplitude.

(a)   (b)
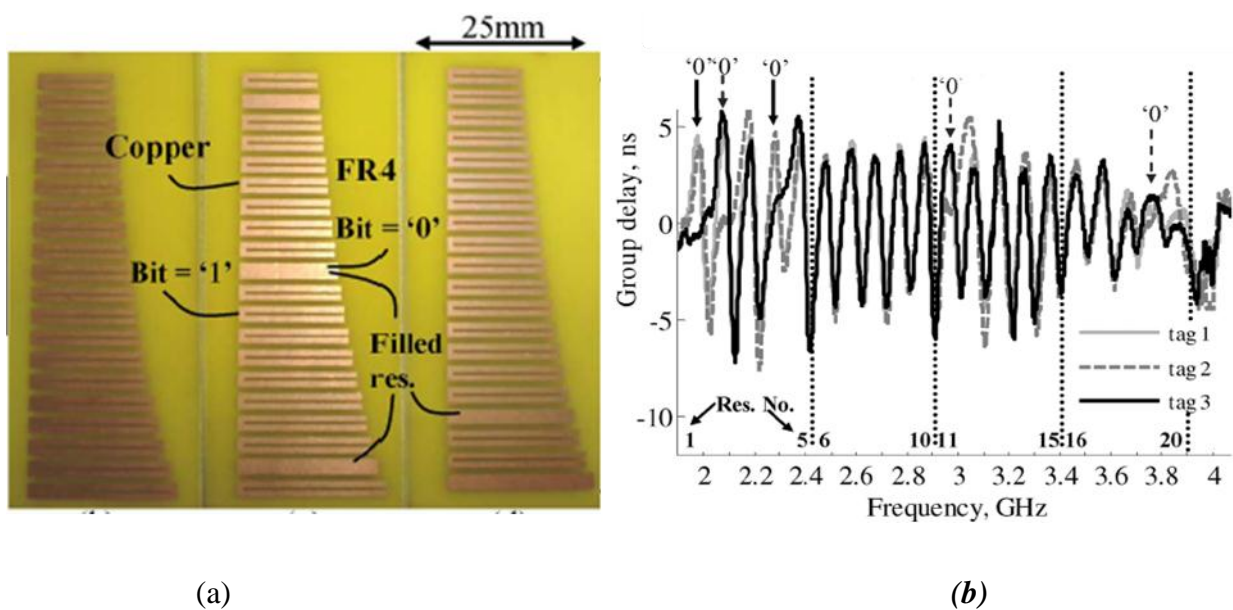
Fig.2. 11: Structure of the chipless tag and correspodning tag response proposed in [43]. a) 20 bit chipless tag in FR-4 substrate ;unfilled resonator creates a logic 1 and filled resonator creates a logic 0. b) Corresponding group delay response. Tag dimension is 70X25 mm^2.

Instead of using two resonators to sense the frequency shift produced by the container permittivity, another approach can be seen in [44] by using a single resonator. The fully printable proposed tag also possess the above explained features such as use of single layer, miniaturized dimension compatible with the size of credit card, structure without tag antennas

etc. The design is based on multiple coplanar $\lambda/4$ strip-line resonators where resonant frequencies can be shifted by setting an additional short circuit at particular locations as shown in Fig.2. 12 (a). It can encode 9 bits. The proposed design also allows the use of a single resonator to detune the effect of container permittivity. Fig.2. 12 (b) shows the measured and corrected resonance frequency when the tag is put on a PTFE (ε_r=2.1, tanδ=0.002) plate.

(a)   (b)
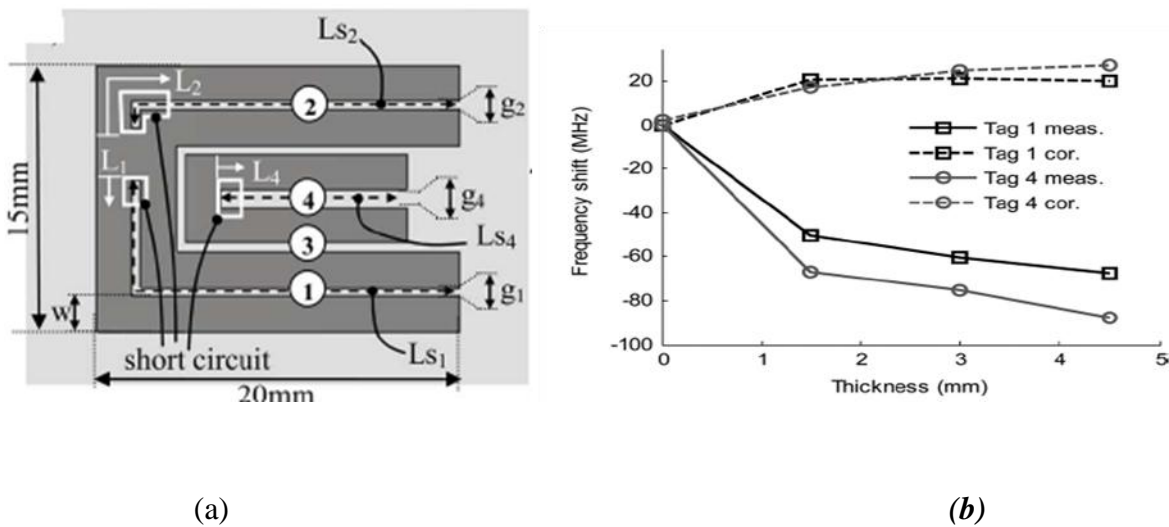
Fig.2. 12: Photograph of the tag proposed in [44] with corrected measured resonance frequency using the proposed detuning technique. a) Proposed tag design ; the initial slot lengths with no short circuit are denoted as L_{s1}, L_{s2} and L_{s4}. Short circuits are denoted as L_1, L_2 and L_4 which allow changing the frequency of each resonator. b)Measured corrected resonance frequency when the tag is put on PTFE plate. The tag dimension is 15X20 mm^2.

Tags having another advanced feature like polarization diversity can also be seen in the literature [46-48], which can be used to increase the coding capacity. Based on the work proposed in [47], in [50] fully printable *slot loaded dual polarized tag* as shown in Fig.2. 13 (a) is used -with four near and far- field reading techniques. This tag consists of four rectangular metallic patches loaded with multiple slot resonators. In order to reduce the mutual coupling between the slots, the same technique proposed in [46] is used, where slots with the same polarization for adjacent frequencies are placed alternately into two patches. Further two similar sets are placed in horizontal and vertical polarizations to double the number of bits within the same frequency bandwidth with an implementation of a new

technique of diversity of polarization. The tag can be detected using dual-polarized waveguide(s) or dual-polarized antennas. It also does not possess any ground plane. It can code up to 16 bits and can be easily printed in plastic and paper substrates. Fig.2. 13 (b) represents the magnitude and phase response of the proposed tag.


(a)   (b)
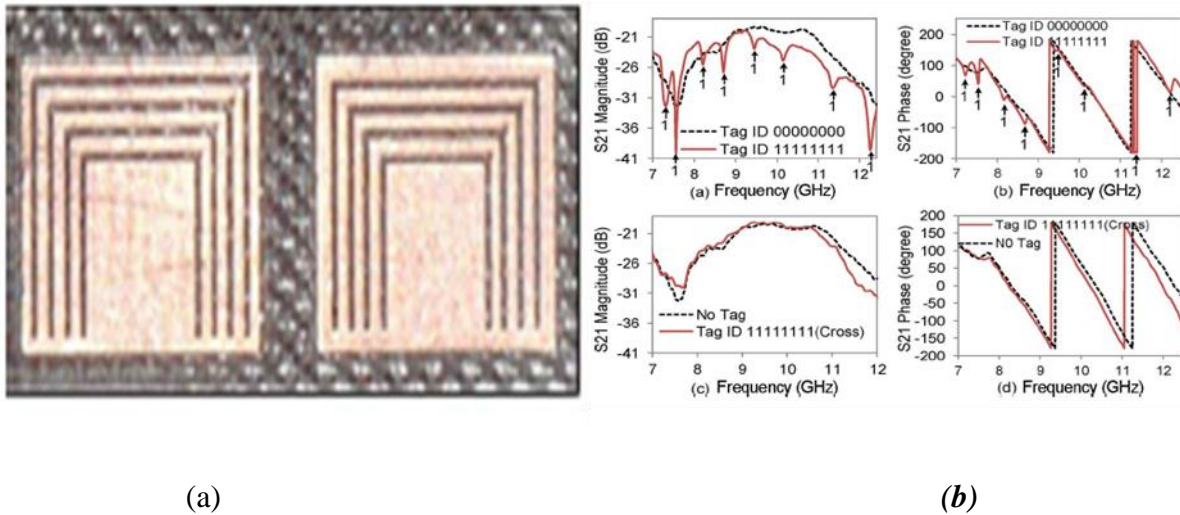
Fig.2. 13: Dual polrized chipless tag proposed in [50] along with the principle of encoding. a)Proposed tag, b) Co polarized (a&b)and cross polarized (c&d) magnitude and phase response along with the corresponding ID. Tag dimension is 7.2X5.8 mm^2.

Another category of miniaturized tag can be found in literature which is based on *electromagnetic code* of the resonators [51-52]. The proposed tag consists of an SRR array printed on very thin paper based substrate which has the size of an identity card as shown in
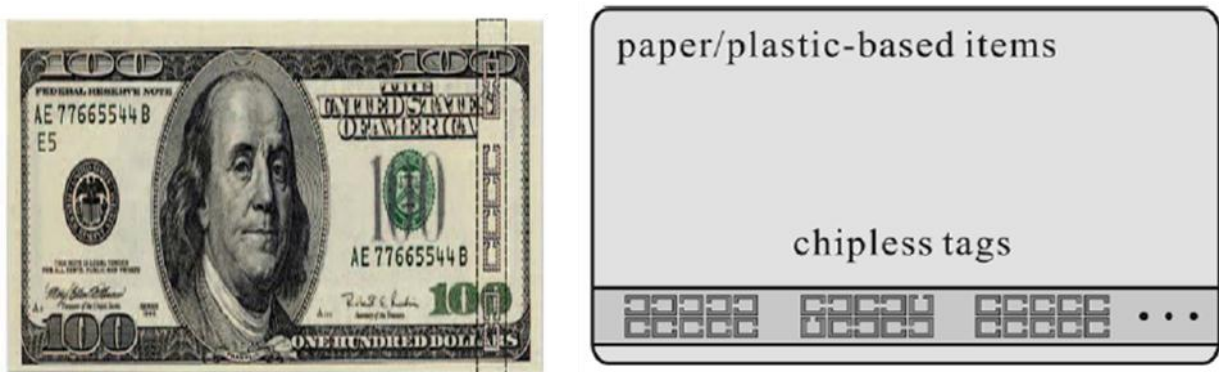
Fig.2. 14: The chipless RFID for paper based bank note proposed in [51-52]. Tag dimension is 85X53 mm^2.

Fig.2. 14. Various combinations of this SRR can produce various electromagnetic signatures. This electromagnetic code can be used to replace the hologram in the bank notes. A 1:1 correspondence can be found in this design also. In the trough, the transmission response can be digitized to 0. The absence of trough can be digitized to 1 (OOK coding).

(a)   (b)
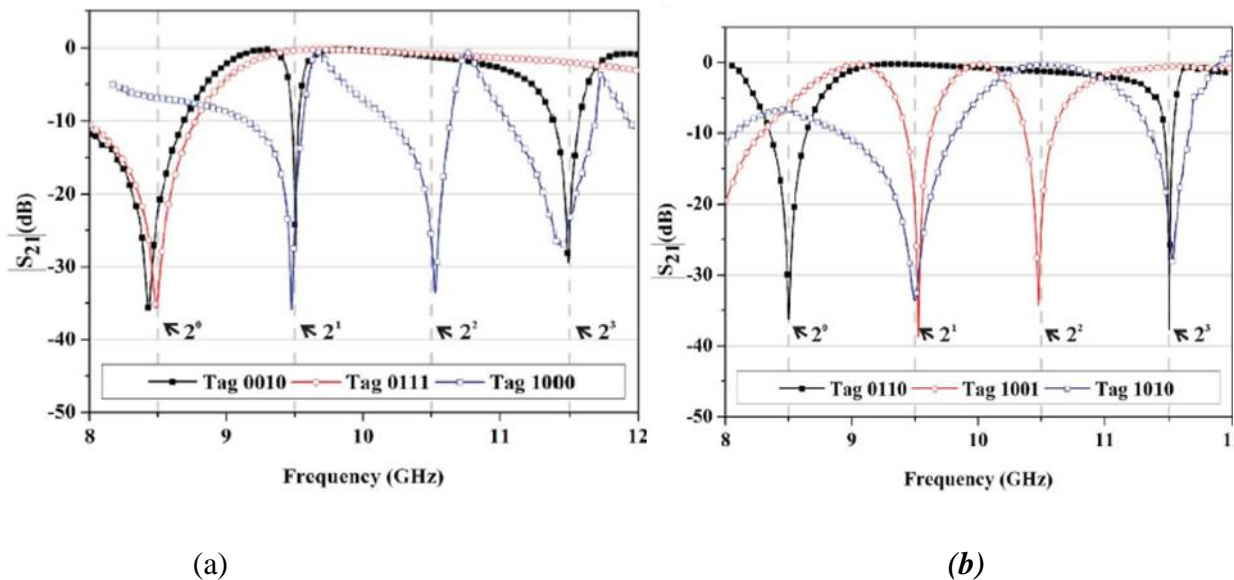
Fig.2. 15: ID generation proposed in [52]. a)Tag (0010, 0111, 1000) and b) Tag (0110, 1001, 1010).

As we already mentioned, if there are transmission responses at N frequency, the N transmission response can be converted to N-bit code. By arranging the gap between each SRR, multiple resonant characteristics can be produced. Even though the structure has a miniaturized dimension like an identity card, it has poor coding capacity. It can code 4 bits. Fig.2. 15 (a) and (b) shows the transmission characteristics along with the corresponding ID.

Thus, all the above explained tags that are categorized under frequency domain tags encode information using amplitude/phase/group delay Vs frequency, i.e. at signal frequency; we will be able to code the information directly. We have found mainly two different categories in this group. One category that possess tag antennas (multi-resonant structure based tags) and the other category that do not have tag antennas (REP). Frequency domain approach permits a high capacity of coding. The maximum number of bits produced by the category with tag antennas is 35 [28] and that of without tag antennas is 49 bits [25]. The REP approach also offer circuit miniaturization and those can be fabricated with the size

compatible with the size of a credit card. However, the main constraint comes while taking the frequency regulation into account since in this approach the coding capacity directly links to the number of bands used. All these tags are designed for short read range (≈50 cm) and own UWB technology which allows smaller amount of emission power (Power Spectral Density of (41.3 dBm/MHz). However, for the application where power level has an importance, it is better to use the ISM bands as in the case of SAW tags. ISM bands allow an emission power of 10mW which in turn will increases the read range (as per ETSI as explained in the preceding chapter).

2.2   FEATURES OF THE PROPOSED TAG

The frequency signature approach uses quite wide band of frequencies because more the band more the number of bits that can be encoded. The limitations of this technique are the frequency regulation and also the requirement of specific calibration process in order to trace the specific electromagnetic signature [43]. All the existing time domain techniques use only single frequency. It is not possible to use several frequencies at a time. Indeed, the transmission line used in this case is not highly dispersive and the delay is not a function of frequency. Also it is not possible to have another frequency to encode the information. Thus the development of tags using dispersive delays lines has an importance while thinking about the increase in coding capacity in time domain. Moreover, from the numerous studies we can pointed out that, it is interesting to use group delay coding rather than amplitude since it is more robust. This is why we stick on group delay encoding by taking the same traditional approach of two antennas and instead of long transmission line, a highly compact dispersive transmission line (known as C-sections, will be explained in detail)The dispersive property of the transmission line allows different spectral component to be arranged in different time. Some investigations have already been done in this domain [53-54]. However, the concept of time domain tags at different frequencies cannot be seen anywhere. While thinking about the technique to increase the coding capacity in time domain, the only solution is to encode at different frequencies. Here comes the importance of temporal multi-frequency technique of coding. The succeeding chapters explain the encoding at single frequency and also at multi-frequency using a highly dispersive transmission line sections also known as C-sections. C-sections are able to produce different delay peaks at different frequencies which are purely function of its geometry (length). Each group delay peak can be assigned by a binary code. By

changing the length of the C-sections, it is possible to shift the delay peaks and hence to encode more number of bits. Thus the proposed tag allows a direct relation between the structure of the tag and the code. Moreover, the proposed tag is compatible with ISM frequencies which allow the increase in read range with the allowed emission power. In order to increase the capacity of encoding of time domain tags, a multi-layer design is also proposed in this thesis. It permits a coding capacity of 5.78 bits using single group of folded C-section and 12.05 bits using multi-group of C-section in the allowed unlicensed ISM band. It can also provide 43.27 bits with UWB regulations. This is significantly large in comparison to the existing time domain tags (except SAW), where the coding capacity is 8 bits [14].

Thus, this thesis proposes a new family of tags which permits temporal coding in multi-frequency [55]. The coding can be done both in frequency and in time. In the case of frequency, different group delay variations can be considered for the coding. In time domain, the time difference between the reference signal and the delayed signal can be used for the encoding. This part will be explained in detail in the succeeding chapters.

2.3   CONCLUSION

This chapter explains the recent (after 2005, except the case of SAW) developments in the domain chipless RFID. Mainly two kinds of categories can be viewed based on the encoding process; time domain tags and frequency domain tags. Time domain tags always use narrow pulse to interrogate the system and they cannot operate at multiple frequencies simultaneously. This limits their coding capacity. On the other hand, frequency domain tags can always operate at multiple frequencies. They use UWB compatible pulse to interrogate the system. Usually the time domain tags possess a common structure; always with tag antennas and delay lines. On the other hand, in frequency domain tags mainly two kinds of categories can be found; structure that owns tag antennas and structure without tag antennas (REP). Moreover, frequency domain tags offer the highest capacity of coding bits. Also, it offers circuit miniaturization with a compatible size of the credit cards. This chapter also proposes the idea of a new family of temporal multi-frequency tag. The proposed tag allows the coding in both frequency and in time.

REFERENCES

1. S.Tedjini , E. Perret , A. Vena, D. Kaddour " Mastering the electromagnetic signature of chipless RFId system", In: Chipless and Conventional Radio Frequency Identification: Systems for Ubiquitous Tagging: Karmakar NC, editor , IGI global; 2012.

2. C. S. Hartmann, "A global SAW ID tag with large data capacity," *Proc. IEEE Ultrasonics Symp.*, Munich, Germany, October 2002, pp.65–69.

3. S. Harma, V. P. Plessky, C. S. Hartmann, W. Steichen, "SAW RFID tag with reduced size", *IEEE Ultrasonics Symposium 2006*, pp:2389-2392, Vancouver,Canada, Oct. 2006.

4. S. Harma, V. P. Plessky, L. Xianyi, P. Hartogh, "Feasibility of ultra-wideband SAW RFID tags meeting FCC rules ", *IEEE Transactions on Ultrasonics,Ferroelectrics and Frequency Control*, vol. 56, no. 4, pp:812-820, April 2009.

5. S. Harma, V. P. Plessky, X. Li, "Feasibility of ultra-wideband SAW tags",*IEEE Ultrasonics Symposium 2008*, pp:1944-1947, Beijing, China Nov. 2008.

6. P. Brown, P. Hartmann, A. Schellhase, A. Powers, T. Brown, C. Hartmann, D.Gaines, "Asset tracking on the international space station using global SAW tagRFID technology", *IEEE Ultrasonics Symposium 2007*, pp:72-75, New York,Oct. 2007.

7. V. P. Plessky, S. N. Kondratiev, R. Stierlin, F. Nyffeler, "Saw tags : newideas ", *IEEE Ultrasonics Symposium 1995*, vol. 1, pp:117-120, Cannes, France,Nov. 1995.

8. T. Han, W. Wang, H. Wu, Y. Shui, "Reflection and scattering characteristics of reflectors in SAW tags", *IEEE Transactions on Ultrasonics, Ferroelectricsand Frequency Control*, vol. 55, no. 6, pp: 1387-1390, June 2008.

9. T. Han, W. Wang, J. M. Lin, H. Wu, H. Wang, Y. Shui, "Phases of carrier wave in a SAW identification tags", *IEEE Ultrasonics Symposium 2007*, pp:1669-1672, New York, Oct. 2007.

10. S. Harma, C. Kim, S. M. Balashov, V. P. Plessky, "Properties of narrow metal reflectors used in reflective array compressors and surface acoustic wave tags",

IEEE/MTT-S International Microwave Symposium 2007, pp:2051-2054, Honolulu, Hawaii, June 2007.

11. S. Harma, W. G. Arthur, C. S. Hartmann, R. G. Maev, V. P. Plessky, "Inline SAW RFID tag using time position and phase encoding", *IEEE Transactions on Ultrasonics, Ferroelectrics and Frequency Control*, vol. 55, no. 8, pp:1840- 1846, August 2008.

12. J. Liu, J. Yao, "Wireless RF identification system based on SAW", *IEEE Transactions on Industrial Electronics*, vol. 55, no. 2, pp:958-961, Feb. 2008.

13. L. Zhang, S. Rodriguez, H. Tenhunen, and L. Zheng, "An innovative fully printable RFID technology based on high speed time-domain reflections", Proc. of International conference on High Density Microsystems Design and Packaging and Component Failure Analysis, HDP'06, Shanghai, China, June 27-30, 2006.

14. L. Zhang, S. Rodriguez, H. Tenhunen, and L. Zheng , "Design and implementation of a fully reconfigurable chipless RFID tag using Inkjet printing technology", IEEE International Symposium on Circuits and Systems, May 2008, pp. 1524 - 1527.

15. M. Schuler, C. Mandel, M. Maasch, A. Giere, R. Jakoby, "Phase modulation scheme for chipless RFID-and wireless sensor tags". Asia Pacific Microwave Conference APMC 2009 May; Singapore.

16. S. Hu, Y. Zhou, C. Law, and W. Dou, "Study of a Uniplanar Monopole Antenna for Passive Chipless UWB-RFID Localization System", IEEE Transactions on Antennas and Propagation, Vol. 58, No. 2, February 2010, pp. 271-278.

17. S. Hu, C. L. Law, and W. Dou, "A balloon shaped monopole antenna for passive UWB-RFID applications", IEEE Antennas and Wireless Propagation Letters, Vol.7, 2008, pp.366-368.

18. S. Shrestha, , M. Balachandran, M. Agarwal, V V. Phoha, and K. Varahramyan, "A Chipless RFID Sensor System for Cyber Centric Monitoring Applications", *IEEE Trans. Microwave Theory & Tech,* Vol. 57, No. 5, May 2009, pp. 1303-1309.

19. A. Chamarti and K. Varahramyan, "Transmission Delay Line Based ID Generation Circuit for RFID Applications", IEEE Microwave and Wireless Components Letters, Vol. 16, No. 11, November 2006, pp. 588-590.

20. J. Vemagiri, A. Chamarti, M. Agarwal, and K. Varahramyan, "Transmission line delay-based radio frequency identification (RFID) tag", Microwave and optical technology letters, Vo.49, No. 8, August 2007, pp.1900-1904.

21. J. Xu, R. S. Chen, "Meandered Microstrip Transmission Line Based ID Generation Circuit for Chipless RFID Tag", 2011 IEEE International Conference on Electrical Design of Advanced Packaging and Systems Symposium (EDAPS), Taiwan, December, 2011, pp.1-4.

22. R. Ling, P. Ufimtsev, "Scattering of electromagnetic waves by a metallic object partially immersed in a semi-infinite dielectric medium", IEEE Transactions on Antennas and Propagation 2001;49(2):223-33.

23. P.V. Nikitin, "Theory and measurement of backscattering from RFID tags", IEEE Transactions on Antennas and Propagation, Vol. 48, Issue 6, December 2006, pp. 212-218.

24. C. Mandel, M. Schussler, M. Maasch, R. Jakoby, "A novel passive phase modulator based on LH delay lines for chipless microwave RFID applications", IEEE MTT-S International Microwave Workshop on Wireless Sensing, Local Positioning, and RFID IMWS; 2009; Croatia: IEEE.

25. A. Vena, E.Perret, and S. Tedjini, "High Capacity Chipless RFID Tag Insensitive to the Polarization", IEEE Transactions on Antennas and Propagation, vol. 60, No 10, 2012.

26. I. Jalaly and I.D. Robertson, "RF barcodes using multiple frequency bands", in IEEE MTT-S Microwave Symp. Dig. Long Beach CA, June 2005, pp.139-141.

27. I. Jalaly and I.D. Robertson, "Capacitively tuned split microstrip resonator for RFID barcodes", 2005 European Microwave Conference, October 4-6, 2005.

28. S. Preradovic, I. Balbin, N. C. Karmakar, "Multiresonator based chipless RFID system for low-cost item tracking", IEEE Transactions on Microwave Theory and Techniques, vol. 57, no. 5, pp:1411-1419, May 2009.

29. S. Preradovic, N. C. Karmakar, "Design of chipless RFID tag for operation on flexible laminates", IEEE Antennas and Wireless Propagation Letters January 2010

30. S. Preradovic, N.C. Karmakar, I. Balbin, "RFID Transponders", IEEE Microwave Magazine, vol. 9, no. 5, pp: 90-103, October 2008.

31. S. Preradovic, N. Karmakar, "Chipless RFID – The barcode of the future", IEEE Microwave Magazine

32. S. Preradovic, N. C. Karmakar, "Design of fully printable planar chipless RFID transponder with 35-bit Data capacity", Proceedings of the 39th European Microwave Conference, Rome, Italy, September 2009

33. S. Preradovic, N. C. Karmakar, "4th generation multiresonator-based chipless RFID tag utilizing spiral EBGs", 40th European Microwave Conference 2010, Paris, France, September - October 2010

34. S. Preradovic, N. C. Karmakar, "Fully printable multiresonator based chipless RFID system for low-cost item tracking", International Microwave Symposium 2010, Anaheim, USA, May 2010

35. N. C. Karmakar and C. K. Pern, "mm-wave chipless RFID tag for low-cost item tagging", Proc. Of Asia pacific Microwave Conference, Melbourne, Australia, December 2011, pp.1462-1465.

36. T. Kim, U. Kim, J. Kwon, and J. Choi, "Design of a Novel Chipless RFID Tag Using a Simple Bandstop Resonator", Proceedings of Asia-Pacific Microwave Conference, Yokohama, Japan, December 2010, pp.2264-2267.

37. R.Padmanabhan, Sree Hari Krishnan Parthasarathi and Hema A. Murthy, "Robustness of Phase based Features for Speaker Recognition," Proc. of Interspeech, 2009.

38. Balbin and N.C. Karmakar, "Phase-Encoded Chipless RFID Transponder for Large Scale Low Cost applications," IEEE Microwave and Wireless Component Letters, Vol. 19, No.8, August 2009.

39. S. Mukherjee and G. Chakraborty, "Chipless RFID using Stacked Multilayer Patches," Proc. of the IEEE international conference on Applied Electromagnetics, Kolkata, India, December 2009.

40. C.M. Nijas, R.Dinesh, U.Deepak, Abdul Rasheed, S. Mridula, K.Vasudevan and P. Mohanan, " Chipless RFID tag using Multiple Microstrip Open Stub Resonators", IEEE Transactions On Antennas And Propagation, Vol. 60, No. 9, September 2012, pp. 4429-4432.

41. C. Mandel, B. Kubina, M. schubler, and R. Jakoby, "Group Delay Modulation with Meta-material Inspired Coding Particles for Passive Chipless RFID, IEEE International Conference on RFID-Technologies and Applications, Nice, France, November 2012.

42. R. Nair, E. Perret, S. Tedjini,"Chipless RFID based on Group Delay encoding" ,IEEE International Conference on RFID technologies and Applications(RFID-TA), Barcelona, Spain, pp. 214-218, September 2011.

43. A. Vena, E. Perret, and S. Tedjini, "A Fully Printable Chipless RFID Tag With Detuning Correction Technique," IEEE Microwave and Wireless Components Letters, vol. 22, pp. 209 – 211, March 2012.

44. A. Vena, E. Perret, and S. Tedjini, "Design of Compact and Auto Compensated Single Layer Chipless RFID Tag", IEEE Transactions on Microwave Theory and Techniques, vol. 60, No 9, pp. 2913 – 2924, 2012.

45. A. Vena, E. Perret, and S. Tedjini, "RFID Chipless Tag Based On Multiple Phase Shifters", International Microwave Symposium, Baltimore, June 5-10, 2011.

46. A.Vena, E. Perret, and S. Tedjini, "Novel compact chipless RFID tag", PIERS proceedings, Marrakesh, Morocco, March 20-23, 2011.

47. A. Vena, E. Perret, and S. Tedjini, "Chipless RFID tag using hybrid coding technique," IEEE Transactions on Microwave Theory and Techniques, vol. 59, pp. 3356-3364, 2011.

48. A. Vena, E. Perret, and S. Tedjini, "A Compact Chipless RFID Using Polarization Diversity For Encoding And Sensing", IEEE International Conference on RFID (RFID), 2012,Orlando, pp.191-197.

49. A. Vena, T. Singh, S. Tedjini, and E. Perret, "Metallic letter identification based on radar approach," in General Assembly and Scientific Symposium, 2011 URSI, 2011, pp. 1-4.

50. Md. A. Islam and Nemai Chandra Karmakar, " A Novel Compact Printable Dual-Polarized Chipless RFID System", IEEE Transactions On Microwave Theory And Techniques, Vol. 60, No. 7, July 2012, pp.2142-2151.

51. W. S. Lee, H. S. Jang , K. S. Oh, and J. W. Yu, "Design of Chipless Tag with Electromagnetic Code for Paper-based Banknote Classification" Proceedings of the Asia-Pacific Microwave Conference 2011, pp. 1406-1409.

52. H. S. Jang, W. G. L, K. S. Oh, S. M. Moon, and J. W. Yu, "Design of Low-Cost Chipless System Using Printable Chipless Tag with Electromagnetic Code", IEEE Microwave And Wireless Components Letters, Vol. 20, No. 11, November 2010, pp.640-642.

53. S. Gupta, B. Nikfal, C. Caloz: "RFID System based on Pulse-Position Modulation using Group Delay Engineered Microwave C-Sections," Asia Pacific Microwave Conference, December, 2010, Yokohama, Japan pp. 203-206.

54. S. Gupta, B. Nikfal, C. Caloz, Chipless RFID System Based on Group Delay Engineered Dispersive Delay Structures. Antennas and Wireless Propagation Letters, IEEE. 2011;10:1366-8.

55. R. Nair, E. Perret and S. Tedjini, "Temporal Multi-Frequency Encoding Technique for Chipless RFID based on C-sections", Progress in Electromagnetics Research B, Vol. 49, 2013, pp.107-123.

CHAPTER THREE MICROSTRIP SINGLE GROUP OF C-SECTIONS AND DELAY BASED ID GENERATION

This chapter deals with the design of chipless tag based on the use of single group of C-sections. The first part deals with the different delay produced by linear transmission line, meandered transmission line, and C-sections. Thereafter, the design of tag prototype (tag without antennas; instead with two ports) using single C-section group is explained along with the ID generation technique. Furthermore, the transformation of tag prototype into a complete chipless tag is explained with the corresponding code. Different time domain measurement techniques with and without a reference tag are explained. Finally those results are validated experimentally. Measurement using commercially available UWB radar is also incorporated. The obtained results confirm the use of the proposed tag for chipless RFID applications.

MICROSTRIP SINGLE GROUP OF C-SECTIONS AND DELAY BASED ID GENERATION

3.1   INTRODUCTION

While considering a practically implementable chipless RFID, several aspects should be taken into consideration. The frequency and power regulation by FCC and ETSI is such an aspect. Chipless RFID systems must be compatible with these existing standards. In frequency domain the only solution to respect these standards while having a broad frequency band is to emit short pulses, i.e. using UWB standard (like in UWB radar) [1]. However, the allowed power level is very low in this case which leads to a low reading range of the order of 50 cm [2]. Hence, for the applications where the power level is more important, the only solution is to use ISM bands. More power will lead to a larger reading range. An example is the SAW (Surface Acoustic Wave) tag developed by RFSAW Inc. [3], in which signal reflections occurred from strips printed on the surface of a piezoelectric material at different
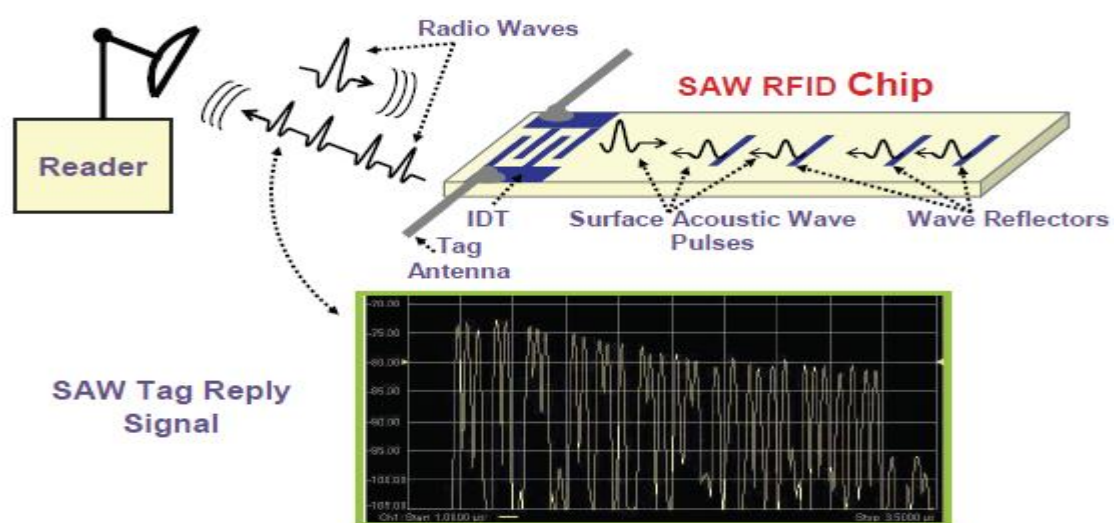

Fig.3. 1 : SAW based RFID system operation. Courtesy: www.rfsaw.com

distances and the reflected signals with different time separations are used for the encoding as shown in Fig. 3.1. The SAW principle is described in the upper portion of Fig. 3.1 where an example of a four pulse encoding scheme is shown. The SAW tag response signal given in the lower portion of Fig. 3.1 shows an example of a 128 bit tag signal. SAW tag operates at 2.45 GHz and permits coding of 256 bits, which is comparable with the EPC data standard or conventional RFID using an IC chip. This high coding capacity is possible because of the slow wave phenomenon in SAW. The SAW tag uses 10 mW of power (as per ETSI regulation) which in turn produces a read range greater than 5 m, depending on the sensitivity of the reader. However, in this case the frequency band is very limited, but it remains compatible with the use of a temporal approach. SAW tags usually uses FMCW radar or model 501 reader as the SAW tag reader [4-5]. The time domain tags have a significant importance while dealing with the practical measurement techniques. In frequency domain approach, the Radar Cross Section (RCS) of the structure has to be determined using specific, and sometimes complex, calibration process in order to extract the tag information contained in the electromagnetic signature (presence/absence of peaks) [2,6-8]. Contrary to this, in temporal encoding, the information detection is simply based on the time position of the reflected pulse [9-10]. This method of detection is less affected by the tag environment [11]. At the same time it is easy to isolate the tag from its external environment by performing a time domain. However, this can be achieved for frequency domain tags also, provided, an additional step of signal processing is necessary to do it. Thus by combing the two preceding observations- the use of ISM bands and the robust communication- it was found in practice that, the reading range of temporal tags is larger than that of the frequency domain tags. Moreover, the easiness in detecting the tag information is also predominant. This explains the communication robustness of time domain RFID tags over frequency domain tags and leads to the design of time domain tags. In the proposed case, the principle used is with the antennas and also with the coding circuit, where the coding circuit is formed by C-sections. In order to get an idea about the amount of delay produced by C-section, a comparison between linear and meandered transmission line has been done in the succeeding section. Microstrip technology is used.

3.2 LINEAR MICROSTRIP TRANSMISSION LINES

Fig.3. 2 shows the general structure of a microstrip transmission line. It consists of a conducting strip (microstrip line) with a width *W* and a thickness *t*, on the top of a dielectric substrate, that has a relative dielectric constant ε_r and a thickness *h,* and the bottom of the substrate is a ground (conducting) plane [12]. The fields in the microstrip extend within two media—air above and dielectric below—so that the structure is inhomogeneous. TEM mode is a good approximation and thus for the frequencies in which we are interested (for ex. UWB), we can consider that the line is not dispersive. Thus as we will see hereafter, in the expression of the delay, there is a relation between the physical size (length) of the line and the delay. Thus, the length plays an important role in the delay. The electric and magnetic waves in a quasi TEM state are represented in Fig.3. 2.
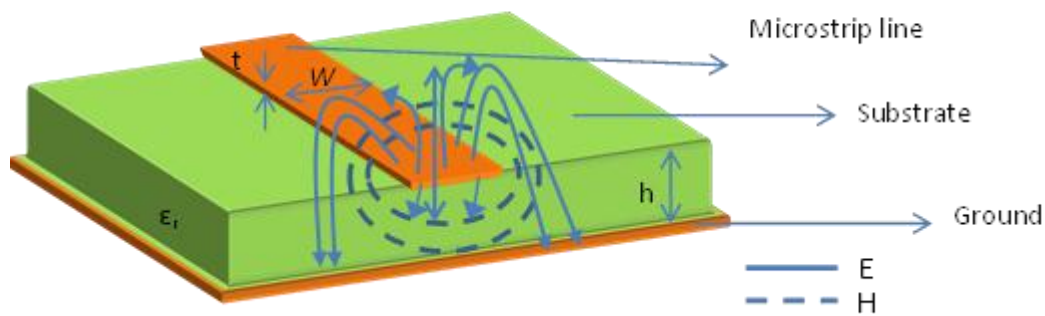
Fig.3. 2 : Structure of a microstrip transmission line.

Transmission characteristics of microstrips are described by two parameters, namely, the effective dielectric constant $\varepsilon_{re,}$ and characteristic impedance Z_c and can be expressed as follows [12].

When W/h≤1:

$$\varepsilon_{re} = \frac{\varepsilon_r + 1}{2} + \frac{\varepsilon_r - 1}{2}\left\{(1 + 12\frac{h}{W})^{-0.5} + 0.04(1 - \frac{W}{h})^2\right\} \qquad (1)$$

$$Z_c = \frac{\eta}{2\pi\sqrt{\varepsilon_{re}}} \ln\left(\frac{8h}{W} + 0.25\frac{W}{h}\right) \tag{2}$$

where $\eta = 120\pi$ ohms is the wave impedance in free space.

When $W/h \geq 1$:

$$\varepsilon_{re} = \frac{\varepsilon_r+1}{2} + \frac{\varepsilon_r-1}{2}\left(1 + 12\frac{h}{W}\right)^{-0.5} \tag{3}$$

$$Z_c = \frac{\eta}{\sqrt{\varepsilon_{re}}}\left\{\frac{W}{h} + 1.393 + 0.677\ln\left(\frac{W}{h} + 1.444\right)\right\}^{-1} \tag{4}$$

Thus, the phase velocity and propagation constant can be expressed as,

$$V_P = \frac{\omega}{\beta} = \frac{c}{\sqrt{\varepsilon re}}, \tag{5}$$

where c is the velocity of light ($c = 3.0 \times 10^8$ m/s) in free space.

The propagation delay can be expressed as a function of length L as: $t = L/v_p$ \hfill (6)

Thus, we see that the propagation delay depends on the geometrical parameters of the line and hence the materials used. In all cases, for modifying the delay, the easiest way is to vary the length of the transmission line.

$$\beta = \frac{2\pi}{\lambda g} \tag{7}$$

Dispersion is a phenomenon in which the phase velocity is a function of frequency or alternatively the group velocity depends on the frequency. There is dispersion in microstrip so that the effective dielectric constant ε_{re} is a function of frequency and can in general be defined as the frequency dependent effective dielectric constant ε_{re} (f). To take into account of the effect of dispersion, the formula for ε_{re} reported in eq. (1) and (3) can be rewritten as explained in the Appendix II,

The delay produced by a linear dispersive transmission line can be obtained as,

Time $t(f) = L/v(f)$ \hfill (8)

where L is the length of the transmission line and V is the velocity of light in free space. Here, contrary to eq.(6), the delay is dependent on the frequency.

From eq. (5), we can write v as $v = 1/\sqrt{\mu \varepsilon_{re}}$ (9)

From eq. (9) it is clear that when the permittivity increases, *v* decreases. It can be found from (6) that a decrease in v(f) increases the time delay. Thus, an increased permittivity can increase the delay. Moreover, it is a common fact that the wave takes more time to propagate in a medium with permittivity ε_r, than in free space. For example, in order to produce 1 ns of delay in free space, a transmission line with 30 cm length is needed using eq. (6)). In order to calculate the delay produced by a linear transmission line, simulation has been done. The substrate was chosen as Rogers R4003 with permittivity of 3.55 and tangent loss of 0.0027. CST microwave Studio 2011 was used as EM solver throughout this thesis. The details of how this simulation tool is used are explained in the Appendix I.

In order to produce 1 ns of delay, a transmission line with length of 19 cm is needed. Fig.3. 3 (a) and (b) shows the corresponding S-parameter and delay produced by a linear transmission line with a length of 19 cm. This group delay is calculated by taking the negative derivative of transmission phase with respect to angular frequency. Thus for a given phase Φ, the group delay will be $\tau = \frac{\partial \Phi}{\partial \omega}$, where Φ is the transmission phase and ω is the angular

(a)   *(b)*
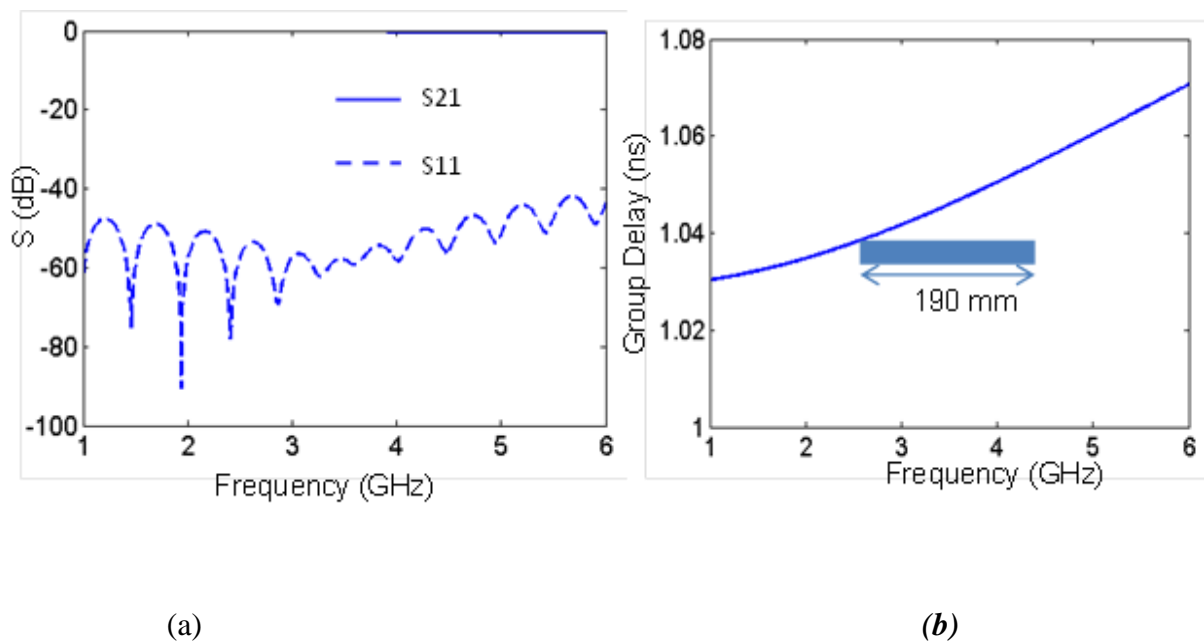
Fig.3. 3 : Simulated S-parameter and delay produced by a linear transmission line. a)S-parameter b) corresponding group delay for 50 Ω line impedance (at 1.8 GHz). Theoretical delay as per eq. (6) is 1.02 ns. L_{Total}=19 cm,w=1.7mm,ε_r= 3.55, tanδ=0.0027, h=0.8 mm.

frequency. We can observe that the behavior is less dispersive. It produces same delay all over the frequency band. Thus, it is clear that we cannot use linear transmission line for producing delay which is independent of the frequency. The only solution to produce a significant amount of delay independent of frequency is to use dispersive lines, which can be realized using C-sections. C-sections make use of the coupling effect to produce a large amount of delay.

3.3   MEANDERED MICROSTRIP TRANSMISSION LINES

A transmission line with length L_{Total} = 19 cm is too large to produce the delay of the order of 1ns and hence cannot be used for coding the information. Hence a technique of miniaturization should be used. Transmission lines are usually meandered in order to provide miniaturization. However these lines cannot be used to produce large amount of delay. There are rules to define the gap between each meander lines. In this case, contrary to what we will see later, the meanders are designed not to get coupling between the arms of the line so as to remain as much as possible on the electrical characteristic of the straight line. The key parameters of a meandered transmission line are the meandered length (M_l), meandered width (M_w) and the bend type used [13]. A meandered transmission line can be considered as a
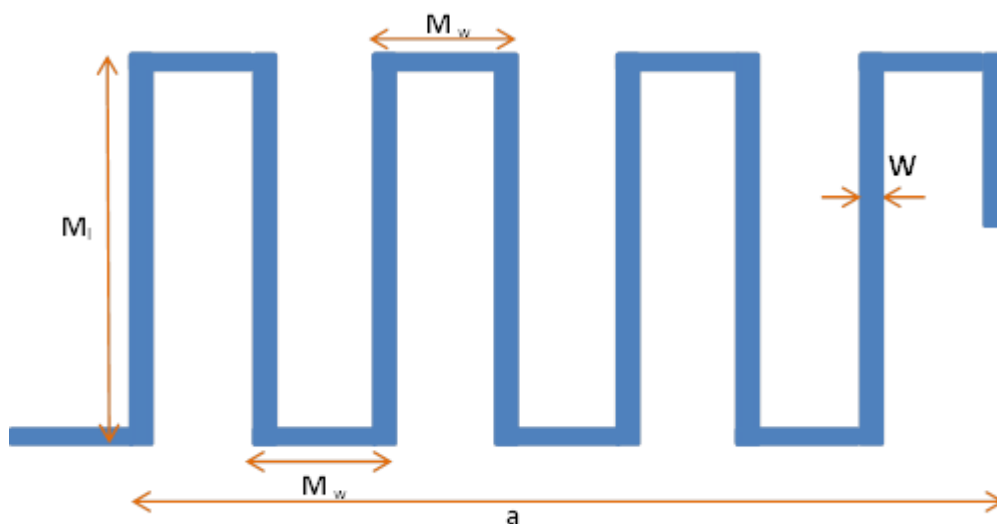

Fig.3. 4 : Structure of a periodic meandered transmission line along with various design parameters.

collection of different transmission line segments connected in series. The length of each transmission line segment is known as the length M_l, while the gap between each segment is known as the meandered width M_w of the transmission line.

According to the rule of thumb in meandered transmission line design, the meandering length M_l should be smaller than the quarter wavelength of the signal wave ($\lambda/4$) and the separation M_w should be more than twice of the transmission line width (w). Fig.3. 4 shows the structure of a meandered transmission line [13].

A simulation has been done with the meandered transmission line as a two port network. The aim was to produce the same amount of delay (1 ns) as in the case of linear transmission line, to have a better comparison. The substrate used was Rogers R4003 with a permittivity of 3.55 and a thickness of 0.8 mm (as in the previous case). The meander length M_l is chosen as 35 mm and the corresponding S-parameter and group delay have been calculated. The total length of the meandered transmission line (L_{Total}) is 20 cm. Fig.3. 5(a) and (b) shows the results obtained. The group delay of the linear transmission line is compared with the meandered transmission line. For a meandered transmission line, the total surface area needed to produce the same amount of group delay as in the case of linear transmission line is 45.2X42 mm^2. For a linear transmission line it was 9.5X 190 mm^2. It is clear that in order to

(a)   (b)
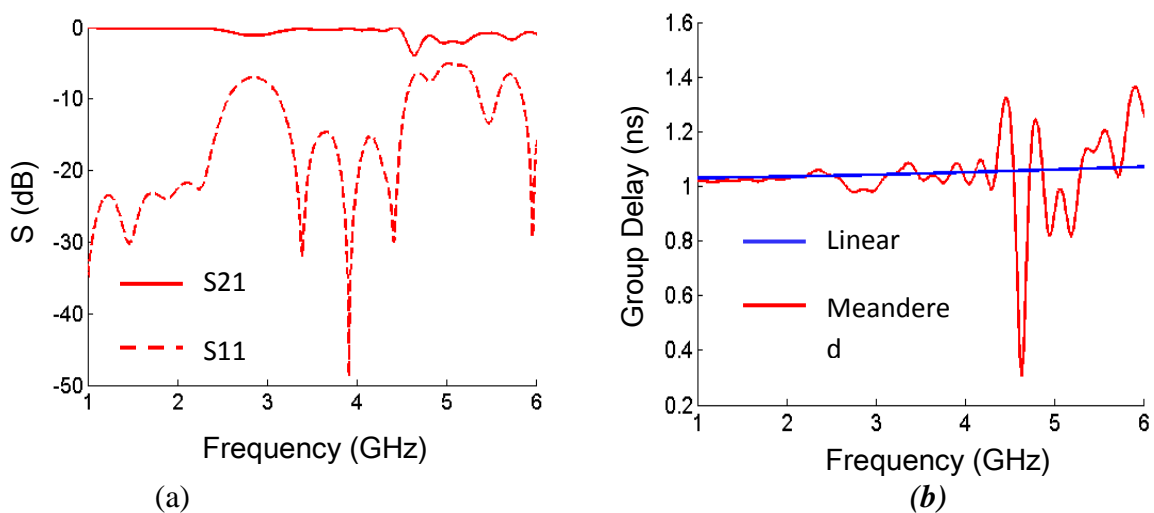
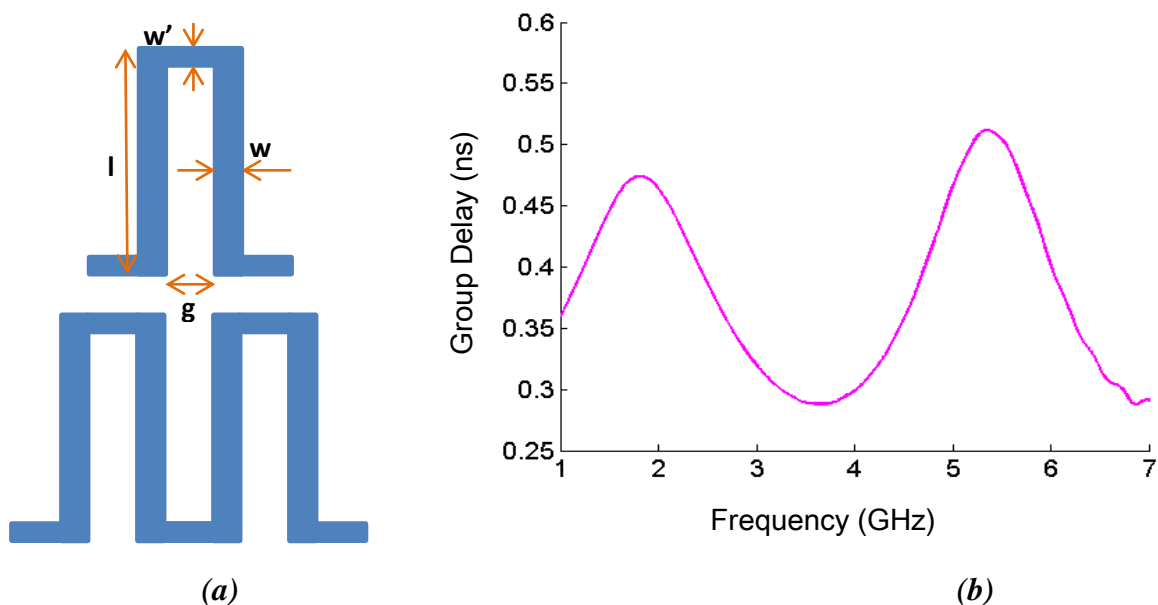Fig.3. 5 : **Simulated *S-parameter and delay produced by a meandered transmission line. a) S-parameter, b) corresponding group delay in comparison with linear transmission line for 50 Ω line impedance (at 1.8 GHz) and four meanders. M_l= 35 mm, M_w= 5 mm, w= 1.7 mm, L_{Total}=20 cm, ε_r=3.55, tanδ=0.0027,h=0.8 mm.***

produce an equal amount of delay the surface area required by a meandered transmission line is less in comparison to a linear transmission line.

Thus, we have observed a small coupling which shows that the line is slightly dispersive. However, it is not enough to produce larger amount of group delays. C-sections can be used for this purpose. However, there is no significant variation in terms of transmission line length was observed. In order to produce a good miniaturization in terms of electrical length and total surface area, coupled lines can be used (C-sections). Moreover, C-sections are dispersive lines which enable them to use different groups to produce different delays at different frequencies.
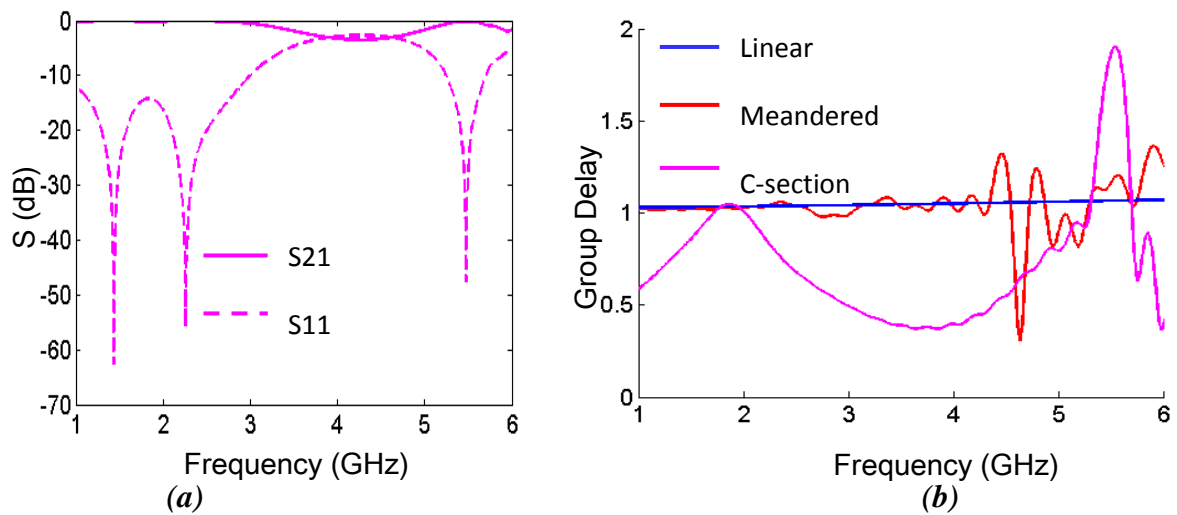
3.4   C-SECTIONS

C-sections can be created by shorting the alternative ends of a coupled transmission line [14-16] as shown in Fig.3. 6(a)**.** Contrary to the meandered transmission line, C-sections make use of the coupling effect between each transmission line sections to produce the delay. A tight

(a)   (b)

Fig.3. 6 : Structure of single and two cascaded C-section, and the periodic delay produced by C-section. a) C-section with its design parameters b) corresponding periodic group delay for 50 Ω line impedance (at 1.8 GHz). Single C-section is simulated here. l= 28 mm, w=w'=1.7mm, g=0.1 mm, ε_r= 3.55, tanδ=0.0027, h=0.8 mm.
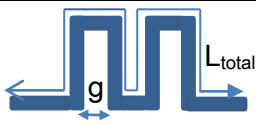
coupling implies a large group delay. The group delay will be always periodic with each period occur at the odd multiple of frequency as shown in Fig.3. 6 (b). Fig.3. 7(a) shows the simulated S-parameters and Fig.3. 7(b) shows the comparison of delay produced by linear and meandered transmission line along with C-sections.


(a)   *(b)*

Fig.3. 7 : Simulated S-parameter and delay produced by two C-sections. a) S-parameter b) comparison of delay produced by linear, meandered transmission lines along with C-section for a 50 Ω impedance line (at 1.8 GHz). Two C-sections are simulated here to produce 1 ns delay. l=28 mm, w=w'=1.7 mm, g=0.1 mm, ε_r= 3.55, tanδ=0.0027, h=0.8 mm.

Table 3. 1 shows the comparison of different parameters of linear transmission line, meandered transmission line and C-section to produce an equivalent amount of delay. The C-section will produce a maximum delay at a single frequency due to its dispersive behavior.

Table 3. 1 : Comparison between the dimensions of linear transmission line, Meandered line and C-sections to produce the same amount of delay.

|		L_{total} (mm)	M_w or g (mm)	Total dimension (mm^2)
Linear transmission line		190	-	9.5X190
Meandered line		200.8	5	45.2X42
C-section		118.3	0.1	12X27
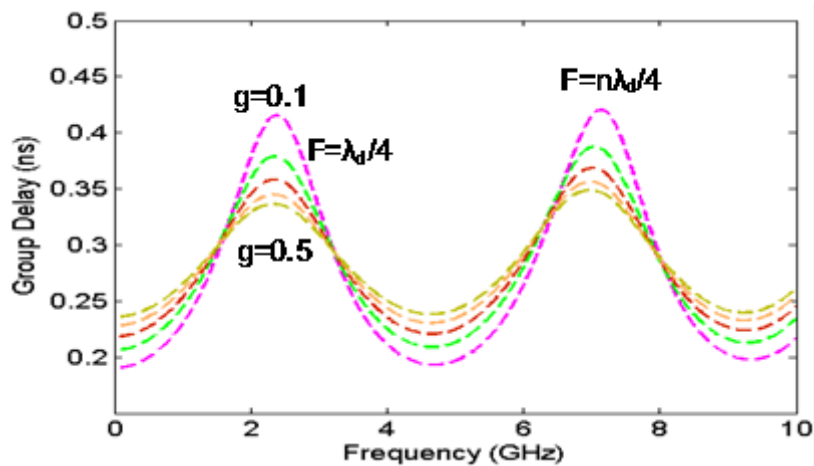
Fig.3. 8 : *Parametric study (simulation) explains the value of group delay a) for different gap 'g' for single C-section. The group delay curve is periodic; b) l=21 mm, w'=w=0.7 mm; ε_r=3.55, tanδ=0.0027, h=0.8 mm.*

A parametric study has been done and it has been found that the group delay increases with decrease in the width and gap in the C-sections. Decreasing the gap will also make the group delay curve narrower. Fig.3. 8 shows the simulated group delay variation for different values of gap 'g' for single C-section. It is evident from the simulation study that the group delay is larger for smaller value of gap g since the coupling between lines increases with a decrease in the gap. As shown in Fig.3. 8, the group delay peaks are periodic in nature with each peak occur almost at $n\lambda_g/4$, where n=1,3,5 etc., of the fundamental frequency. For a given length l, the frequency at which the group delay peaks appear for a single C-section will be,

$$F(l_i) \approx c/(4\, l_i\, (\varepsilon_{\text{reff}})^{1/2}), \qquad (10)$$

where $c=3\text{x}10^8$ m/s and $\varepsilon_{\text{reff}}$ is the effective permittivity of the microstrip line which can be calculated using the eq. (1). This expression is used in the preliminary design. The lengths are further optimized by simulation. However, in order to have an idea of the system design, this expression is included here. In fact, the behavior here is similar to that of a microstrip coupler where the maximum coupling occurs under the same conditions.
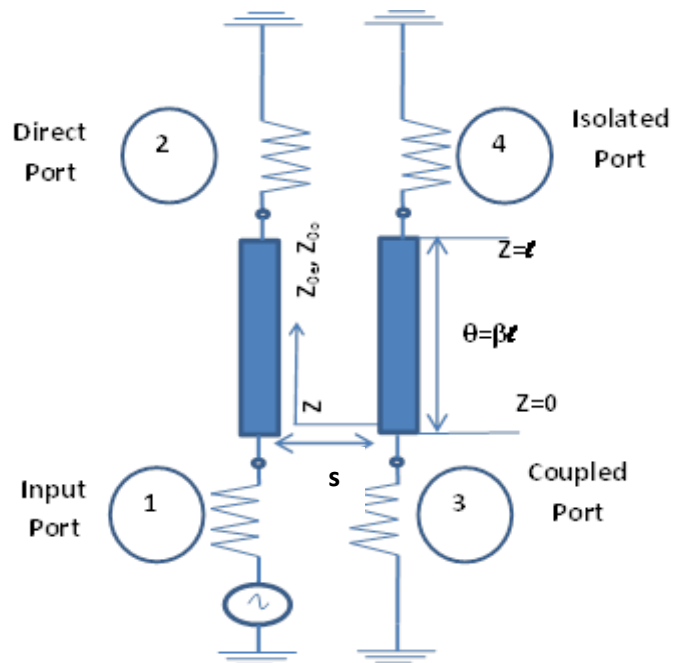
Fig.3. 9 : A typical backward wave directional coupler.

The coupling coefficient k between each line has been simulated using Ansoft Planar EM. For this purpose the C-sections have been considered as a coupled line as shown in Fig.3. 9. The coupler shown in Fig.3. 9 is also known as a backward wave directional coupler.

Two important factors that determine a directional coupler are coupling and directivity.

$$\text{Coupling (dB)} = 10 log \frac{P_1}{P_3} \qquad (11)$$

$$\text{Directivity (dB)} = 10 log \frac{P_3}{P_4} \qquad (12)$$

where P_1 is the power input at port 1 and P_3 and P_4 are power outputs at port 3 and port 4, respectively. There will not be any power at port 4 in an ideal case. However, in practice, a small amount of power is always coupled to this port. If the coupling and directivity are known, the isolation of the coupling can be determined using the following equation [17].

$$\text{Isolation (dB)} = 10 log \frac{P_1}{P_4} \text{ or Isolation (dB) = Coupling (dB) + Directivity (dB)} \qquad (13)$$

The scattering parameters of the network can be defined as

$$S = \begin{bmatrix} 0 & \frac{\sqrt{1-k^2}}{\sqrt{1-k^2}\cos\theta + j\sin\theta} & \frac{jk\sin\theta}{\sqrt{1-k^2}\cos\theta + j\sin\theta} & 0 \\ \frac{\sqrt{1-k^2}}{\sqrt{1-k^2}\cos\theta + j\sin\theta} & 0 & 0 & \frac{jk\sin\theta}{\sqrt{1-k^2}\cos\theta + j\sin\theta} \\ \frac{jk\sin\theta}{\sqrt{1-k^2}\cos\theta + j\sin\theta} & 0 & 0 & \frac{\sqrt{1-k^2}}{\sqrt{1-k^2}\cos\theta + j\sin\theta} \\ 0 & \frac{jk\sin\theta}{\sqrt{1-k^2}\cos\theta + j\sin\theta} & \frac{\sqrt{1-k^2}}{\sqrt{1-k^2}\cos\theta + j\sin\theta} & 0 \end{bmatrix}$$

where $\theta = \beta l$ denotes the electrical length of the coupler and k is the coupling co-efficient which is given by

$k = \frac{Z_{0e} - Z_{0o}}{Z_{0e} + Z_{0o}}.$ $\qquad$ (14) , where Z_{0e} is the even mode impedance and Z_{0o} is the odd mode impedance and is defined in the Appendix II.

The maximum amount of coupling occurs when $\theta = \beta l = \pi/2$ radians or $l = \pi/2\beta = \lambda_g/4$.
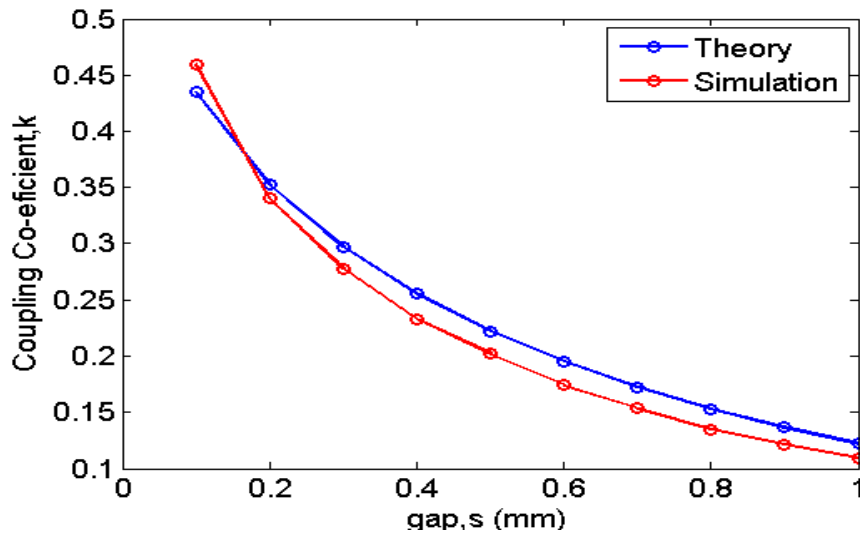
Fig.3. 10 : Simulated and theoretically calculated coupling co-efficient k, at f=λ$_g$/4, as a function of gap s. l=21 mm, w=w'=0.7 mm ; ε$_r$=3.55, tanδ=0.0027, h=0.8 mm. "Theory" represents k calculated using eq.(14).

The coupling coefficient of the coupler is calculated using the eq. (14) as shown in Fig.3. 10, where even and odd mode impedances were obtained from simulation. Further, a typical coupler has been designed using Ansoft Designer and the coupling coefficient k has


(a)

(b)
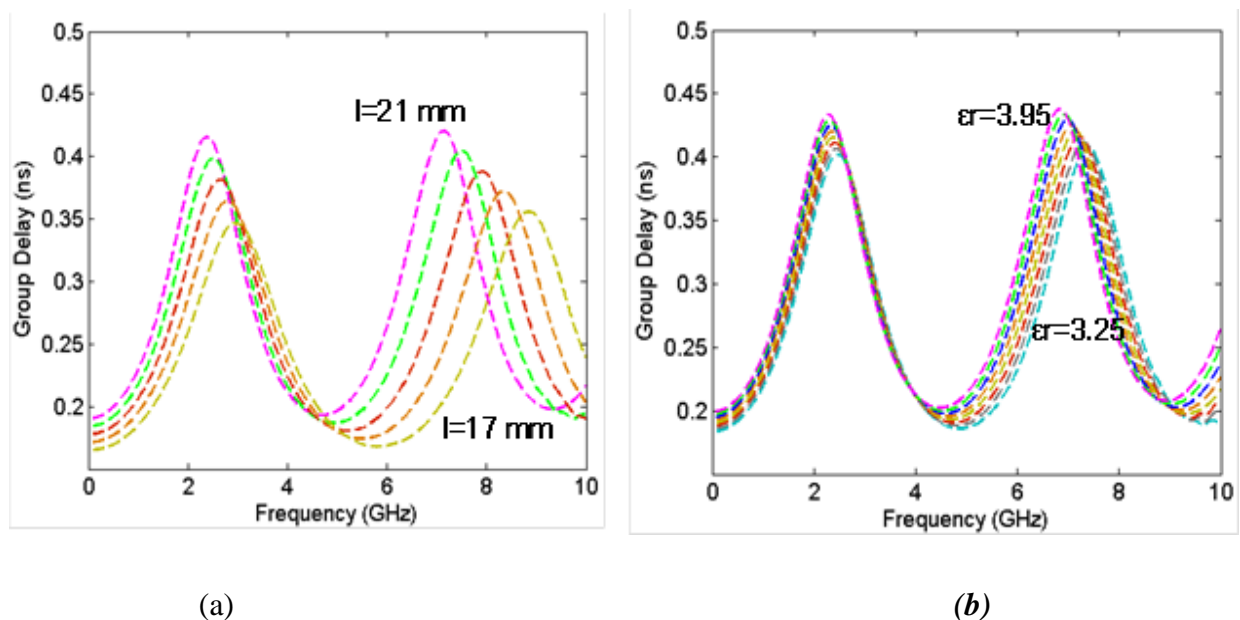
Fig.3. 11 : *Parametric study explains the value of group delay for different, a) length l for a step size of 1mm and b) permittivity ε$_r$ for a step size of 0.1 Two C-sections are simulated. g=0.1 mm, w'=w=0.7 mm; ε$_r$=3.55, tanδ=0.0027, h=0.8 mm.*

been determined from the S-parameters (precisely S12) by substituting θ= π/2 in the S-matrix. Fig.3. 10 shows the comparison between calculated and simulated k, as a function of gap s. It is clear from the figure that the coupling coefficient increases for a small gap which in turn enhances the group delay.

Group delay increases with an increase in length and permittivity with a shift in frequency towards the lower region and will makes more frequency selective peaks. Fig.3. 11(a) and (b) shows the variation of group delay as a function of length and permittivity respectively.

The width of the transmission line w and the gap width w' also have their own influence in group delay. The parametric study reveals that a decrease in width will increase the group delay. Fig.3. 12(a) shows the variation of group delay as a function of width w. The

(a)   *(b)*
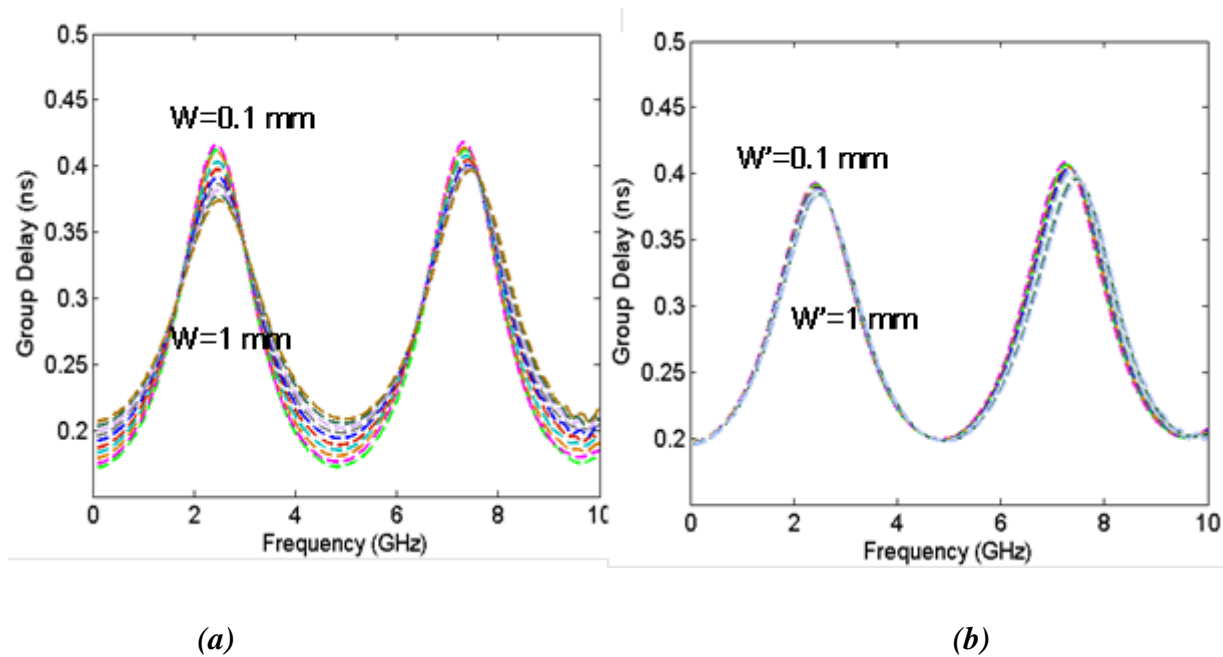
Fig.3. 12 : Parametric study explains the value of group delay for different a) width w and b) gap width w'. The step size is 0.1 mm. Two C-sections are simulated. g=0.1 mm, l=21 mm; ε_r=3.55, tanδ=0.0027, h=0.8 mm.

gap width w' has less influence on group delay as shown in Fig.3. 12(b). However the gap width can be chosen as the same as the width w in order to reduce the unwanted reflections due to mismatching, while using the tag in the backscattering measurement. In short, using C-sections it is possible to have a significant amount of group delay (3 ns using 10 C-sections).

We have also seen in Table 3. 1 that, contrary to linear or meandered transmission line, C-sections miniaturizes the circuit size. It can be as compact as credit card and hence can be used in the chipless RFID applications to code the information. Moreover, the dispersive characteristics make possible the coding of the information at different frequencies.

3.5   CASCADED SINGLE GROUP OF C-SECTIONS

3.5.1   PROTOTYPE DESIGN

Thus considering the different aspects of parametric study, the design parameters of the C-section have been determined and a prototype of the tag is designed as shown in Fig.3. 13. Prototype is a term used to define the tag without antennas, i.e. tag when acts as a two port network as shown in Fig.3. 13.
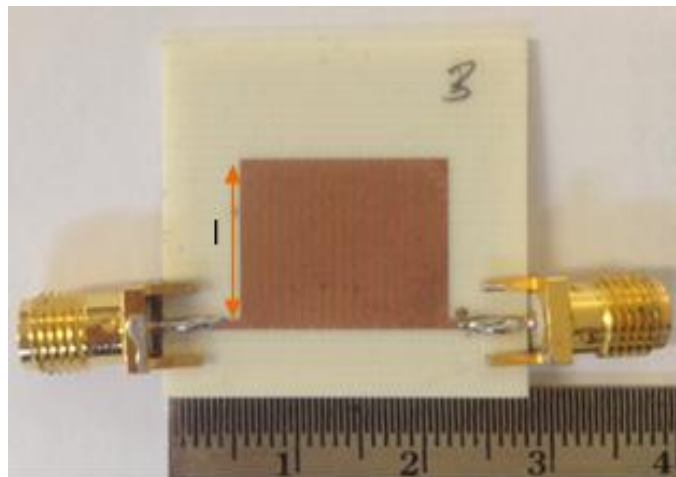
Fig.3. 13 : Prototype of the tag with one group of 10 C-section; g=0.1 mm, w' = w = 0.7 mm, l_3=13.8 mm; ε_r=3.55, tanδ=0.0027, h=0.8 mm.

Rogers 4003 is used as the substrate with a permittivity of 3.55 and tangent loss of 0.0027. The height of the substrate is 0.8 mm. Rogers were chosen instead of the low cost FR-4 substrate because of its low tangent loss which can enhance the backscattering characteristics of the tag. It was found in [14] that high tangent loss significantly reduces the amplitude of the tag modes which will explain in the succeeding section.

The structure of a single C-section and two C-sections cascaded together can be seen in Fig.3. 6 (a). In the same manner, ten consecutive C-sections with equal lengths have been

cascaded here as shown in Fig.3. 13. This was to increase the group delay. It was found in simulation that decreasing the width increases the group delay, so that the width has been optimized to 0.7 mm which corresponds to the characteristic impedance of 82 ‘Ω. Additionally, it is not necessary to design the width for 50 ‘Ω; instead the width can be designed to match with the input impedance of the antenna. The gap *g* has been assigned a value of 0.1 mm to provide tight coupling between the C-sections. As already explained decreasing the gap increases the group delay. However, due to fabrication accuracy the gap is limited to 0.1 mm and the number of C-sections was increased in order to have a significant delay. Also the gap's width *w'* is made equal to 0.7 mm to avoid any unwanted reflections due to impedance mismatch while integrating to the tag antennas. These design parameters are kept as constant and only the length *l* of the C-sections has been changed for designing various tag configurations.

In order to have a preliminary study, the prototype of the C-section is considered first. Here the group delay produced is simply due to the particular length of the C-section. The principle of encoding of such a prototype will be explained in the succeeding section. Further, two cross-polarized antennas have been added to the two ports of the prototype in order to convert into a chipless tag. In this case, the conception of antennas, problems of adaptation, and finally the group delay introduced by tag antennas has been treated.

3.5.2   PRINCIPLE OF PROTOTYPE ENCODING

Fig.3. 14 shows an example of principle of encoding of C-section prototype. In this case the simulation results represented in Fig.3. 11(a) has been considered and just the lengths are varied between l_1-l_k. Different combinations of prototypes can be designed by decreasing the length by a factor of Δl_i, where i=1,2,…k, from the reference length. Let l_1 be considered as the reference length (maximum length considered) corresponding to the frequency f (l_1). It will produce a periodic group delay Gd (l_1) which will be maximum at f(l_1) as shown in Fig. Fig.3. 14(b).

In time domain, it can be seen that the corresponding frequency component is shifted by the same amount Gd (l_1), from the reference as shown in Fig.3. 14(c). This time domain response is obtained by applying a numerical filter at f(l_1) on the signal that passes through the C-sections and obtained at the other end. The reference signal in this case is the input

signal filtered at f (l_1). The frequency f (l_1) is considered as the operating frequency of the C-sections. The amount of group delay Gd (l_1-Δl_i) at f (l_1) is calculated each time. The delay produced by each length represents a binary code. In this case k is chosen as 8 and thus in total 8 different lengths are considered which in turn corresponds to 3-bit code.

(a)   (b)   (c)
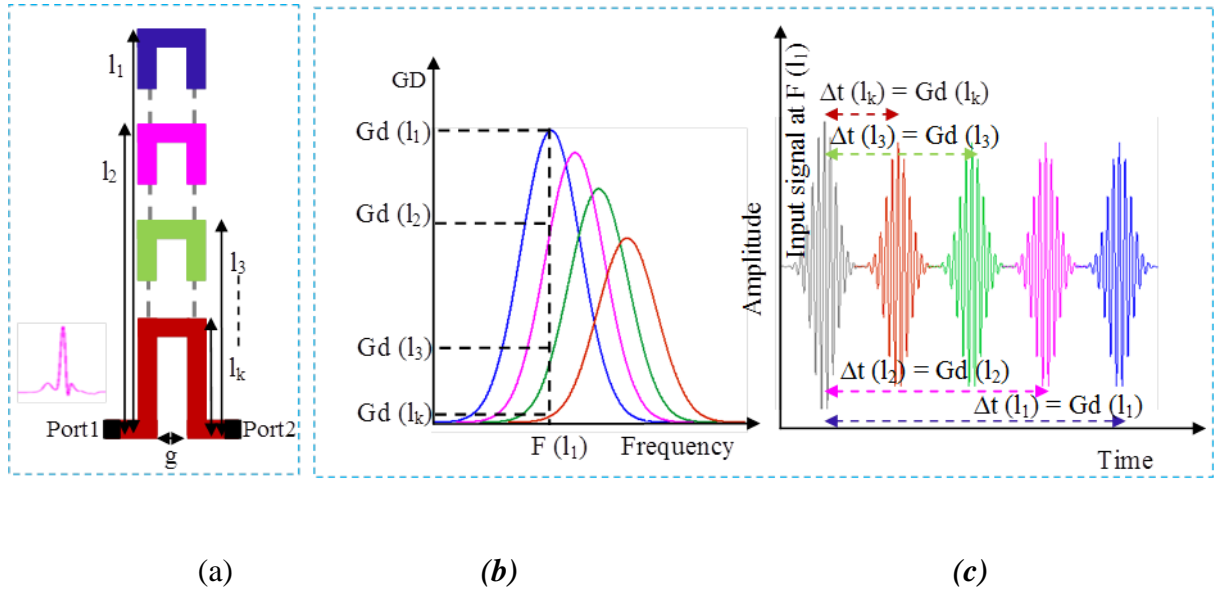
Fig.3. 14: Principle of encoding for cascaded commensurate C-sections. a) Prototype (for simplicity, only one C-sections is represented). b) Group delay Vs frequency response. c) Corresponding time domain response for the spectral component at f(l_1).

3.5.3   SIMUATION STUDY

Simulation has been done for the given prototype as a two port network (see Fig.3. 13) as explained in the Appendix. Group delay has been calculated for the given prototype as a function of frequency. The group delay can be calculated by taking the negative derivative of transmission phase with respect to angular frequency. Thus for a given phase Φ, the group delay will be $\tau = \frac{\partial \Phi}{\partial \omega}$, where Φ is the transmission phase and ω is the angular frequency.

Fig.3. 15 shows the group delay calculated for different values of length l (corresponds to Fig.3. 14 (b)). As explained in the operating principle, from Fig.3. 15 it is clear that for each length, a delay is possible. Hence it allows a single frequency with different delay variations which in turn permits to encode different bits.

Time domain simulations were also done for the two port network (see Fig.3. 13), as per the operating principle (corresponds to Fig.3. 14(c)). A Gaussian signal modulated at a carrier
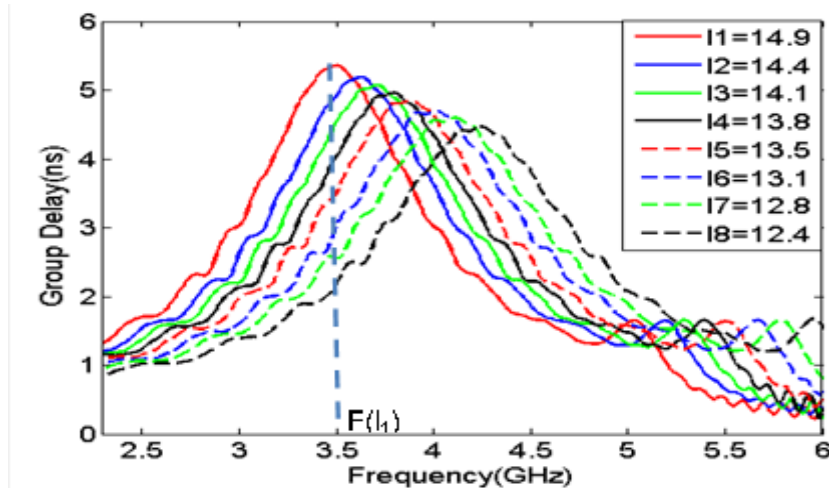
Fig.3. 15 : Simulated group delay for different values of lengths of 10 C-sections given in the previous figure. All units are in mm; g=0.1, w' = w = 0.7, l₃=13.8; εᵣ=3.55, tanδ=0.0027, h=0.8.
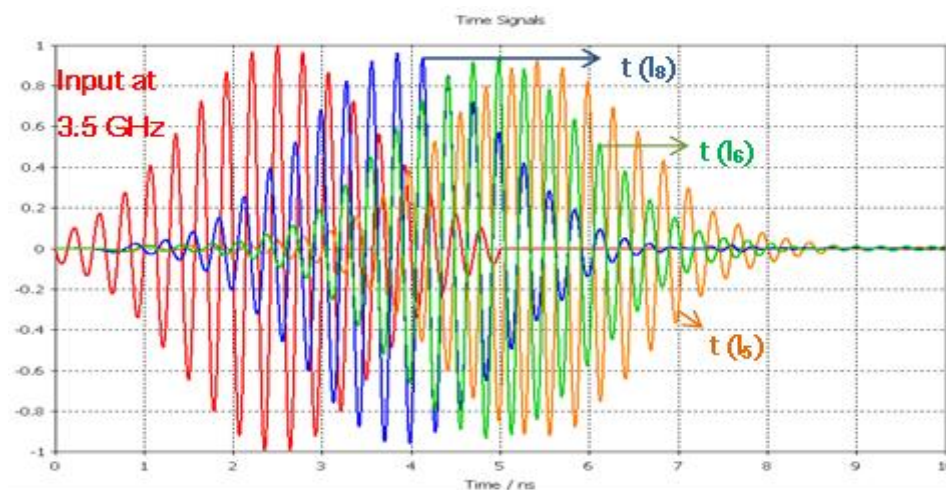
Fig.3. 16 : Simulated time delay for different values of lengths of C-section with a Gaussian modulated signal at f(l₁)=3.5GHz as the input signal. All units are in mm; l₅=13.1, l₆=12.8, l₈=11 ,g=0.1, w' = w = 0.7, l₃=13.8; εᵣ=3.55, tanδ=0.0027, h=0.8.

frequency of f(l₁) is used as the input signal i(t).

$$i(t) = e^{\left(\frac{-t^2}{2tv}\right)}.\cos(2\pi F_{(l_1)}t) \qquad (15)$$

, where t_v is the time domain parameter which consider the bandwidth of the signal (*BW*=0.15). The delayed output signal at the output port is used to calculate the time delay as shown in Fig.3. 16. The time difference between the input and output peaks has been calculated.

Table 3. 2: Comparison between simulation delays (CST) produced in frequency domain and time domain (extracted from Fig.3. 15 and Fig.3. 16).

| l_n(C) ;n=1-8 (mm)	GD(C-section) in frequency domain (Fig. 3.15)(ns	GD(C-section) in time domain (Fig. 3.16)(ns)
14.9	5.32	5.3
14.1	4.5	4.5
13.8	4	4
13.5	3.49	3.48
13.1	3	3.01
12.8	2.55	2.56
12.4	2.19	2.19
11	1.24	1.23

It is found that this time shift is exactly equal to the group delay that we have calculated in the group delay-frequency curve (Fig.3. 15). Here the difference is that the input signal used in CST is the signal generated using eq.(20). Fig.3. 15 is generated using the excitation provided

by CST which corresponds to a Gaussian signal that covers the frequency band of interest. Table 3.2 shows the comparison of delays produced in frequency domain and time domain.

3.5.4   MEASUREMENT

In order to prove the encoding of 3 bits, eight tag configurations have been realized by varying the length l_1 of the C-section. The tag prototype i.e. tags without antennas was measured separately (see Fig.3. 13). The two ports of the prototype have been connected to the Vector Network Analyzer (VNA HP 8570D). Fig.3. 17 shows the simulated and measured group delay response with respect to frequency for three different prototypes. The corresponding group delay at f (l_1) =3.5 GHz is marked in the figure.

For time domain experimental validation, an impulse of 80 ps width has been generated using Picosecond Pulse Labs-Model 3500 and used as the input to the structure. The delayed spectrum for the reference prototype has been measured by using the Agilent Digital Oscilloscope DSO91204A. Numerical filter in MATLAB has been applied in order to extract the spectral component at f (l_1) = 3.5 GHz. For this purpose, the MATLAB function
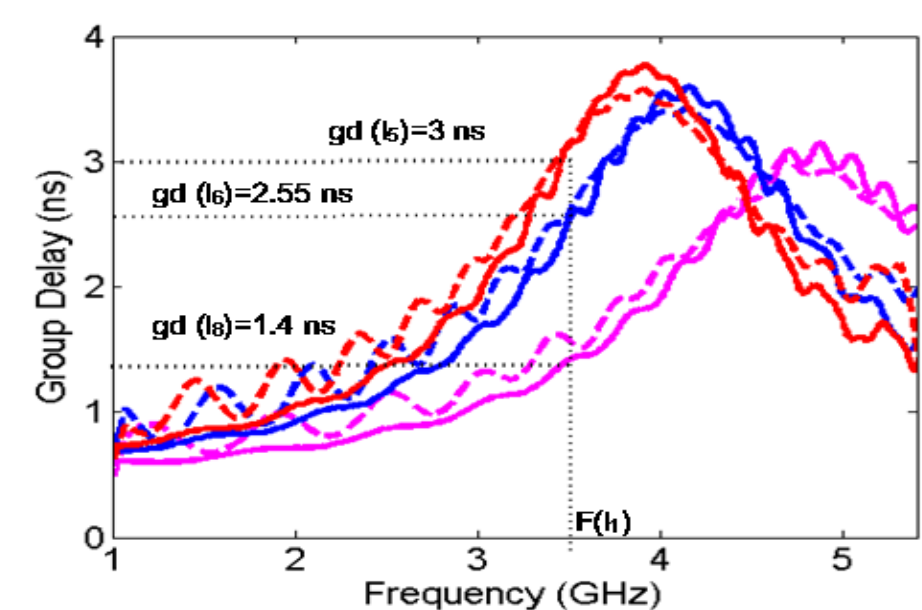
Fig.3. 17 : Simulated and measured (measurement using VNA)group delay for single group of 10 C-section as a 2-port network (see Fig.3. 13); l_5=13.1 mm, l_6=12.8 mm, l_8=11 mm, g=0.1 mm, w'=w=0.7 mm; ε_r=3.55, tanδ=0.0027, h=0.8 mm.

Butterworth filter with third order and lower cutoff frequency as 3.4 GHz and upper cutoff

frequency as 3.6 GHz is used. Finally signal envelope has been taken using the 'Hilbert' MATLAB function to determine the time difference between the input signal and delayed output signal at f (l_1). This process will be explained in the succeeding section of information separation part. Fig.3. 18 shows the obtained time domain response. Six other combinations of the prototype were also measured to verify the characteristics.
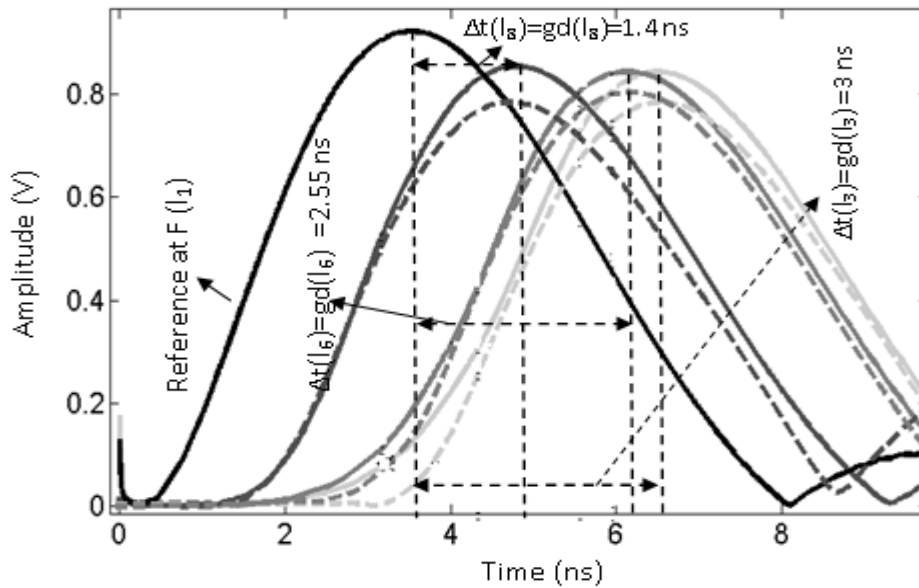
Fig.3. 18 : Simulated (solid line) and Measured (dashed line) time delay for single group of 10 C-section as a 2-port network; The reference signals are superimposed. l_5 =13.1 mm, l_6=12.8 mm, l_8=11 mm, g=0.1 mm, w'=w=0.7 mm; ε_r=3.55, tanδ=0.0027, h=0.8 mm.

Here, the same excitation signal used for the measurement (signal generated by the pulse generator) is used as the input for the simulation. This is why reference signals for both simulation and measurement are superimposed. Simulation was also done using a UWB compatible pulse and the same results were obtained.

3.6 TRANSFORMATION OF PROTOTYPE INTO A CHIPLESS TAG

The prototype can be transformed into a chipless tag by adding receiving and transmitting antennas at the two ports of the prototype as shown in Fig.3. 19. This is just a schematic representation. The structure of the tag will be explained in the succeeding parts.

In this work, a monopole disc UWB antenna has been used as the tag antenna since it can operate in the desired frequencies [6]. Moreover, it has an omnidirectional radiation pattern which allows exciting even from the back side of the tag which is not the case of a simple patch antenna. As we already explained in the introduction, while considering the regulation imposed by FCC and ETSI, there are mainly three possibilities: 1) either works on the narrow bands (ISM bands); in this case we can take the advantage of multi-layer C-section which will be explained in the chapter 5. In this case, a dual band antenna can be used (2.45 and 5.8 GHz). Or 2) works on UWB band where a broadband antenna can be used as the tag antenna. In this work, even though the operating frequencies of the tags are limited to one or more narrow bands, it was preferred to use broadband antenna in order to illustrate the frequency versatile characteristics of these tags.

The tag antennas are cross polarized in order to reduce the interference between the
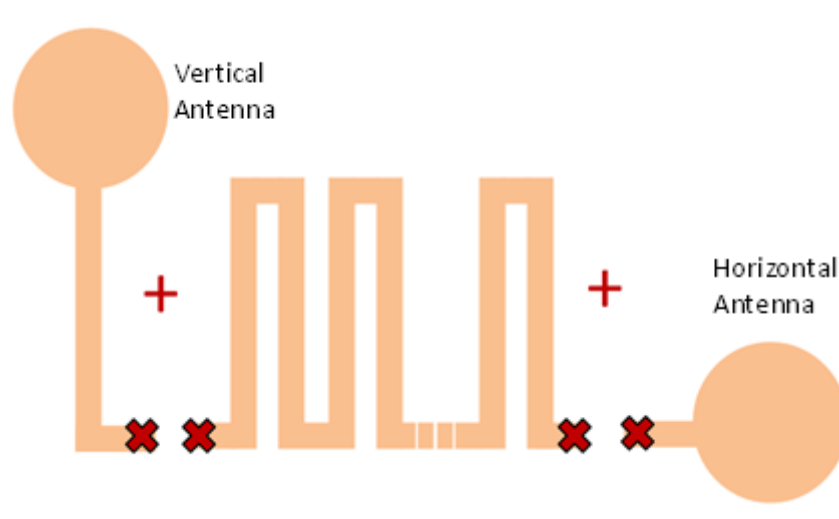

Fig.3. 19 : Process of transformation of tag prototype into a chipless tag by adding UWB antennas at the two port of the tag prototype.

interrogation signal and the backscattered signal which contains the tag information. Indeed,

most of the objects will reflect back the signals in the same direction of the signal emitted. In this case, while labeling the tags, the reflections from any of the objects at a particular distance and hence a particular time may interfere with the tag information. A cross-polarization can avoid these problems. This is the reason why cross polarized antennas are used here. Indeed, a single antenna can also be envisaged. A circularly polarized antenna with a matched load at the end of the C-section will cause the signal to travel through the C-section two times. The principle advantage in such a case is the size reductions. Even though it improves the delay, the amplitude of the back scattered response of the C-section (tag mode) will be very low to detect. This is the reason why two cross polarized antennas have been used here in a more practical point of view [6].

3.7   ULTRA WIDEBAND ANTENNA

In February 14, 2002, the Federal Communications Commission (FCC) of the United States adopted the first report and order that permitted the commercial operation of ultra wideband (UWB) technology [18]. Since then, UWB technology has been regarded as one of the most promising wireless technologies that promises to revolutionize high data rate transmission and enables the personal area networking industry leading to new innovations and greater quality of services to the end users. Ultra-wideband (UWB) communication systems have the promise of very high bandwidth, reduced fading from multipath, and low power requirements [6, 19]. In recent years, the circular disc monopole antenna has attracted considerable research interest due to its simple structure and UWB characteristics with nearly omni-directional radiation patterns [20-21].The parameters of the antenna have been optimized to satisfy the matching conditions and the operating frequency with the C-sections in particular. The width is kept as 0.7 mm to provide impedance matching with the C-section. Fig.3. 20 (a) & (b) respectively show the structure of the UWB antenna along with its response. The group delays of the tag antennas have been simulated separately.

(a)   *(b)*
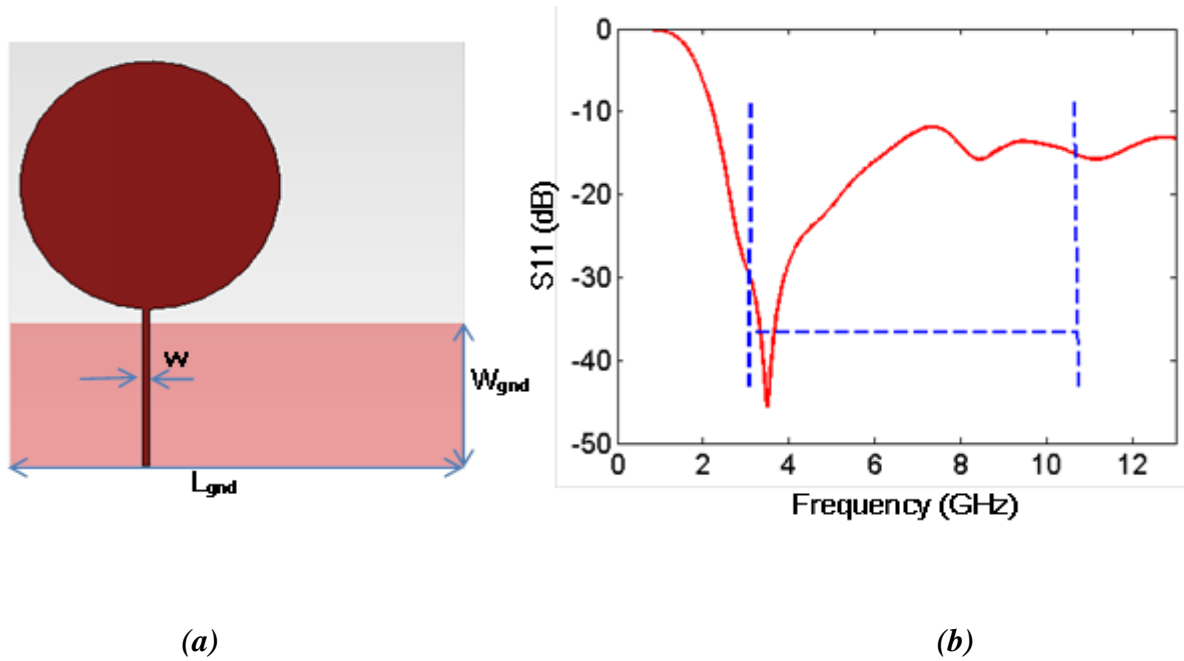
Fig.3. 20 : *Structure of the UWB antenna and the simulated S11. a) Antenna layout, b) simulated S parameter. The UWB band is marked in between the dotted blue lines w=0.7 mm, L_{gnd}=45.3 mm, W_{gnd}=14.97 mm; ε_r=3.55, tanδ=0.0027, h=0.8 mm.*

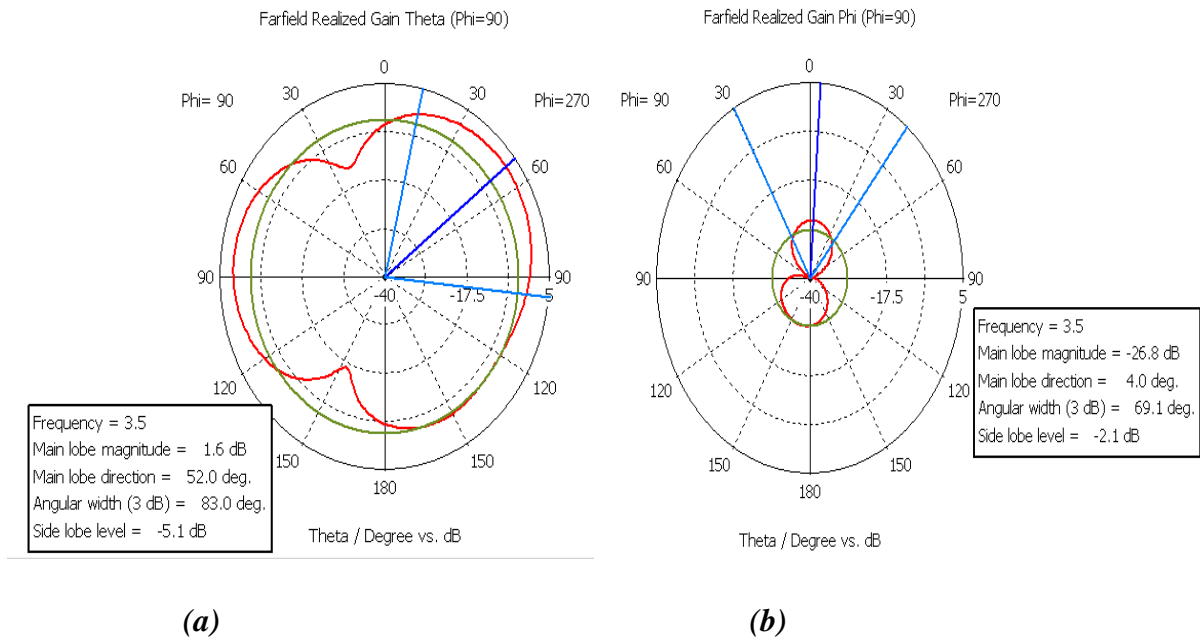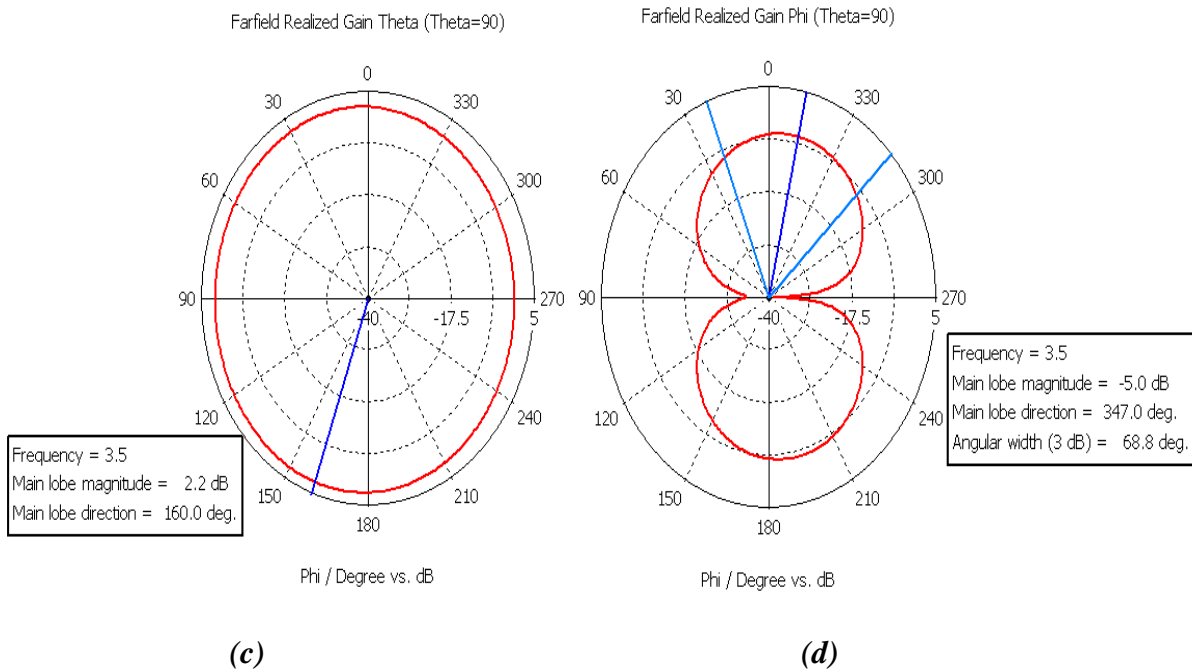*(a)*   *(b)*

Fig.3.21(a) & (b) represent the co and cross polarized simulated radiation pattern of the antenna presented in Fig.3. 20, in the E-plane at 3.5 GHz. Corresponding pattern in the H-pane can be seen in Fig. 3.21 (c) and (d)

(c)   *(d)*

Fig.3. 21 : Simulated radiation pattern of the disc monopole antennas in the E-plane and in H-plane. a) Co-polarized form in E-plane, b) cross polarized pattern in E-plane, c) Co-polarized pattern in H-plane, d) cross polarized form in H-plane.

The group delays of the antennas have also been simulated. To do so, the antennas have been excited using waveguide port which is kept at the feed-line and far-field probes (probes in CST which can be positioned outside the computation domain to record the electromagnetic far field) are placed at a distance greater than the far-field distance, R [22] as shown in Fig.3. 22 (a). Group delay of the transmission phase has been calculated by considering the phase of the signal emitted by the antenna, (see the port represented in Fig.3. 22 (a)) and collected at the far-field probe. From the values obtained, the delay between the antenna and the probe, i.e. R / c has been subtracted. This was to obtain the value of group delay produced by the two antennas (vertical and horizontal antennas, see Fig.3. 19). Fig.3. 22(b) shows the simulated group delays of the horizontal and vertical UWB antennas.

(a)   *(b)*
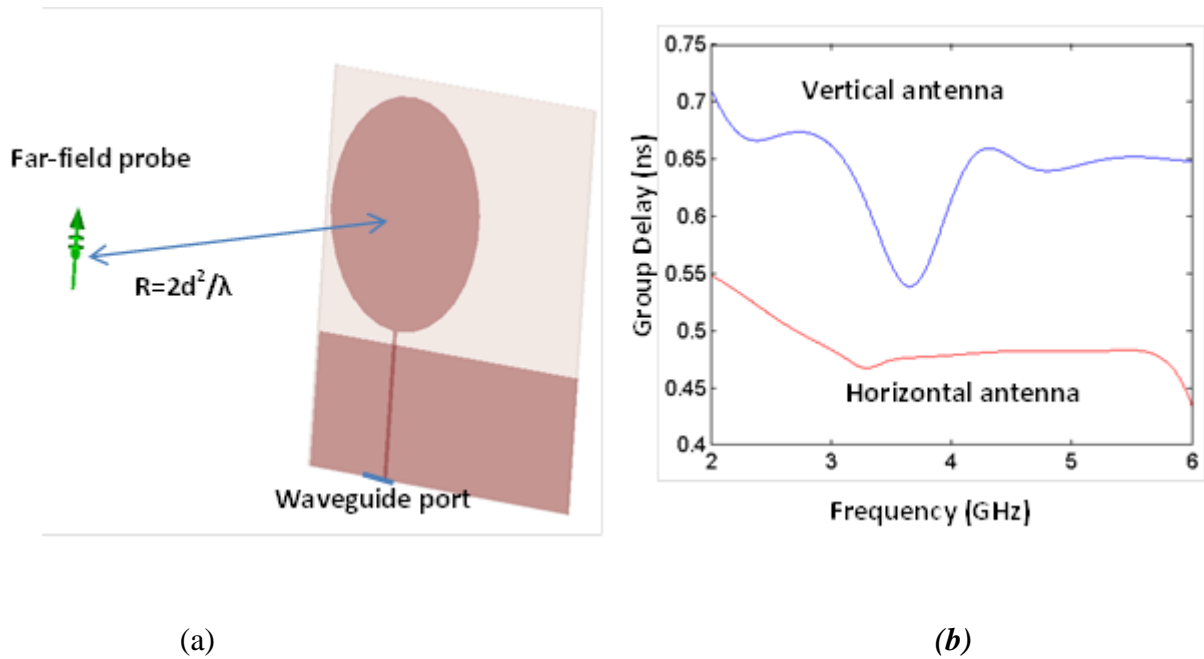
Fig.3. 22 : Simulated model of antenna in order to calculate the group delay. a) Antenna model along with the far-field probe. b) Simulated group delays. w=0.7 mm; ε_r=3.55, tanδ=0.0027, h=0.8 mm.

Here what we are measuring is the time difference between the reference signal and the delayed signal due to C-sections. The reference signal here is the signal reflected directly from the tag and in literature we will call it as a structural mode. The two backscattering modes of the antenna can be seen in the next part.

In the literature, different formulations can be noticed for a field scattered by an antenna connected to a load [23-24]. This field can be expressed as the sum of two modes:

- Structural mode: It occurs at the physical surface of the antenna due to the current produced on the antenna while an electromagnetic wave is incident on it.

- Antenna mode: it is due to the presence of the load. A part of the signal captured by the antenna is guided to the load and reflected on it and re-radiated by the antenna.

Here the two tag antennas are terminated with C-sections and hence the corresponding antenna mode, also called as tag mode, will be the signal guided through the C-section and re-

emitted by the second tag antenna. Now, we are interested in the group delay produced by the tag (can be de-composed into the delay produced by each antenna and the C-section), which can be calculated by the time difference between structural mode and tag mode.

While integrating the antennas to the C-sections, it was found that the antennas modify the total group delay of the tag. In this case, we were able to determine that the total group delay is the sum of group delays produced by the C-sections and the two tag antennas. In all cases it is not a problem. In the measurement, even though the delay produced by the antenna is not known (it will be always constant), it will not affect the coding since coding depends purely on the length of the C-section. We have determined the delays produced by antennas just to make sure that the signals reflected by each tag is temporarily well shifted as a function of the length of C-section. From Fig.3. 22 (b), the value of group delay at 3.5 GHz can be calculated. For vertically polarized antenna the delay (Delay $_{VA3.5GHz}$) was found to be 0.57 ns and for horizontally polarized antenna the delay (Delay $_{HA3.5GHz}$) was found to be 0.46 ns.

3.8   CHIPLSS TAG CONSISTS OF SINGLE GROUP OF C-SECTIONS: SIMULATION STUDY

As already explained, the chipless tag consists of two cross polarized UWB tag antennas and the C-sections. A time domain simulation has been done using the plane wave as an excitation source. An impulse signal can be used as the excitation signal (same as the practical case). However, in this study a Gaussian signal modulated at carrier frequency of $f(l_1)$ is used as the excitation signal as explained earlier, which permits the visualization of both structural mode and tag modes and hence the delay, without filtering. Throughout this thesis, the backscattered signal is the signal which guided through the C-section and re-transmitted by the tag transmitting antenna. Two far-field probes with a polarization same as that of the tag antennas have been placed at a far-filed distance R, where $R \geq 2d^2/\lambda$; d is the largest possible dimension of the antenna. Fig.3. 23 (a) shows the structure of the chipless tag and Fig.3. 23 (b) shows the simulation model.

(a)   *(b)*
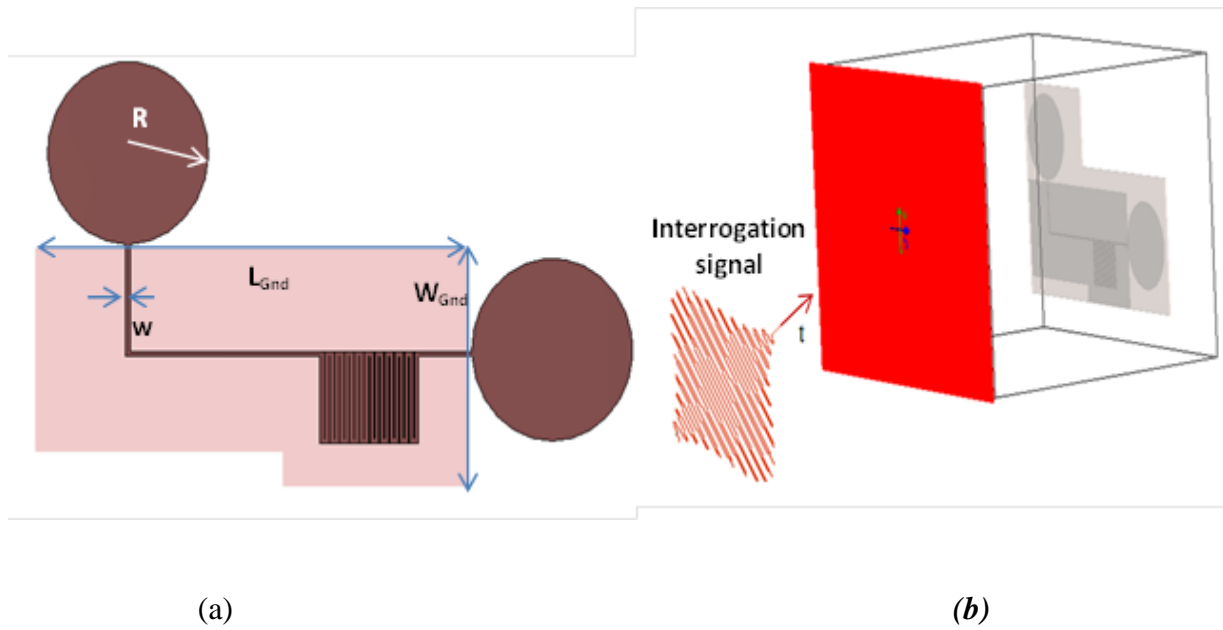
Fig.3. 23 : Structure of the chipless tag with simulation model. a) Tag layout with different design parameters; R=13 mm, w=0.7 mm, L_{gnd}=70 mm, W_{gnd}=34 mm. b) Simulation model with a plane wave as an excitation signal.
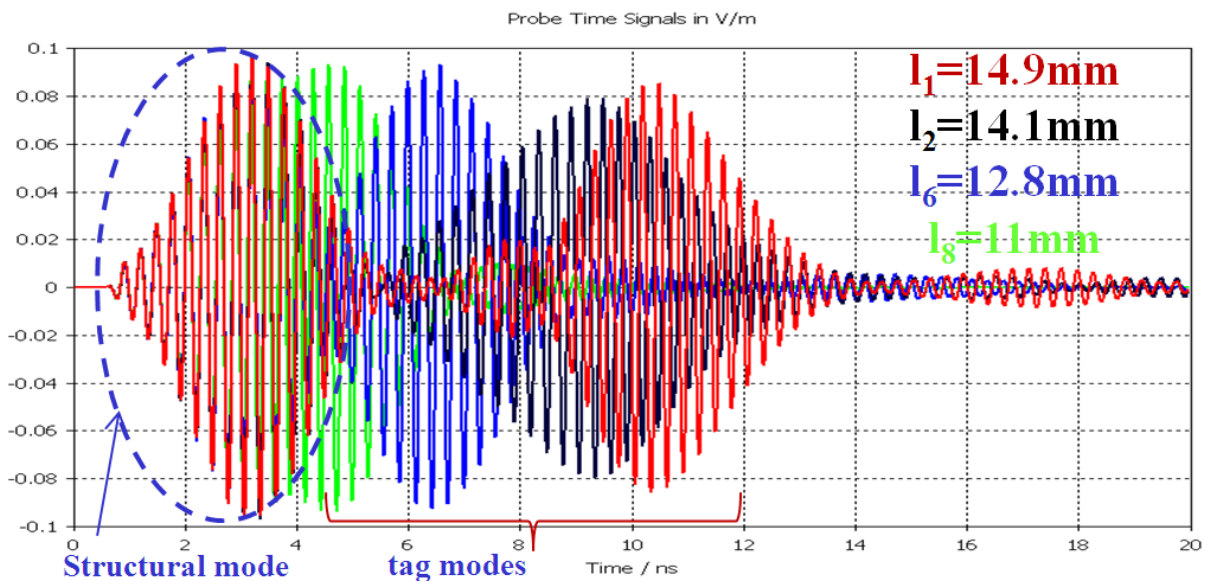
Fig.3. 24 : Simulated backscattered signals of different tags (one tag is represented in Fig.3. 23) collected at the horizontally oriented probe for different lengths of C-section.

Simulation has been done for different tags by varying the length of the C-section. As already explained, as a proof of concept, 3 bit coding is explained in this work. Three bit coding can

be realized with 8 different tags, each tag with different length. Backscattered signal can be collected at the far-field probe (as explained in the Appendix). Fig.3. 24 shows the backscattered signal collected at the horizontally oriented probe (output) for different lengths of C-section.

As shown in the figure and also as explained previously, the backscattered signal consists of two components, the structural mode, and the tag mode. As mentioned, the time delay between the structural mode and tag mode is used for encoding. Table 3. 3 shows the simulated delays obtained along with different binary codes. The first column corresponds to different lengths of C-section. The second column corresponds to different delays obtained when the C-section acts as a two-port network (see Fig.3. 15 and Fig.3. 16). Third column corresponds to the calculated delay. It is the delay determined by adding the delay produced by C-sections and two cross polarized antennas at $f(l_1)$. Fourth column corresponds to the delay obtained by taking the time difference between the structural and tag modes (see Fig.3. 24) in the case of a complete chipless tag. And final column is the assigned binary code.

For this study, the lengths of the C-sections are chosen in order to have a minimum delay difference of 0.5 ns between each combination. This value can easily detect practically using an oscilloscope. However, in the Table 3, a small amount of mismatch can be observed (7 % of error) which may be due to the error in the modelization of the antennas in order to calculate the group delay.

Table 3. 3 : *Chipless tags : comparison between the simulated and calculated delay*

$$\text{Delay}_{VA3.5GHz}+\text{Delay}_{HA3.5GHz}= 0.57 \text{ ns} + 0.46 \text{ ns} =1.03 \text{ ns}$$

$l_n(C)$; n=1-8 (mm)	Delay(C-section) (ns) Simulation as 2-port network	Delay $_{tag}$ (Delay $_{Antennas}$+ Delay $_{C-section}$) Calc. Δt (ns)	Delay $_{tag}$ (Δt between two modes) Sim. Δt (ns)	Binary Code
14.9	5.32	6.35	7.1	000
14.1	4.5	5.53	6	001
13.8	4	5.03	5.3	010
13.5	3.49	4.52	4.7	011
13.1	3	4.03	4	100
12.8	2.55	3.58	3.37	101
12.4	2.19	3.22	2.7	110
11	1.24	2.43	1.93	111

3.9   FABRICATED CHIPLESS TAGS

Different combinations of tags were fabricated in Rogers 4003 substrate. As already said this substrate has very less loss tangent which is of the order 0.0027 and permittivity of 3.55. The height of the substrate is 0.8 mm. Fig.3. 25 (a) & (b) shows the fabricated reference tag and chipless tag respectively. What we will call as the "reference tag" is made by short

circuiting the two cross polarized antennas each other (Fig.3. 25 (a)). Measurement has been done using these tags. Different time domain measurement techniques were used which will be explained in the succeeding section.

(a)   (b)
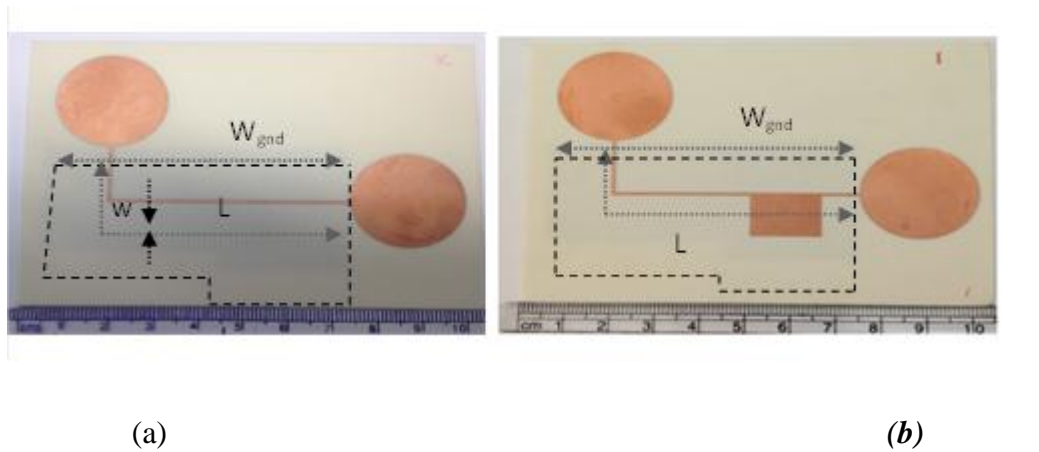
Fig.3. 25 : *The* **reference** *tag and chipless tag used. a)* **Reference tag.** *b) Chipless tag with 10 C-sections; bottom ground plane is marked as dashed lines.* W_{gnd}*=70 mm, L= 79.1 mm, w=0.7 mm.*

3.10   TIME DOMAIN MEASUREMENT TECHNIQUES

The time domain measurement set-up is explained in the Appendix. Homemade Lab software is used to pilot the DSO. Fig.3. 26 represents the set-up used. The specification of DSO and
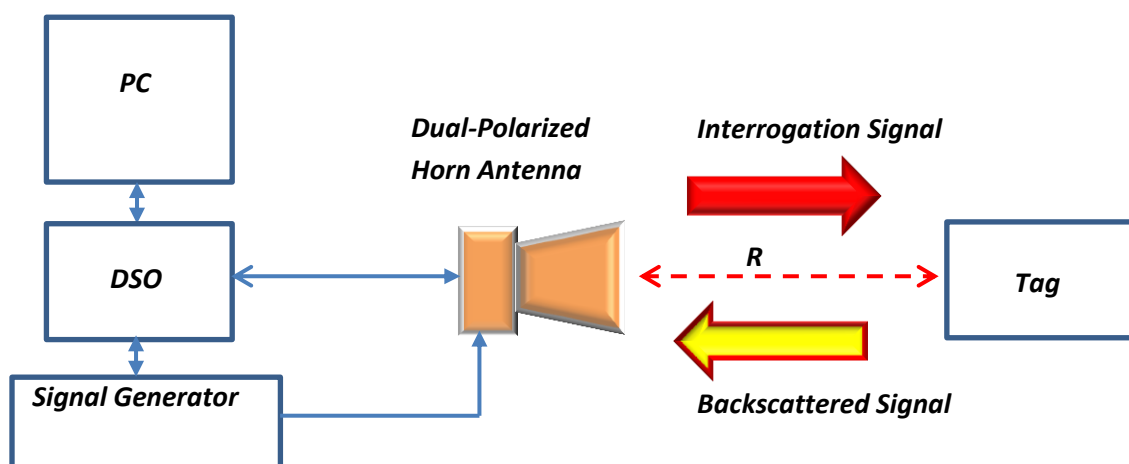
Fig.3. 26 : Time domain measurement set-up.

the picosecond pulse generator used is explained in the Appendix I. Both dual polarized and two single polarized horn antennas (oriented 90° each other) were used in the measurement to prove the robustness of the tag with different reader antenna conditions. The distance R between tag and the horn antennas were set as 1.2 m for the measurement explained in this chapter. The backscattered signal is a temporally delayed signal.

The most challenging part of the backscattering measurement is the information separation (delay produced by the tag), especially when the delay due to the environment has a predominant effect along with the delay produced by the tag. In the following part, two kinds of techniques can be seen for validating the concept. Fig.3. 27 explains the procedures carried out. An empty room (without tag) measurement has been conducted throughout the backscattering measurement explained in this thesis except for the measurement with reference tag. The reference tag is used to get directly the delay induced by the C section and to compare the measurements with the prototype (without tag antennas). A background subtraction of the empty room response can eliminate most of the unwanted contributions from the nearby objects cables and antenna coupling, assuming that they are constant.

Two techniques were used. Former technique explains (Part A in Fig.3. 27) the de-embedding with a reference tag (de-embedding tag). This was to eliminate the delay produced by the tag antennas and to validate the delay produced by C-sections. In this case, it was noted that the delay produced is the same as the delay produced by the C-sections while it is acting as a 2-port network. Latter proves the efficiency of time domain encoding in information separation, without using a reference tag (Part B in Fig.3. 27). In this case a time windowing has a significant importance. A time windowing can eliminate the coupling due to the reader antennas. Once the time windowing is performed, continuous wavelet transform or filtering can be used to extract the information at the frequency of interest.
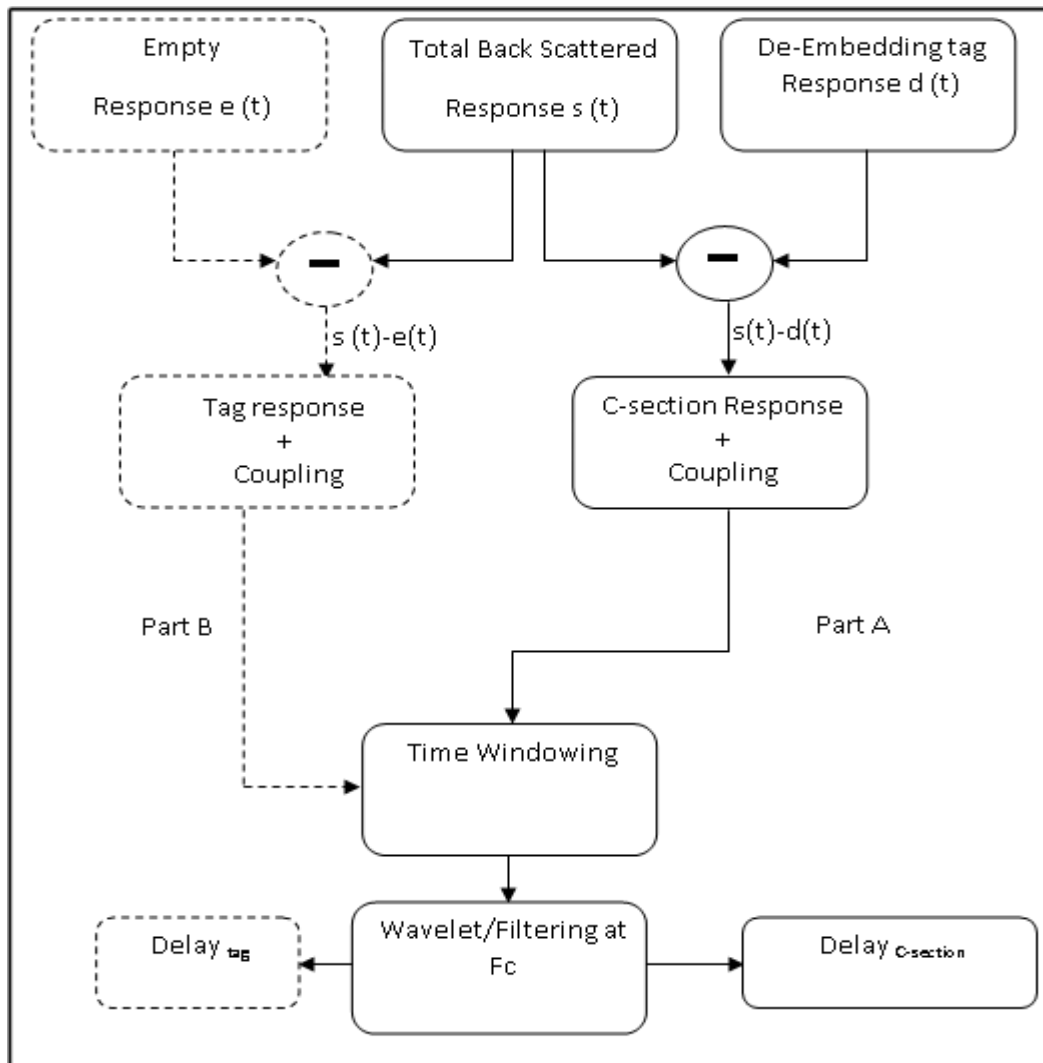
Fig.3. 27 : The process of information separation.

3.10.1   De-embedding with tag antennas

To overcome the distortions created by the tag antenna and also by the whole environment of the tag (coupling of antennas, the presence of support, cable length etc.), we have used a reference tag in which the C-sections are replaced by a transmission line section as shown in Fig.3. 25 (a). The antennas used here are the same antennas used in the real tag. The length of this transmission line is equal to the length L as shown in Fig.3. 25 (b) for the tag with C-sections. Fig.3. 28 shows the above formulated conclusion. As we already explained, the backscattered signal from the horizontally polarized tag transmitting antenna consists of structural mode and tag mode. The time Δt between these two modes is given by,

$$\Delta t= \text{Delay}_{\text{tag}} = \text{Delay}_{\text{HA}} + \text{Delay}_{\text{C-section}} + \text{Delay}_{\text{VA}} + \text{Delay}_{\text{CA}} \qquad (16)$$

where Delay $_{\text{HA}}$ is the delay produced by the horizontally polarized tag antenna and Delay $_{\text{VA}}$ is that of the vertically polarized tag antenna. Delay $_{\text{C-section}}$ is the corresponding delay produced by the C-sections. Delay $_{\text{CA}}$ is due to the coupling effect with the reader antenna, which is very weak (will show this feature in the following section) and hence one can consider the total delay as the sum of the first three parameters.

Delay $_{\text{VA}}$ Delay $_{\text{C-section}}$ Delay $_{\text{HA}}$
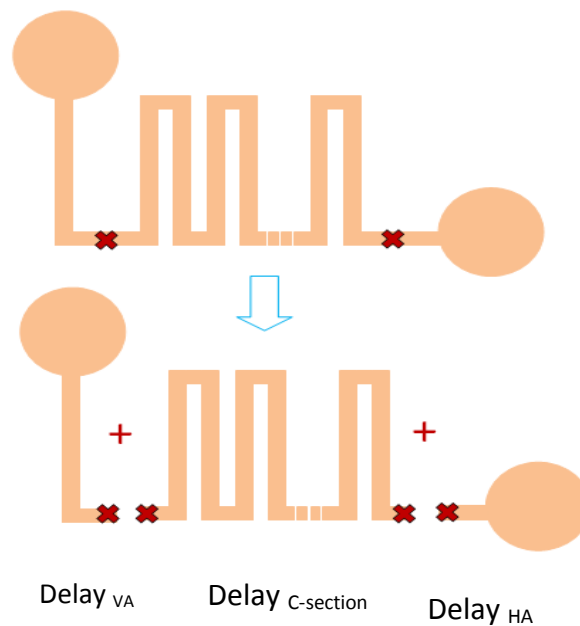
Fig.3. 28 : Principle used to extract the group delay and hence the tag information which contains antennas.

Another interesting fact to be noticed here is the time T, at which structural mode starts in comparison to the excitation signal. It has been defined by the equation T=2R/c, where R is the distance between tag and reader and c is the speed of light. This time has a greater importance when the tags are used for localization applications. By determining the time T, the distance at which the tag is placed can be calculated or vice versa.

As explained in Fig.3. 27, for de-embedding, the response of the reference tag has been subtracted from each of the chipless tag response, which in turn gives the response of the C-section without antennas. This response also consists of structural mode and tag mode and the time between the two modes is given by,

Δt= Delay $_{\text{C-section}}$.

Since the tag is designed for a single frequency f (l_1), the corresponding tag response can be determined by numerical filtering in MATLAB or via wavelet transform as explained in [25].

3.10.2   Information separation without reference tag

As already said, the time domain technique has a predominant role in the information separation since it can be done without an additional reference tag. A background subtraction of the empty room response can eliminate most of the unwanted contributions from the nearby objects cables and antenna coupling, assuming that they are constant. Other parasitic effects can be again eliminated by an averaging and also by an efficient time windowing in the post signal treatment process. Time windowing is interesting in practice since it can be used to extract the tag information directly without the use of a reference tag. Thus, it reduces the need for reference tag measurement taking place with each tag combinations [2]. It has been found that when the distance between the tag and reader antenna increases, the time between the coupling signal (signal between the antennas) to the reader antenna and the structural mode increases. It is in accordance with the already defined equation T=2R/c. The rising edge of the window can be determined from this equation while the trailing edge can be determined by an optimization process, assuming that most of the decaying part of the signal is noise. Also knowledge about the total time response of the tag can also help to fix the trailing edge. So in practice we use both edges in order to increase the robustness of the measurement.

3.11   CASCADED SINGLE GROUP OF C-SECTION: MEASUREMENT

As previously explained, the prototype of the tag can be transformed into a chipless tag by adding a transmitting and receiving antenna at the two ends. The entire system has been simulated and the backscattered signal from the receiving antenna has been used for the encoding purpose. In order to prove the predicted theories and the flexibility of the proposed tag with different kinds of reader antenna conditions, two kinds of measurements have been carried out in the anechoic chamber; with and without a reference tag.

Moreover, measurements with different distances were also carried out in order to validate the equation $T=2R/c$ and hence the possibility of using these tags for localization applications. Also in two cases two different kinds of reader horn antennas have been used.

A dual polarized horn antenna has been used in the former case and two horn antennas oriented in a cross polarized form have been used in the latter case. The two experimental results prove the earlier theoretical predictions.

3.11.1   With reference tag

The tag shown in Fig.3. 25 (a) was used as the reference tag. A dual polarized horn antenna, which can operate in 2-32 GHz with an average gain of 17 dBi, was used as the reader antenna as shown in Fig.3. 29 (a).

(a)   *(b)*
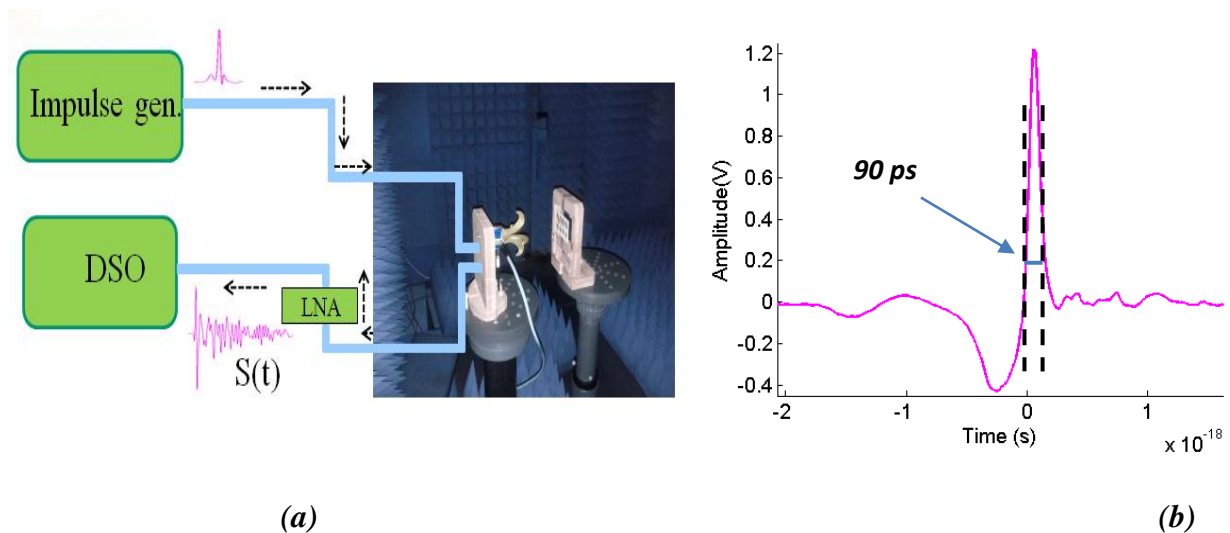
Fig.3. 29 : The proposed measurement set-up and the excitation signal used. a) Measurement set-up used in the anechoic chamber. b) The impulse signal used as the excitation signal.

The chipless tag and the reader antenna were mounted on plastic stands and the tag was placed at a distance R. Measurements were conducted at different distances of 30 cm, 50 cm, 1 m and 1.2 m. The previously defined impulse signal is used as the input for horn antenna. The delayed spectrum for each tag has been measured by the Agilent Digital Oscilloscope

DSO91204A. A 90 ps pulse width impulse signal has been used as the excitation signal as shown in Fig.3. 29 (b).

As already explained, the de-embedded tag response was subtracted from all tag combinations, which gives the response of C-section only. In order to separate the tag information at the frequency of interest, MATLAB filtering was done as explained earlier. A 3rd order butterwort filter with upper cut-off frequency and lower cut-off frequency as 3.4 GHz and 3.6 GHz respectively were used. The same filter is used for all combination of tags. Fig.3. 30 (a) shows the backscattered tag response (with length l4=13.1 mm). Fig.3. 30 (b) shows the filtered signal for two tag responses (with length l5=13.8 mm & l4=13.1 mm) at f(l1)=3.5GHz along with their envelopes.

(a) *(b)*
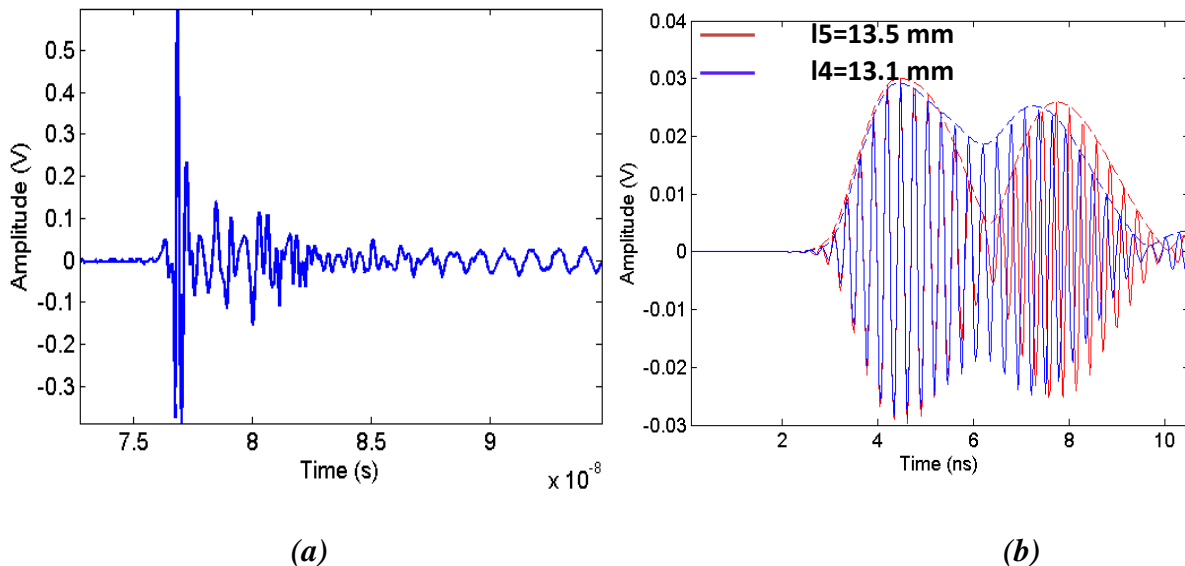
Fig.3. 30 : Tag response before and after numerical filtering. *a) Backscattered tag (l4=13.1 mm) response. b) Filtered signals at f(l1)=3.5 GHz, along with their envelopes for two different tags (l4=13.1 mm & l5=13.5 mm).*

Fig.3. 31 shows some of the de-embedded response obtained for tags at a distance of 30 cm. These results were obtained after a numerical filtering at 3.5 GHz and by taking the envelopes as explained in Fig.3. 30(b).
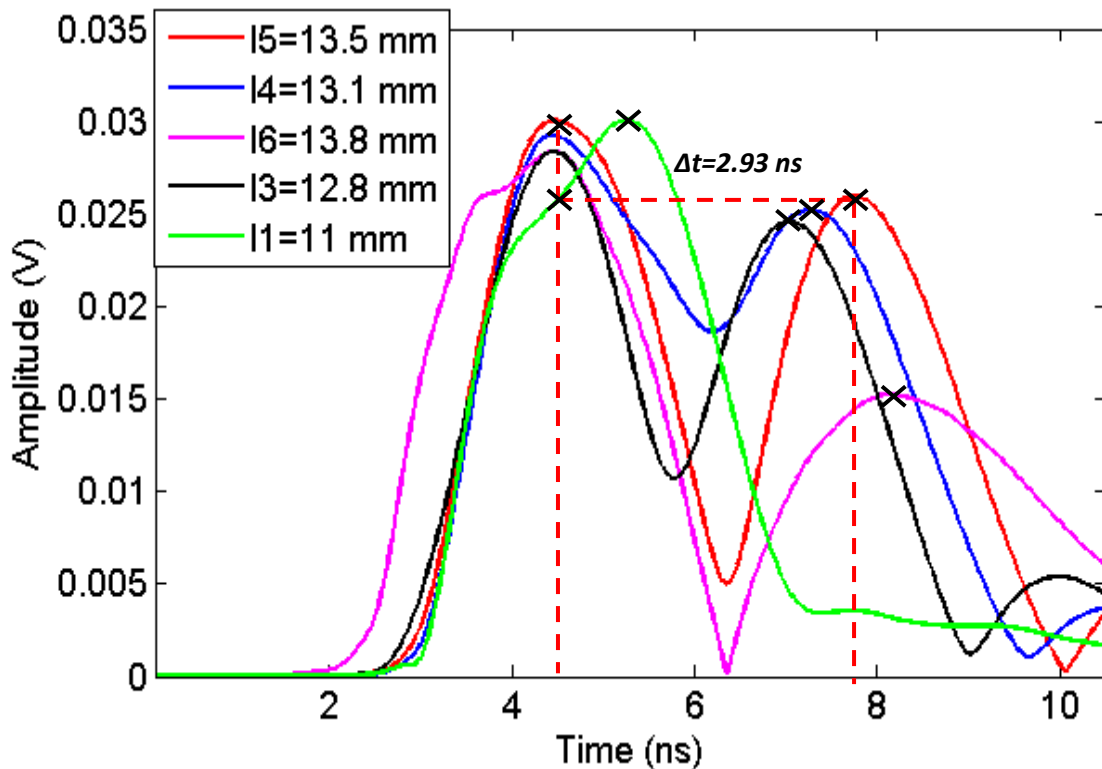
Fig.3. 31 : Some of the de-embedded C-section response measured for different lengths f (l1) = 3.5 GHz. One of the tags is represented in Fig.3. 25 (b).

Again, we see that the obtained responses contain two modes, structural mode which seems to be constant for all tag combinations and tag mode which changes each time depending on the length of the C-section. The time Δt has been calculated by taking the difference of structural mode peak and tag mode peak as shown in the figure (the time difference between black cross of different peaks). This time has been compared to the delay produced by the C-sections when they are connected as a two-port network as shown in Fig.3. 15, Fig.3. 16 and also in Table 3.2. It is clear that the delay changes with a change in the length of the C-section.

If the delay is too small, the structural mode and tag mode intersects as in the case of l_1. Table 3. 4 shows the comparison of delays. A good agreement has been obtained, which proves the concept of de-embedding.

Table 3. 4 : Comparison of delay produced by C-section after de-embedding

$l_n(C)$; n=1-8 (mm)	Gd(C-section) (ns) Simulation as 2-port network	Measured Δt (ns)
14.9	5.32	5.3
14.1	4.5	4.65
13.8	4	3.9
13.5	3.49	3.35
13.1	3	2.93
12.8	2.55	2.5
12.4	2.19	2.22
11	1.24	0.95

Measurement has been done with commercially available UWB radar, 'Novelda' [26] in a real environment which can serve as the front end of a chipless reader. The radar is specified to be FCC compliant and to operate over a frequency range of 0.45 to 9.55 GHz and a sampling rate greater than 30 Gs/s. To verify the characteristic of the radar, the emitted pulse has been measured and it was found that the radar is able to detect tags until 7 GHz. The radar sends UWB pulse and samples the response of the tag. The measurement was done in a room with lot of interference objects such as walls, computers, cardboards, tables etc.

In this case a short pulse is used to interrogate the system. Measurement with the reference tag was also performed. All the signal processing remains the same as explained earlier. The dashed lines in Fig.3. 32 represent the results obtained for some of the combinations. As shown in figure, there is a good agreement with the results obtained using a digital oscilloscope and impulse generator. Table 3. 5shows a comparison of different delays obtained using Novelda and digital oscilloscope. Contrary with the use of oscilloscope [2], it is essential to use a LNA with the radar Novelda to correctly retrieve the ID of the tag. This shows the limitations in terms of sensitivity of the radar. The maximum amplitude produced by Picosecond pulse generator is 2 V into a 50 Ω load giving a maximum instantaneous power of 19 dBm and that of Novelda is of the order of 200 mV (6 dBm).

$l_n(C)$; n=1-8 (mm)	Measured Δt-Oscillo (ns)	Measured Δt-Radar (ns)
14.1	4.65	4.6
13.8	3.9	3.95
13.1	2.93	3.03
12.8	2.5	2.44
11	1.2	1.1

Table 3. 5 : *Comparison of de-embedded measured delays (Δt between structural mode and tag mode) with DSO and UWB radar*

In order to prove the feasibility of these kinds of tags in localization applications, measurements with different distances were also carried out. Fig.3. 33 shows the de-embedded response for a randomly chosen tag with the length of C-section as 13.5 mm. In this particular example, the different Δt shown in the figure is the same since it is the response for the same tag. The time T at which the structural mode starts is also marked in Fig.3. 33. It has been found that the time varies with distances and has a very good agreement with the

theoretical expression 2R/c. It has been found that the starting point of each curve produces an additional time delay of 800 ps, which is due to the numerical filter used in the signal processing routine. Measurements for tags with different lengths were also carried out to confirm the results. In practice the "luxury" of using a de-embedding tag may not be practical. Hence the measurement without a de-embedding tag was also carried out. The de-embedding was included in the study just to verify the delay produced by C-section with our theoretical predictions.
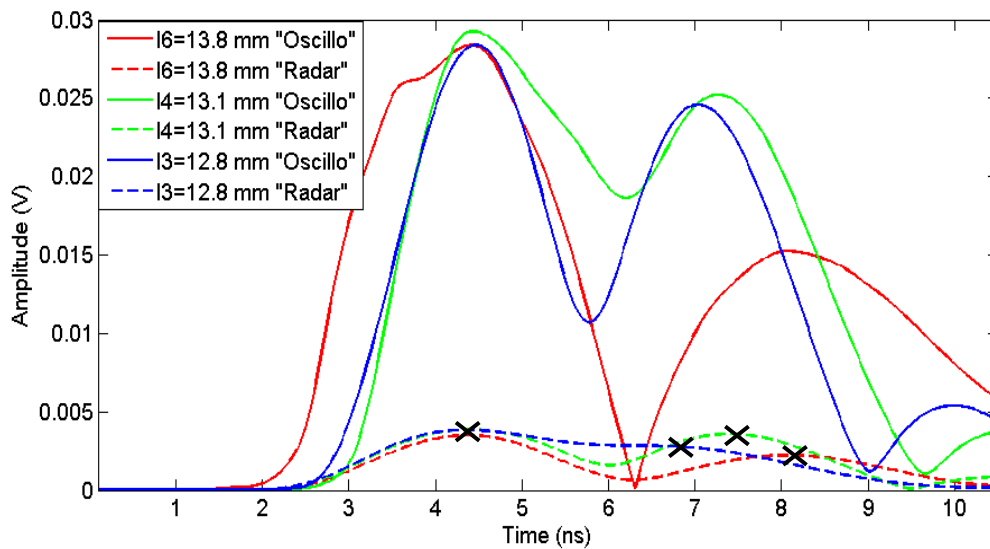
Fig.3. 32 : Some of the de-embedded C-section response measured for different lengths at F (l1) = 3.5 GHz. "Oscillo" stands for results using digital oscilloscope and "radar" stands for results using a commercially available UWB radar which can serve like a chipless RFID reader. One of the chipless tag is represented in Fig.3. 25.

In short, different measurement results using a reference-tag was presented in this section. It also explains measurement using both DSO and UWB radar. The possibility of using C-sections for producing different IDs and measurements at different distance were also conducted. The next part explains measurement without a reference tag.
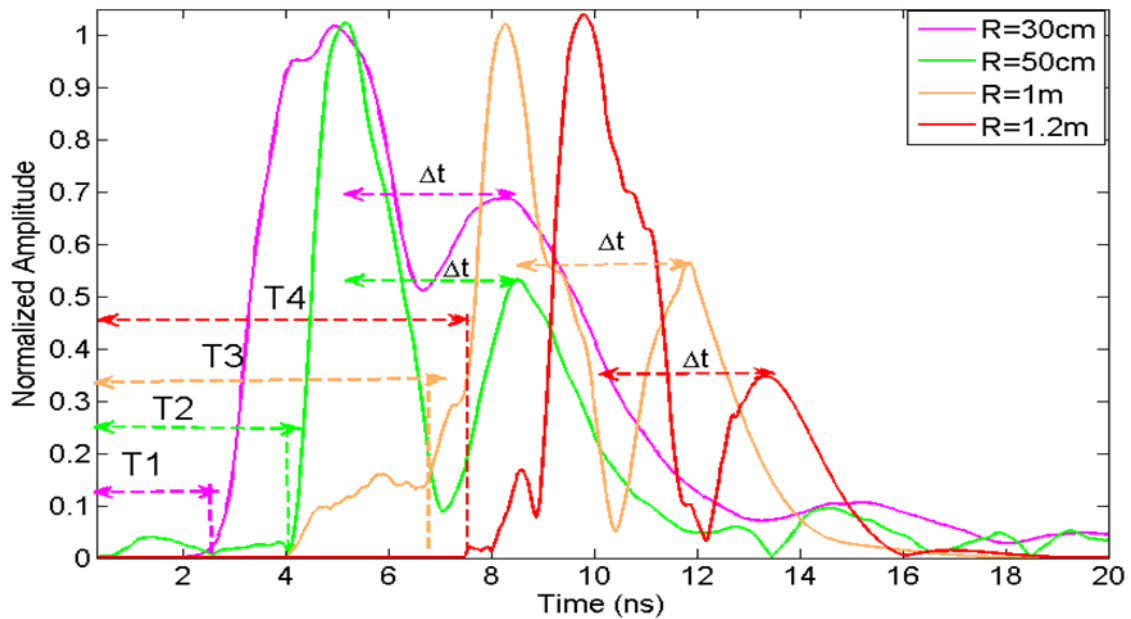
Fig.3. 33 : De-embedded C-section response measured at different distances R (T=2R/c)for the tag with length of C-section as 13.5 mm.

3.11.2   Without a Reference tag

In this case, two horn antennas were used as the reader antennas. They are oriented in a cross-polarized form. These horn antennas are placed at a distance of 10 cm from each other and they can operate within 700 MHz-18 GHz with a gain of 12 dBi. The chipless tag and the reader antennas were placed at distance of 1.2 m. All other measurement set-up remains the same. One remarkable thing in this case is that the de-embedding tag is not used and hence can avoid all the calibration techniques which make the whole system complex [2]. The only measurement needed is the measurement for empty chamber and with tag, which is not difficult to implement in practice. This is a prime advantage of the time domain and cannot be used in frequency domain where the amplitude of the signal (RCS) is used for the encoding. This again proves the robustness of temporal approach. Contrary to [27], where LNA is not utilized in the measurement and hence read range of 50 cm was obtained, in this measurement LNA has been used in the receiving end which enables read range of 1.2 m.

In order to separate the structural mode and different tag modes at the frequency of interest, Continuous Wavelet Transform (CWT) is used [28]. The CWT performs a

correlation analysis and as a consequence maximum output can be expected when the input signal mostly resembles the wavelet template. This input signal will be the time domain signature of the tag with amplitude in Volt. Consider the backscattered response of the tag after time windowing as *B(t)*.

A Gaussian signal modulated at a carrier frequency of F_C is chosen as the known deterministic signal *p(t)*.

Thus, $p(t) = e^{\left(\frac{-t^2}{2tv}\right)}.\cos(2\pi F_C t)$

where t_v is the time domain parameter which consider the bandwidth of the signal(*BW=0.1*) and here i=1,2. Thus the wavelet template signal *p(t)* is a signal which can be parameterized in frequency and bandwidth. A cross correlations of this signal with *B(t)* has been done. Finally the maximum of this cross-correlation gives the unknown location parameter τ.

τ=max (B (t)*p(t)), where * represents the cross-correlation operation.

In our case, τ will be a combination of two peaks, the first peak represents the structural mode and the second peak represents the tag mode. The difference between these two peaks gives the delay of the tag (Delay $_{Tag}$). This principle is the basis for a matched filter, which is the optimum detector of a deterministic signal in the presence of additive noise.

In the proposed case, a Gaussian modulated signal at a carrier frequency of 3.5 GHz is used as the known deterministic signal. Fig.3. 34 shows the maximum output of the correlation, which in turn corresponds to the group delay produced by the C-section and the two cross polarized antennas. It is seen that the signal comprises of two components, the structural mode and the tag mode. The delay between structural mode and tag Δt mode can be used for the encoding. CWT was preferred other than filtering in this case because this approach can easily separate the spectral components from a noisy environment with the help of an efficient windowing [23,26]. It follows the concept of a matched filter. CWT was also tested in simulation studies in order to separate the spectral components at frequency of interest, while interrogating the whole system using a short UWB compatible pulse. The results were quite comparable with those produced in Fig.3. 24 (Simulation results).
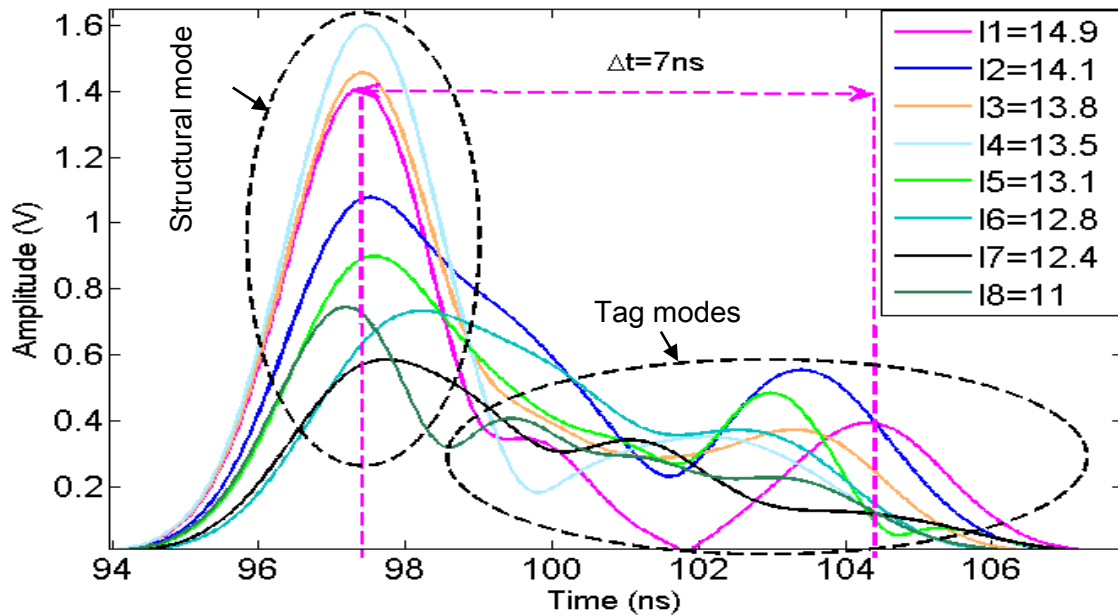
Fig.3. 34 : Measured delays of chipless tag obtained using wavelet approach for single group of 10 C-section with different lengths l1-l8 mm at f (l1) = 3.5 GHz. This measurement was done without a reference tag.

Table 3. 6 gives the calculated, simulated and measured delays obtained along with the delay produced by the tags with different length of C-sections at 3.5 GHz. Calculated delay is the sum of simulated delay produced by cross polarized antennas and C-sections at 3.5 GHz, by using the equation (16) (see Fig.3. 28). It is clear from the table that there is a good agreement between the simulated and measured delays. However, calculated delay shows a 7% of average error from those of simulated and measured values. This may be due to the coupling between the antennas and the C-section which may also be a function of the length of the C-section. The delay produced by the reference tag is assigned by the binary code '000' and that by the second tag is assigned as '001'. The subsequent delays have been assigned by other binary values.

Table 3. 6 : *Chipless Tag: Calculated, simulated and measured delays obtained without a reference tag.*

$Delay_{VA3.5GHz} + Delay_{HA3.5GHz} = 0.57$ ns $+ 0.46$ ns $= 1.03$ ns

1_{1n} , n=1-8 (mm)	Delay $_{C\text{-}section}$ Sim. (ns)	Delay $_{tag}$ Calc. Δt (ns)	Delay $_{tag}$ Sim. Δt (ns)	Delay $_{tag}$ Meas. Δt (ns)	Code
14.9	5.32	6.35	7.1	7	000
14.1	4.5	5.53	6	6.1	001
13.8	4	5.03	5.3	5.4	010
13.5	3.49	4.52	4.7	4.9	011
13.1	3	4.03	4	4.4	100
12.8	2.55	3.58	3.37	4	101
12.4	2.19	3.22	2.7	3	110
11	1.4	2.43	1.93	2.1	111

Further, in order to evaluate the performance of the proposed tag with different orientations, a simulation has been done by rotating the tag with different angles. It has been found that the tag keeps the same performance with different angles.

(a)   *(b)*
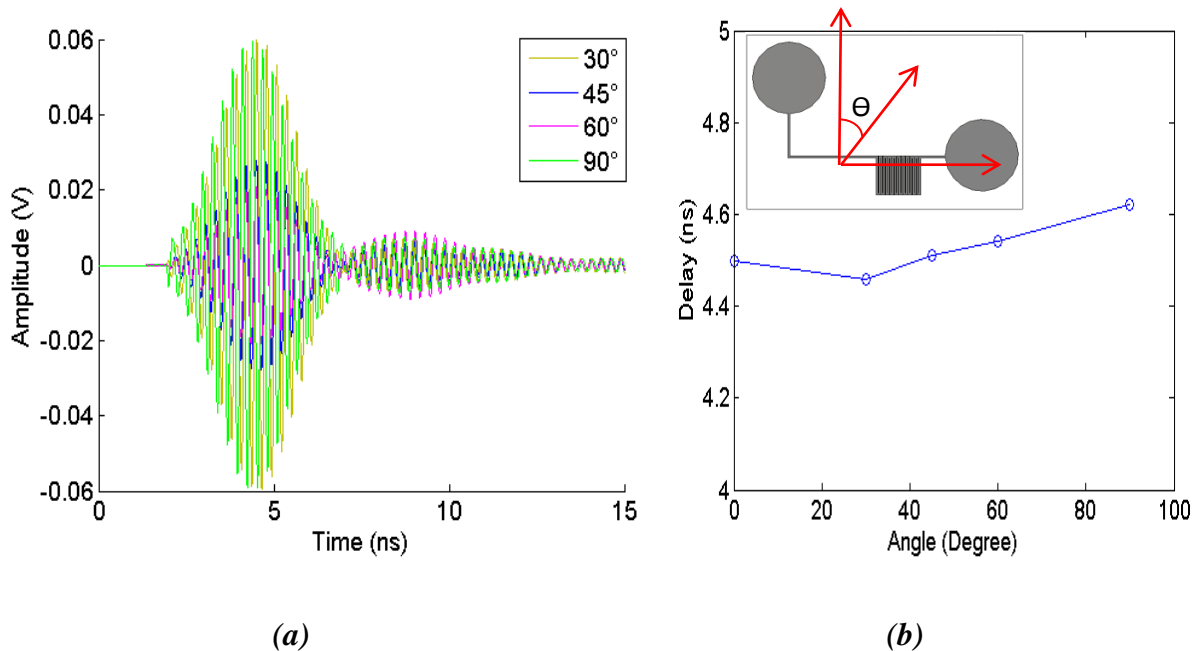
Fig.3. 35 : Simulated results for the tag with different orientations. a) Simulated backscattered results obtained when the tag is rotated for different angles Ө. b) Obtained delayed between structural mode and tag mode as a function of angle. Insight: tag with coordinates.

Fig.3. 35 (a) shows the simulated backscattered signal collected at the probe when the tag is rotated with different angles as shown in Fig.3.35 (b). Fig.3. 35 (b) shows the obtained delay (Δt) between structural mode and tag mode as a function of different angles. It is clear that despite of the amplitude, the delay keeps almost a linear behavior with different angles. Since the information is encoded only using delay, we can conclude that the proposed tag can operate independent of the orientation. Moreover, simulations have been done for other angles also. The tag was excited from the bottom ground plane. It was found that in this case also, the time delay remains the same. In short, the tag can be operated irrespective of the orientation with reader. This is an advantage of working with two antennas. Unlike the REP tags [29], where the tag orientation has to be considered prior to the tag design, these kind of tags works well with different orientations.

3.12   CONCLUSION

A time domain chipless tag using microstrip C-sections are explained in this chapter. A Chipless tag using dispersive transmission line sections are presented elaborately. The time domain chipless tags permit to operate in some limited bands for example the unlicensed ISM bands that are compatible with the FCC and ETSI in terms of allocation of frequency and emission power. Moreover, the reading system is more easier than that of the frequency domain approach because it doesn't demand the implementation of some advanced calibration techniques to trace the electromagnetic signature of the tag and hence its identifier. Time domain Chipless tags offer more robust communication together with the use of ISM bands offers significantly large reading range compared to the frequency domain tags. Even though time domain tags have number of advantages, researchers are mostly interested in the frequency domain approach because of the high number of bits it can be encoded. Frequency domain approach has reached a maximum of 49 bits [29]. In contrast, the maximum number of bits that are encoded so far with time domain approach is 8 (except the case of SAW tag) [9]. The robustness of the temporal approach is proved since it allows the measurement without the use of calibration tag. The tags were also simulated for different orientations and it was found that the performance remains the same.

The coding capacity can be increased by decreasing the time resolution or by including more number of variations rather than considering 8 variations. Cascading multi C-section groups with different lengths can also increases the capacity of encoding. The dispersive lines allow using multiple C-sections at different frequencies. In this case there will be multi operating frequencies rather than single, depending on the number of multi C-section groups. The following chapter explains this concept.

REFERENCES

1. S. Harma, V.P. Plessky, X. Li and P.Hartogh, "Feasibility of Ultra-Wideband SAW RFID Tags Meeting FCC Rules", IEEE Transactions on Ferreelectronics and Frequency Control, Vol. 56, No.4, April 2009.

2. A. Vena, E. Perret, and S. Tedjini, "Design of Compact and Auto Compensated Single Layer Chipless RFID Tag", IEEE Transactions on Microwave Theory and Techniques, vol. 60, No 9, pp. 2913 – 2924, 2012.

3. C. S. Hartmann, "A global SAW ID tag with large data capacity," Proc. IEEE Ultrasonics Symp., Munich, Germany, pp.65–69, October 2002.

4. Model 501 SAW RFID reader system, [online] Available:www.rfsaw.com.

5. C.S. Hartmann and L.T. Claiborne, "Fundamental limitations on reading range of passive IC based RFID and SAW based RFID", 2007 IEEE International Conference on RFID, TX, USA, March 26-28, 2007.

6. S. Preradovic, I. Balbin, N.C. Karmakar, and G.F. Swiegers, "Multiresonator-based chipless RFID system for low-cost item tracking", Microwave Theory and Techniques, IEEE Transactions on, vol. 57, No 5, pp. 1411-1419, 2009.

7. A. Vena, E. Perret, and S. Tedjini, "Chipless RFID Tag Using Hybrid Coding Technique", IEEE Transactions on Microwave Theory and Techniques vol. 59, No 12, pp. 3356-3364, 2011.

8. S. Preradovic, N. C. Karmakar, "Design of fully printable planar chipless RFID transponder with 35-bit Data capacity", Proceedings of the 39th European Microwave Conference, Rome, Italy, September 2009

9. L. Zheng, S. Rodriguez, L. Zhang, B. Shao, and L.R. Zheng, "Design and implementation of a fully reconfigurable chipless RFID tag using Inkjet printing technology", IEEE International symposium on Circuits and Systems, May 2008, pp. 1524-1527.

10. L. Zhang, S. Rodriguez, H. Tenhunen, and L.R. Zheng, "An innovative fully printable RFID technology based on high speed time-domain reflections". Proc. High Density Microsystem Design and Packaging and Component Failure Analysis 2006 (HDPapos 06) pp. pp. 166 – 170,27-28 June 2006.

11. A. Ramos, A. Lazaro, D. Girbau, and R. Villarino "Time domain measurement of time-coded UWB chipless RFID tags", Progress In Electromagnetic Research, vol. 116, pp. 313-331, 2011.

12. J. Hong and M. Lancaster, "Microstrip Filters for RF/Microwave Applications", A WILEY-Interscience Publication, ISBNs: 0-471-38877-7 (Hardback); 0-471-22161-9 (Electronic), 2001.

13. S. Shrestha, "Chipless Rfid Sensor Tag System with Microstrip Transmissionline Based Id Generation Schemes", PhD Dissertation from College Of Engineering And Science Louisiana Tech University, March 2009.

14. R. Nair, E. Perret, S. Tedjini,"Chipless RFID based on Group Delay encoding" ,IEEE International Conference on RFID technologies and Applications(RFID-TA),September 2011,Barcelona,Spain,pp. 214-218.

15. R. Nair, E. Perret and S. Tedjini, "Temporal Multi-Frequency Encoding Technique for Chipless RFID Applications", IEEE MTT-S International Microwave Symposium IMS 2012, Montréal, Canada, June 17-22.

16. S. Gupta, A. Parsa, E. Perret, R.V. Snyder, R.J. Wenzel, and C. Caloz, "Group delay engineered non-commensurate transmission line all-pass network for analog signal processing," IEEE Transactions on Microwave Theory and Techniques, September, 2010, vol. 58, issue. 9, pp. 2392-2407.

17. R. K. Mongia, I. J. Bahl, P. Bhartia, and J. Hong, *RF and Microwave Coupled-Line Circuits*, 2nd ed. Norwood, MA: Artech House, 2007.

18. FCC, First Report and Order 02-48. February 2002.

19. J. Liang, "Antenna Study and Design for Ultra Wideband Communication Applications" PhD Dissertation from Department of Electronic Engineering Queen Mary, University of London United Kingdom, July 2006.

20. N. P. Agrawall, G. Kumar, and K. P. Ray, \Wide-Band Planar Monopole Antennas", *IEEE Transactions on Antennas and Propagation*, vol. 46, no. 2, February 1998, pp. 294-295.

21. M. Hammoud, P. Poey and F. Colombel, "Matching the Input Impedance of a Broadband Disc Monopole", *Electronics Letters*, vol. 29, no. 4, 18th February 1993, pp. 406-407.

22. H.J. Lam, Y. Lu, H. Du, P.M. Poman, and J. Bornemann, "Time-domain modeling of group-delay and amplitude characteristics in ultra wide band printed circuit antennas", Springer Proc. in Physics, vol. 121, pp. 321-331, 2008.

23. R. Ling, and P. Ufimtsev, "Scattering of electromagnetic waves by a metallic object partially immersed in a semi-infinite dielectric medium", IEEE Transactions on Antennas and Propagation vol. 49, No 2, pp. 223-233, 2001.

24. W.T. Wang, Y. Liu, S.X. Gong, Y.J. Zhang, and X. Wang, "Calculation Of Antenna Mode Scattering Based On Method Of Moments", *Progress In Electromagnetics Research Letters, Vol. 15, pp.117-126, 2010.*

25. A. Lazaro, A. Ramos, D. Girbau and R. Villarino, "Chipless UWB RFID tag detection Using Continuous Wavelet Transform", *IEEE Antennas and Wireless Propagation Letters*, vol. 10, pp. 520-523, 2011.

26. Novelda Nanoscale Impulse Radar (2013 January) [Online] Available : https://www.novelda.no/

27. A. Vena, E. Perret, and S. Tedjini, "Novel compact RFID chipless tag," presented at the Proc. Progress in Electromagnetic Research Symp., Marrakesh, Morocco, 20–23, March 2011.

28. A. Lazaro, D. Girbau, and R. Villarino, "Wavelet-Based Breast Tumor Localization Technique Using UWB Radar", Progress In Electromagnetic Research, Vol. 98, pp. 75-95, 2009.

29. A. Vena, E. Perret, and S. Tedjini, "High Capacity Chipless RFID Tag Insensitive to the Polarization", *IEEE Transactions on Antennas and Propagation*, vol. 60, No 10, 2012.

CHAPTER FOUR MICROSTRIP MULTI-GROUP OF C-SECTIONS AND DELAY BASED ID GENERATION

This chapter deals with the design of tag using multi- group of C-sections. C-sections are dispersive lines. This characteristic enables the C-section producing delay peaks at different frequencies. This is major advantage that solely possessed by C-section in comparison to linear or meandered transmission line which enables producing delay at single frequency. As per our knowledge, this is the first chipless tag that allows coding in both frequency and time. Thus, we can consider this tag as third category; just after frequency domain tags and time domain reflectometric tags; here comes temporal-multi frequency tags. The tag is designed to operate in the two ISM bands at 2.45 GHz and 5.8 GHz respectively. Since the tag enabled coding at different frequencies, it provides a solution for increasing the coding capacity in time domain tags. The design of tag prototype is explained in the chapter. Furthermore the transformation of the prototype into a chipless tag is incorporated. Measurement using commercially available UWB radar which can act like a chipless reader is also incorporated. The results have been validated. The obtained results confirm the use of proposed tag in chipless RFID applications.

# MICROSTRIP MULTI-GROUP OF C-SECTIONS AND DELAY BASED ID GENERATION

4.1 INTRODUCTION

The core of the proposed chipless tag design is the C-sections. C-sections are dispersive structures. In a dispersive structure, the group velocity v_g is a function of frequency, which results in a frequency dependent group delay. Consequently, a wide band signal travelling along such a structure experience time spreading since its different spectral components travel with different group velocities and are therefore temporally rearranged [2]. In the following sections, a time domain chipless RFID tag based on cascaded microstrip coupled transmission line sections (C-sections), which can operate in multi-frequency bands is presented. The group delay characteristics of the C-sections are exploited to generate the tag Identification (ID). The tag comprises of cascaded commensurate group of C-sections and two cross-polarized ultra wide-band (UWB) antennas (see Fig.4. 1 (a)). Since the proposed tag can operate in multi-frequency, this chapter proves the possibility of increasing the coding capacity compared to the existing time domain designs. A tag operating at ISM (Industrial Scientific and Medical) bands at 2.45 GHz and 5.8 GHz together with conformance of frequency and power regulations is discussed elaborately in the succeeding sections. The proposed device is designed, prototyped and experimentally verified. The time domain characteristic of the tag is also validated experimentally by interrogating with a short pulse. Furthermore, measurement results obtained using commercial UWB radar which can be used a chipless RFID reader is also incorporated. The obtained results confirm the concept and the possibility of using temporal multi-frequency in chipless RFID. In this chapter a chipless RFID using C-sections which can operate in multi-frequency bands is proposed. Indeed, the dispersive characteristics of C-sections are exploited for this purpose. As already explained, C-sections are highly dispersive transmission delay lines and are used here so that signal at certain frequencies can be delayed in a controlled manner which is independent from one frequency to another. A proof of concept for practical implementation of the tag is developed here. Each frequency band is directly related with the length of the C-sections. On the other

hand, for the first time, the direct relation between the tag geometry and code is carried out in a comprehensive way. If the ID is known, the tag geometry can be obtained directly and hence it is easy to implement in practice. Also, contrary to [3], the structural and tag modes (back scattering response of C-sections which will be explained later) are used for the encoding. Moreover, narrow band multiple frequencies that are potentially compatible with ISM bands are employed. Additionally as explained in chapter three, the structure makes use of the coupling effect to increase the amount of delay, which miniaturizes the transmission line in comparison to a linear or meandered transmission line. This chapter also presents the experimental verification using Novelda radar [4]. The obtained results have been compared with the results obtained using DSO and Vector Signal Generator, and good agreement is obtained. As already explained in the preceding chapter, the reference tag is not used and hence can avoid all the calibration techniques that make the whole system complex [5]. Moreover, the proposed tag can operates at N-frequencies (here N=2) and explains a novel time-frequency encoding technique.

4.2   OPERATING PRINCIPLE

The frequency dispersive property of transmission line can be utilized to rearrange different spectral components at different times. Frequency dispersion results from propagating different spectral components at different speeds. This characteristic is used for realizing chipless tags. Fig.4. 1 (a) depicts the operating principle of the proposed system which comprises a chipless tag composed of two cross polarized broadband antennas and cascaded commensurate (equal length) C-section groups which is the core of the system. The criteria for cascading the C-sections will be explained in the following section. The frequency dispersive characteristics of the microwave transmission line provides different spectral components rearranged in time and is utilized for encoding of chipless RFID tags. The group delay indicates time taken by a signal to propagate through a structure as a function of frequency.

(a)

(b)
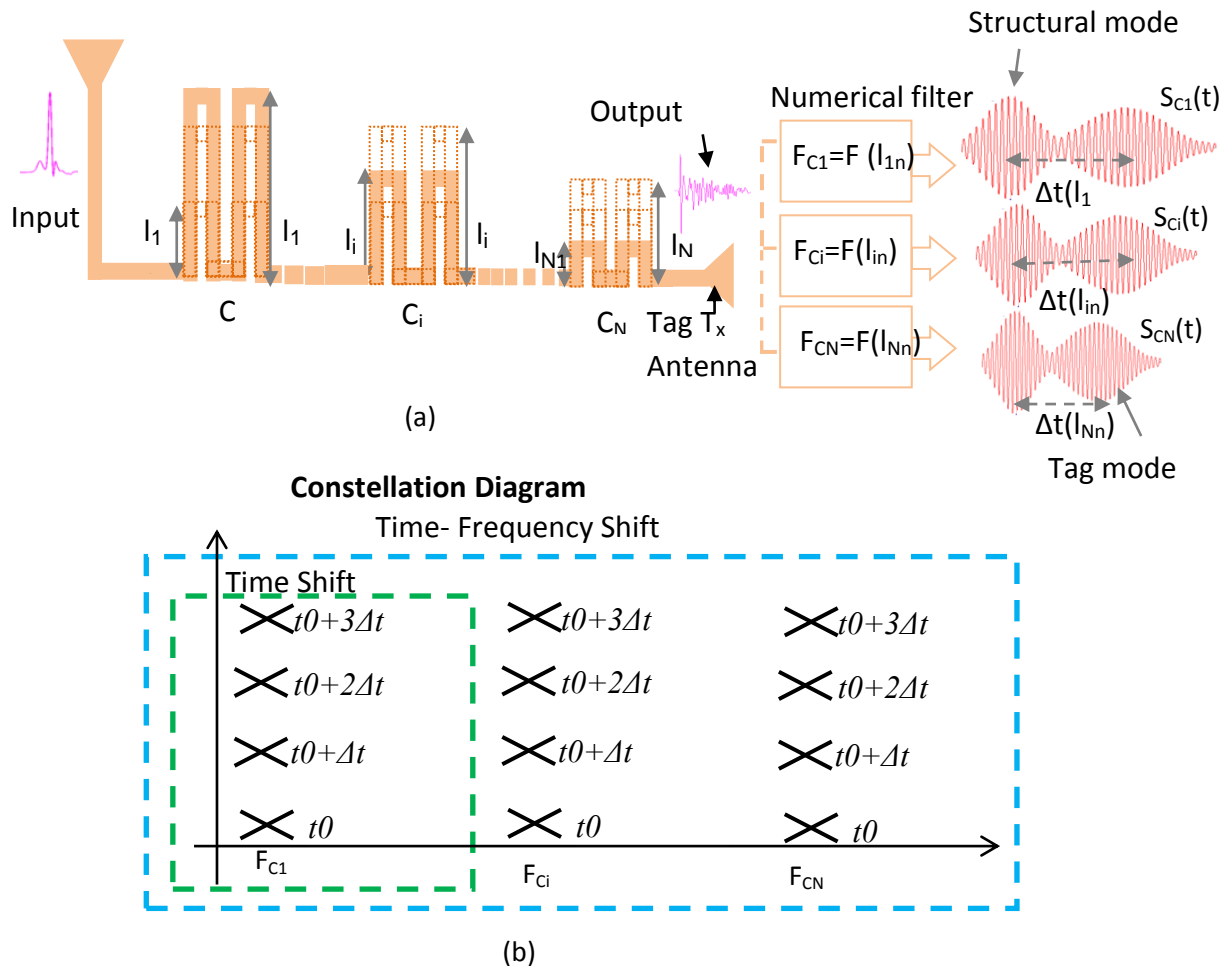
Fig.4. 1 : Proposed Chipless RFID system along with the ID constellation diagram, a) Operating principle. In the illustration each group of C sections consists of two C-sections. b) Proposed time-frequency encoding principle.

For better understanding let us consider a system with N group of C-sections $C_1 \ldots C_i \ldots C_N$, where C_1 is the first group, C_i is an intermediate group and C_N is the last group. As shown in Fig.4. 1(a), each group can have a finite number of lengths such as l_{11}, $l_{12 \ldots}$ l_{1n} , where l_{1n} is the maximum length and l_{11} the minimum length of the C-sections for group C_1. The maximum length l_{1n} for a single C-section, is directly linked to the fundamental frequency F_{C1} by the following relation:

$$F_{C1} = F (l_{1n}) \approx c/(4* l_{1n} (\varepsilon_{eff})^{1/2})   (1)$$

where ε_{eff} is the effective permittivity of the microstrip line and F_{C1} is the frequency at which the group delay is maximum i.e. when the length of C-section is l_{1n}. This is exactly the same expression as we already explained in the preceding chapter for the case of a single group of C-section. As we will explain in the following sections, for all other lengths, the

group delay will be lower than this value. This relation is true in the case of a single C-section. When consecutive C-sections are cascaded, a negligible shift is observed in the frequency to the lower region because of the strong coupling between the C-sections, which increases the capacitive effect. This expression is used in the preliminary design. The lengths are further optimized by simulation. However, in order to allow the reader to have an idea of the system design, this expression is included here. In fact, the behavior here is similar to that of a microstrip coupler where the maximum coupling occurs under the same conditions.

Similarly for the group C_N, l_{Nn} is the maximum possible length of the C-sections among N different configurations at frequency F_{CN}. This allows a single tag to operate at multi-frequency. When this system is interrogated by an UWB compatible pulse, different commensurate group of C-sections modulate the interrogation signal in time and it backscatters the response which will be the sum of the response of each group of C-sections $C_1 \ldots C_i \ldots C_N$. Here, the backscattered signal which contains the ID of the tag will be the signal guided through the C–section and re-transmitted by the tag transmitting antenna.

The frequency F_{Cp}, where p=1...i...N, is geometrically related to the C-section as explained in eq. (1). As already said, it is the frequency at which the C-section with length l_{pn} produces a group delay peak and is assigned as the operating frequency for each group such as an ISM band. Later it will be shown that the group delay peaks for each C-section groups can be independent of each other and can vary if and only if the length of the corresponding group is varied. This is the advantage that belongs solely to C-section because of its dispersive property, which discriminates it from linear or meandered transmission line. In the case of linear or meandered line, any variation in length can cause a change in the total delay and will be independent of the frequency, which is the case for the entire existing time domain chipless RFID [6-12].

The filtered signal S_{Cp} (t), the total signal reflected by the tag and arriving at the reader antenna, will consist of two components. The first component, the structural mode, is due to the reflection from the tag and is independent of the length of the C-sections. The second component hereafter called as the tag mode is a part of the signal guided through each group of C-sections and modulated in time at different frequencies and re-transmitted by the output antenna. This will be explained in detail in the results and discussion sections. The time between structural mode and tag mode will be $\Delta t(l_{pn})$, which in turn corresponds to the group delay produced by the C-sections group with length l_{pn} and the delay produced by the two cross polarized antennas at the frequency F_{Cp} since the delay produced by other C-section

groups at this frequency will be negligible. This re-transmitted signal will be sent back to the reader for decoding. The structural mode can be used as the reference and the time difference $\Delta t(l_{pn})$ between the structural mode and different tag modes can be used for generating different combinations of ID. Fig.4. 1 (b) shows the ID-constellation diagram corresponding to the new temporal multi frequency encoding technique.

The tags were manufactured on Rogers R4003 (ε_r=3.55, tanδ=0.0025 and h=0.8 mm). As already explained in the preceding chapter, Rogers were chosen instead of the low cost FR-4 substrate because of its low tangent loss which can enhance the back scattering characteristics of the tag. It was found in [6-7] that high tangent loss significantly reduces the amplitude of the tag modes. The chipless tag consists of two cross polarized UWB antennas, in between we have cascaded commensurate groups of C-sections Fig.4. 2) as shown in Fig.4. 2 (b). CST Microwave Studio 2011 has been used as the simulation platform as explained in the Annexure.

(a)   *(b)*
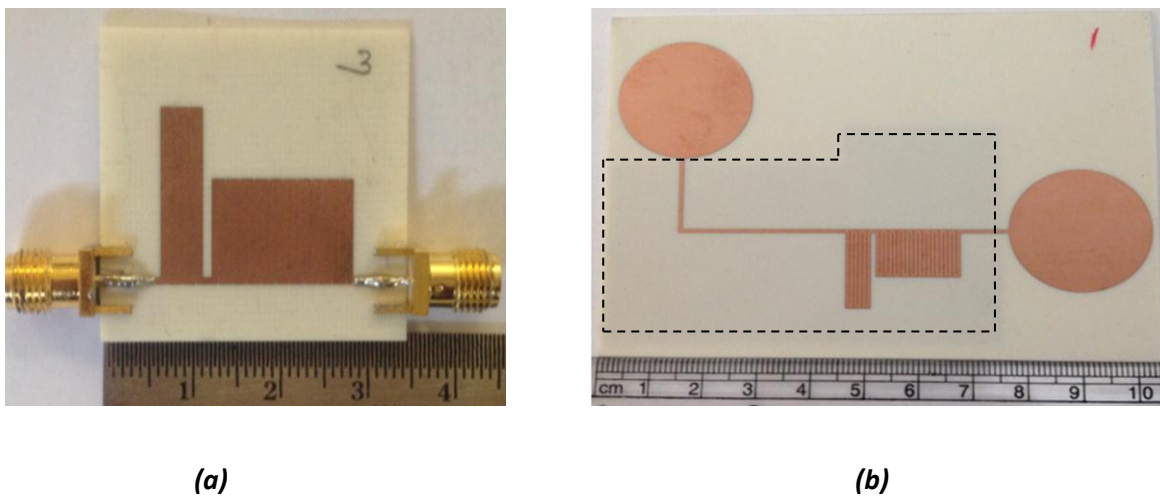
Fig.4. 2: Chipless tag comprised of two groups of C-section; a) prototype, b) chipless tag; g=0.1 mm, w'=w=0.7 mm; ε_r=3.55, tanδ=0.0027, h=0.8 mm. The lower ground plane is indicated by the dashed lines.

4.3   CRITERIA FOR CASCADING THE C-SECTIONS

As already said, the group delay peaks are periodic and each peak can vary by varying the length of the corresponding C-section as shown in Fig.4. 3 (a). In order to increase the group delay, 3 C-sections are used here in a single group. As shown here, the group delay peaks are

(a)

(b)

(c)

(d)
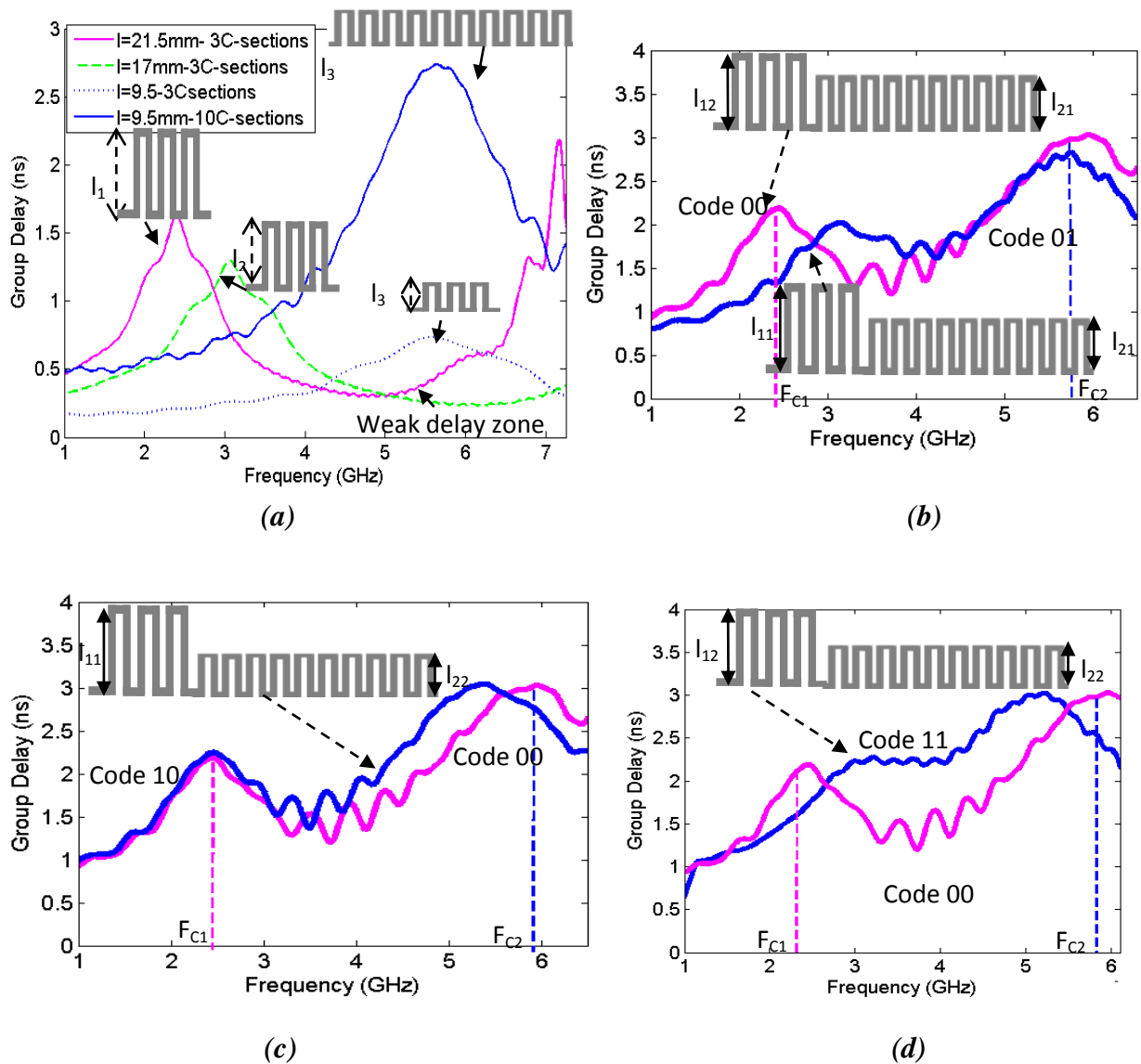
Fig.4. 3 : Principle of Cascading C-sections a) group delay peaks for different lengths of C-sections along with the cascading group delay curve produced by 10 C-sections. Group delay curve of cascaded C-sections corresponding to the code. b) 00 & 01. c) 00 & 10. d) 00 & 11. Each time only the peaks corresponding to the change in length of C-section is varying making the other independent.

periodic and changing the length of the C-section will vary the group delay magnitude and frequency peak. However, for three groups of C-sections, there is a zone where the group delay variations are negligible even though the delay peaks are changing as marked in the figure. This zone, named as weak delay zone, has an importance while cascading commensurate multi-group of C-sections. This zone permits the delay peaks for different

lengths to be independent of each other. In this case, a second group can be added as shown in Fig.4. 3 (b). However, the most important feature of C-section which permits to cascade different groups and hence to produce different delay peaks is its dispersive nature. In the proposed tag, two groups of C-sections are used.

Here in the second group, instead of three, ten C-sections are used because of two reasons (see Fig.4. 3 (a)). First, the value of delay will be less in high frequencies since the length of the C-section is small (l_3 = 9.5 mm). Hence, while utilizing the same number of C-sections, the obtained delay will be very small to detect. Second, increasing the number of C-sections will increase the coupling between C-sections as already explained and hence will make the group delay curve more selective in frequency as shown in Fig. 4.3 (a). However, more number of groups can be incorporated by increasing the coupling within each group so that the group delay peaks will be narrower resulting in a wide range of weak delay zone. This can be achieved by again increasing the number of C-sections in each group or by using multi-layer C-sections as explained in [8]. Thus, it permits the information encoding at several frequencies. Fig.4. 3(b), (c) and (d) respectively represent the evolution of coding results from cascading two groups of C-sections.

4.4   TIME DOMAIN MEASUREMENT TECHNIQUES

The most challenging part of the back scattering measurement is the information separation (delay produced by the tag), especially when the environmental delay has a predominant effect along with the delay produced by the tag. Fig.4. 4 explains the principle used to extract the group delay and hence the tag information. It is the same principle that has been explained in chapter 3 (Fig.3.27 Part B). As we already explained in chapter 3, the back-scattered signal from the horizontally polarized tag antenna consists of structural mode and tag mode. The time Δt between these two modes is given by the equation (16) in chapter 3.
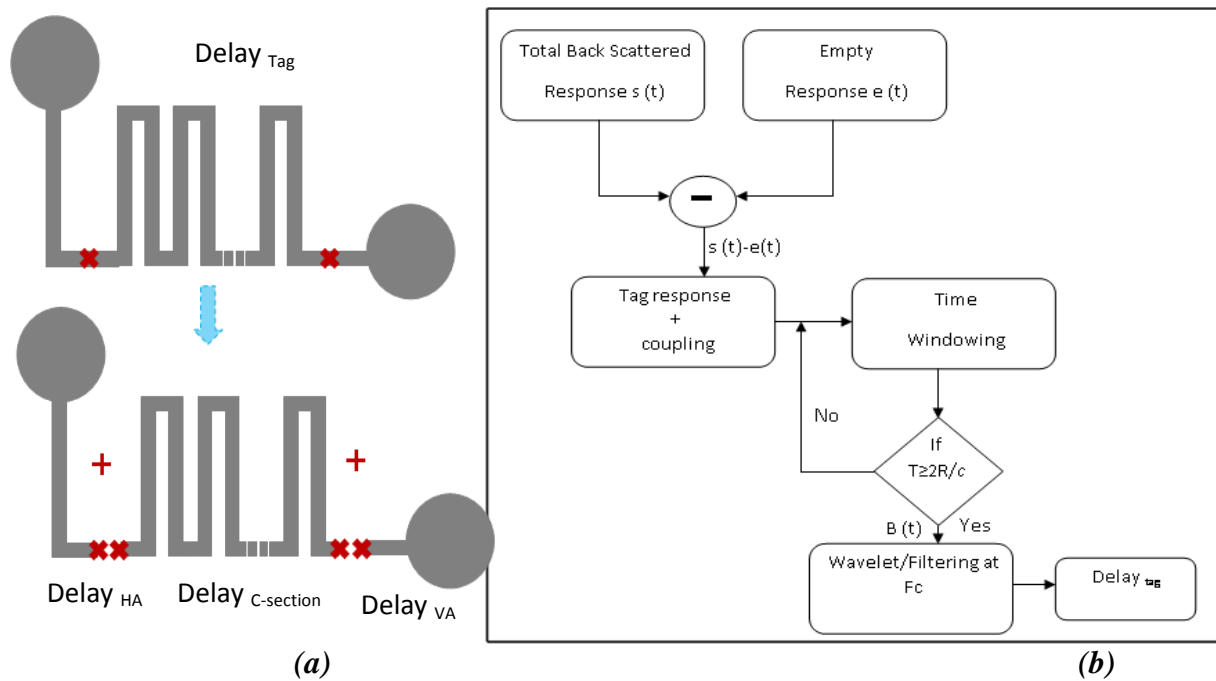
Fig.4. 4 : Principle used to extract the group delay and hence the tag information; a) formulated conclusion, b) process of information separation.

4.5   MICROSTRIP MULTI GROUP OF C-SECTION: PROTOTYPE SIMULATION AND MEASUREMENT RESULTS

In order to prove the concept, 4 different variations have been considered. The lengths are optimized as 21.5 mm and 9.5 mm that correspond to the two ISM bands 2.45 GHz and 5.8 GHz respectively. The prototype with this configuration is chosen as the reference and the corresponding delay obtained has been assigned as the code '00'. The three other combinations were also designed by changing the length of the C-section. In the second combination, length l_{11} is changed to l_{12} by subtracting an amount of length Δl_1 and by keeping the length l_{21} as such. Similarly in the third combination, the length l_{21} is changed to l_{22} by adding an amount of length Δl_2 by keeping the length l_{11} as such. Finally both the lengths l_{11} and l_{21} have been changed to l_{12} and l_{22} and corresponding delay obtained has been assigned as the code 11.

Fig.4. 5 (c) and (d) shows the simulated and measured group delay response of the cascaded commensurate multi group of C-section prototype as a two-port network (see Fig.4.5 (a)).

(a)

(b)

(c)

(d)
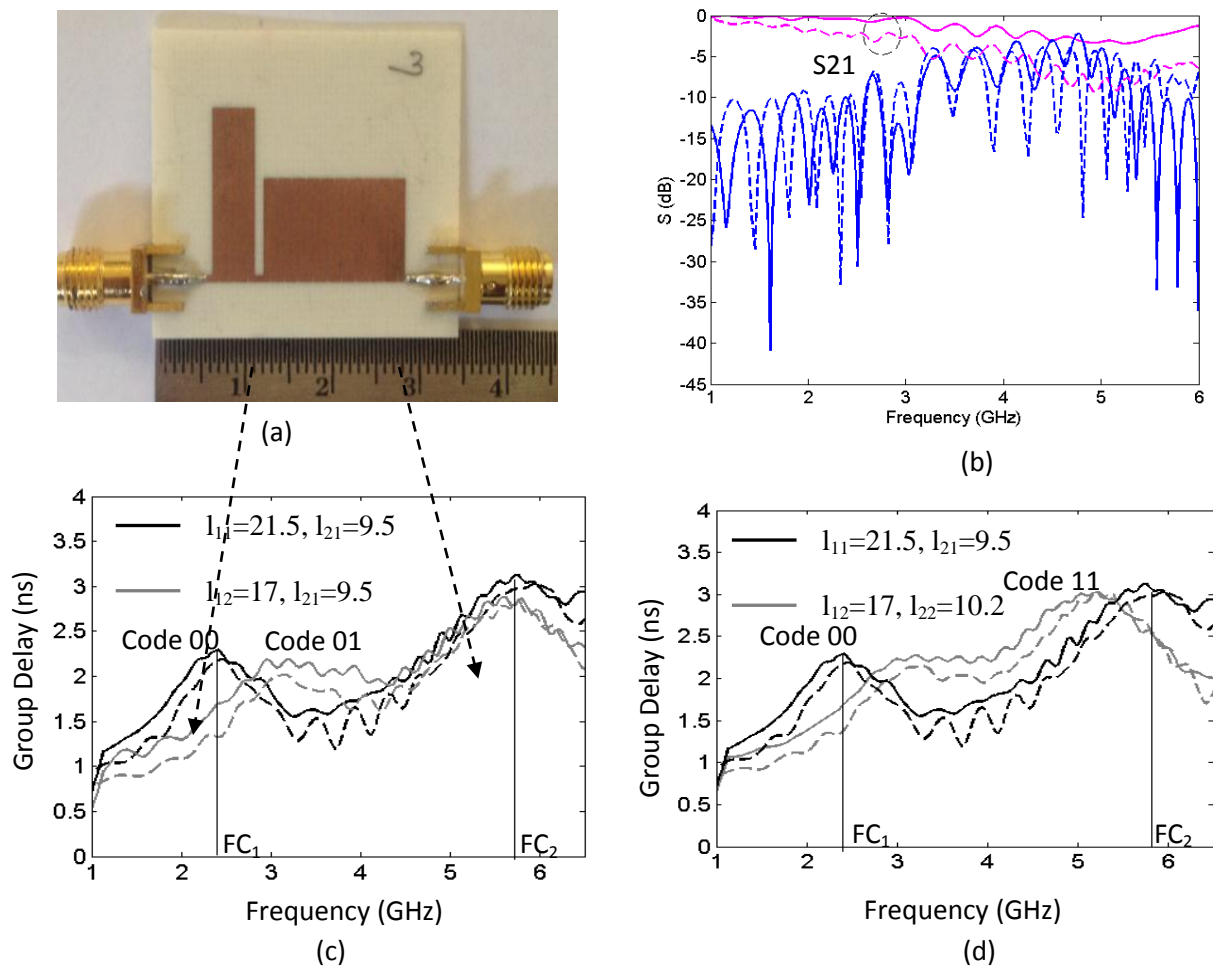
Fig.4. 5 : Results obtained along with the prototype. a) Corresponding prototype. b) Simulated (solid line) and measured (dashed line) S-parameter. Simulated (dashed line) and measured (solid line) group delay for two groups of C-section at two frequencies represent the evolution of different codes; measurement is done using VNA c) 00 & 01, d) 00 & 11; g=0.1, w' =w=0.7; All the units are in mm. ε_r=3.55, tanδ=0.0027, h=0.8 mm.

The two ports of the prototype have been connected to the Performance Network Analyzer (PNAN5222A). The delay produced by each prototype has been measured. As depicted in the figure, the two delay peaks are independent of each other and can be varied by changing the corresponding length of the C-section, which leads to different combination of tags. Thus in general the total number of peaks depends on the total number of C-section groups used. Fig.4. 5 (b) shows the comparison between simulated and measured S-parameter curves. It is found that in measurement the amount of loss is higher than that of simulation. It may be due to the losses occurred while connecting a standard 50 Ω SMA connector to the designed 82 ohms feed line.

However, the group delay is based on phase, which is independent of the magnitude variations; it doesn't reflect in the predicted group delay curves. This again proves the robustness of phase based encoding. As already stated, the group delay peaks are periodic and each peak appears at odd multiple of frequency. This fact should be taken into account while designing tags for multiple frequencies. However, there is also the possibility of using the subsequent periodic harmonic while considering increasing the reliability of the reader. Thus the C-sections open a new path for temporal identification method for multi-frequency.

## 4.6   MICROSTRIP MULTI GROUP OF C-SECTION: CHIPLESS TAG SIMULATION

As already explained, the prototype can be converted to a chipless tag by adding a receiving and transmitting antenna at the two ports of the prototype. Simulation has been done for such a tag. A plane wave in CST microwave Studio has been used to interrogate the chipless tag. A
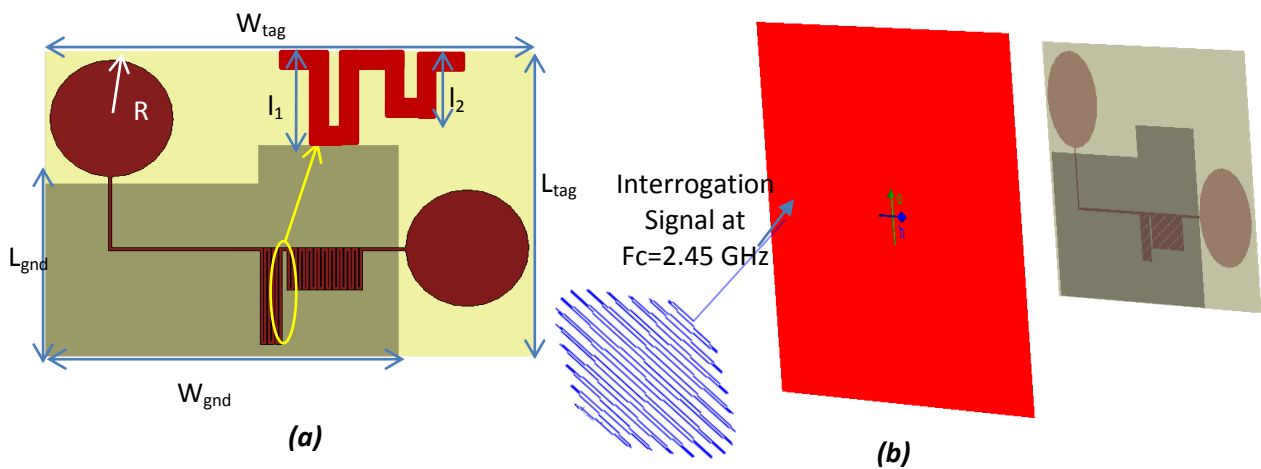
Fig.4. 6 Structure of the tag and simulation in CST. a) Tag structure with various design parameters; l_1=21.5 mm, l_2=9.5 mm, W_{gnd}=74.5 mm, L_{gnd}=38.5 mm, L_{tag}=68 mm, W_{tag}=103 mm and R=13 mm. b) Plane wave excitation using a carrier signal modulated at 2.45 GHz.

Gaussian signal modulated at a carrier frequency of 2.45 GHz is used as the excitation signal. It is the same signal which we have already explained in chapter 3; except the carrier frequency (Fc=2.45 GHz, BW=0.1).Fig.4. 6 (a) shows the structure of the tag and Fig.4. 6 (b) represents the plane wave excitation in CST Microwave Studio.

Two far-field probes were placed at a distance $R \geq 2D^2/\lambda$, where R is the far-field distance and D is the largest possible dimension of the antenna. The probes were oriented with the same polarization as the tag antennas. The plane wave was interrogated using vertical linear polarization since the tag receiving antenna has the vertical linear polarization. The tag receiving antenna receives the signal which further guided through the C-sections, modulated by its length and re-transmitted by the transmitting antenna. Different excitation signals corresponding to the operating frequencies of the two C-section groups were used. This was to easily understand the behavior of the tag. Further, an impulse signal can be used as the excitation signal and the corresponding tag response can be filtered at the specific operating frequencies. Fig.4. 7 (a) and (b) shows the backscattered signal collected by the far-field probes at 2.45 GHz (F_C (l_1)) and 5.8 GHz (F_C (l_2)) [10].

(a)

(b)
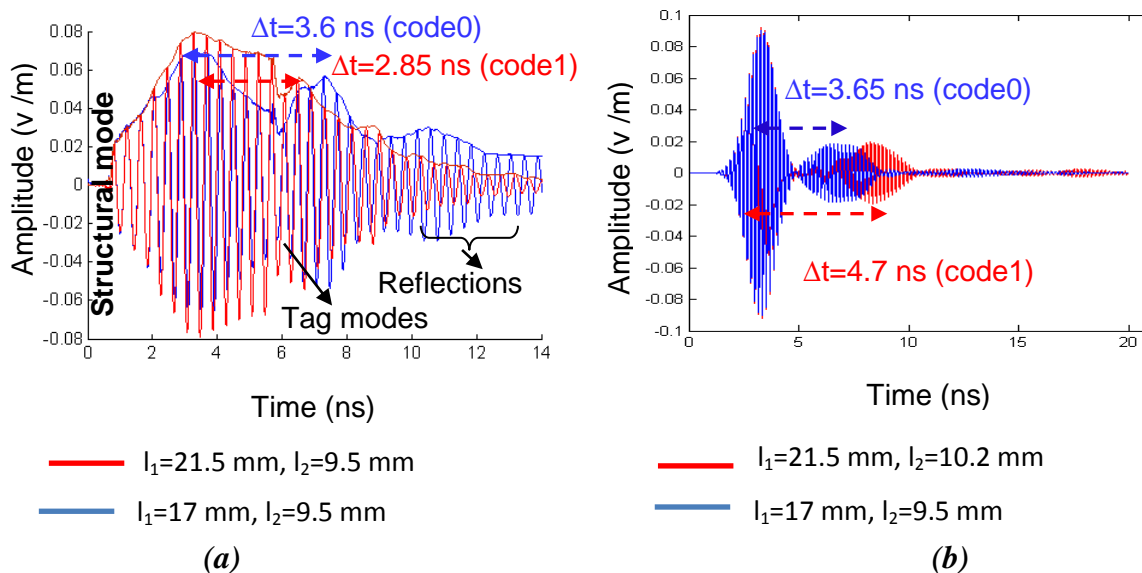
Fig.4. 7 : Back scattered signal collected by the far-field probe corresponds to the code 00 and 11. a) at 2.45 GHz, b) at 5.8 GHz. Gaussian modulated signals with BW as 0.1 and cut off frequencies as 2.45 GHz and 5.8 GHz are used as the excitation signals.

Different tag modes can be seen in the figure. Unwanted reflections can be seen in Fig.4. 7 (a) which may be due to the poor impedance matching of the tag antennas at the selected frequency. As shown in Fig.4. 7, the tag modes are separated depending on the length of the C-section. The difference between structural mode peak and tag mode peak can be used to calculate the time delay. It is clear from the figure that structural mode is constant in all simulations irrespective of the length of the C-section and only tag mode varies with respect

to the length of the C-section. Table 4. 1 shows the different delays obtained through simulation and by calculation. Calculated delay is the delay obtained using the eq. (21). Group delay corresponding to the tag antennas has been calculated by the same procedure as explained in the chapter three.

Table 4. 1 : Chipless tag (tag with antennas and C-section) : Calculated and simulated delays obtained along with the percentage error.

$Delay_{VA2.45GHz}+Delay_{HA2.45GHz}= 0.68$ ns $+ 0.53$ ns $=1.21$ns

l_{11} (mm)	l_{21} (mm)	GD_C Sim. (ns)	Calc. Δt (ns) Sim.	Sim. Δt (ns)	Percentage Error between simulated and calculated delay %
21.5	10.2	2.24	3.45	3.65	5.7
21.5	9.5	2.18	3.39	3.6	6.19
17	10.2	1.44	2.65	2.89	9
17	9.5	1.33	2.54	2.85	12
$Delay_{VA5.8GHz}+Delay_{HA5.8GHz}= 0.64$ ns $+ 0.47$ ns $=1.11$ns					
21.5	10.2	2.97	4.08	4.7	15.1
21.5	9.5	2.56	3.67	3.75	2.1
17	10.2	2.83	3.94	4.6	16
17	9.5	2.65	3.76	3.65	2.9

Here, in order to prove the concept, only four group delay levels have been considered which corresponds to 2 bit coding. More group delay levels can be considered at each frequency and hence can improve the coding capacity. In this case, each group delay peak should be more selective. Such an approach can be seen in chapter 5 in the case of multi-layer approach. The next section explains the chipless tag measurement conducted in the anechoic chamber using an oscilloscope and vector signal generator. It also incorporates the real environment measurement conducted using commercially available radar.

4.7   MICROSTRIP MULTI GROUP OF C-SECTION: CHIPLESS TAG MEASUREMENT

For experimental validation, two horn antennas were used as the reader antennas, which are oriented in a cross-polarized form as shown in Fig.4. 8 (a). These horn antennas are placed at a distance of 10 cm to each other and they can operate within 700 MHz-18 GHz band with a gain of 12 dBi. The chipless tag and the reader antennas were placed at distance

(a)   *(b)*
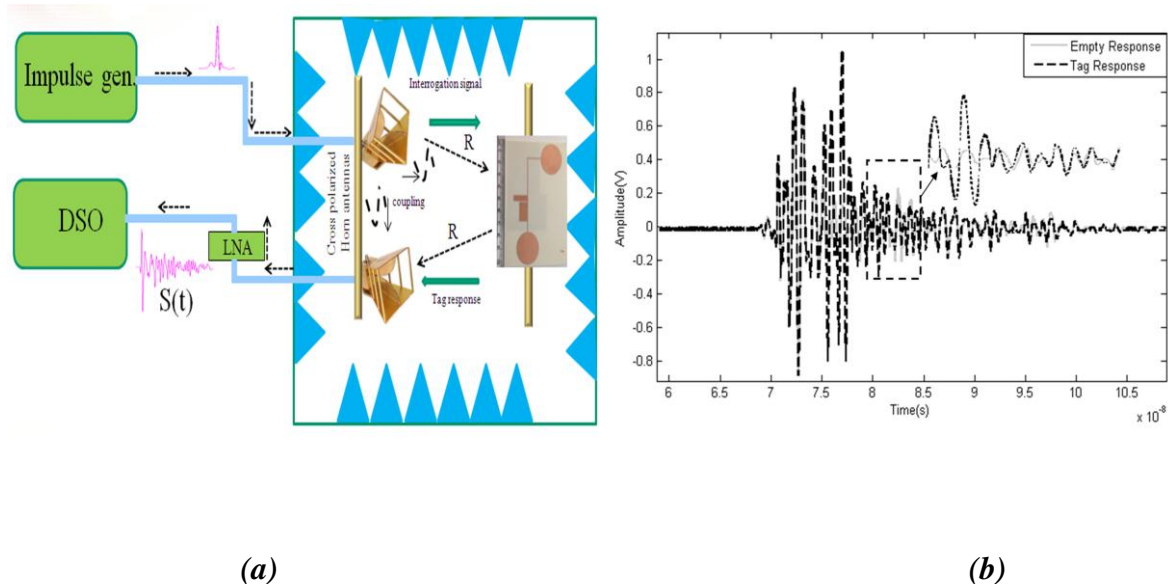
Fig.4. 8 : Experimental set up together with empty ad tag responses. a) Measurement Set-Up. b) The measured empty response and tag response, insight view: zoomed version of the two responses.

of 1.5 m.

Both reader antennas and tags were mounted on plastic stands. A Gaussian signal with pulse width of 90 ps and maximum amplitude of 1.2 V has been generated by Picosecond 10060A and used as the input for the system. The back scattered signal has been measured using digital oscilloscope DSO91204A which is connected to the receiving horn antenna through an LNA (low noise amplifier). Contrary to the measurement reported in [11] where read range is limited to 50 cm, the presence of LNA increases the read range until 1.5 m. The only measurement needed is the measurement for empty chamber and with tag, which is not difficult in a practical point of view.

As discussed in chapter 3, this is a prime advantage of the time domain and cannot be used in frequency domain where the amplitude of the signal (RCS) is used for the encoding. This again proves the robustness of temporal approach. Background subtraction has been done and a time windowing is applied as already explained. This background signal has a comparable magnitude with the scattering from the tag itself as shown in Fig.4. 8 (b). Thus an empty measurement (measurement without any tag) was done to perform the background subtraction. This time domain signal was subsequently subtracted from the all other measurements for different chipless tags. The impulse signal used is the same signal that we have represented in chapter 3 with 90 ps pulse width.

As we already discussed in chapter 3, in order to separate the structural mode and different tag modes at the frequency of interest, Continuous Wavelet Transform (CWT) is used [12]. The sole difference here is that each time two deterministic Gaussian signal will be used with different carrier frequencies F_{C1} and F_{C2}. The CWT performs a correlation analysis and as a consequence maximum output can be expected when the input signal mostly resembles the wavelet template. This input signal will be the time domain signature of the tag with amplitude in Volt. Consider the backscattered response of the tag after time windowing as *B(t)* (see Fig.4. 4).

A Gaussian signal modulated at a carrier frequency of F_{C1} and F_{C2} is chosen as the known deterministic signal *p(t)*. The rest all operations are as explained in chapter 3. At each time, a Gaussian modulated signal at a carrier frequency of F_{C1} = 2.45 GHz and F_{C2} = 5.8 GHz respectively is used as the known deterministic signal. A cross correlation of the tag response with these modulated signals will results in two different peaks as shown in Fig.4. 9 (a) & (b) shows the measured delays obtained at 2.45 GHz and 5.8 GHz respectively along with the corresponding binary code. For better view, here the envelope of τ is represented.

First peak is the structural mode, which remains constant for all the tag combinations while the second component seems to be changing according to the length of the C-section. The delay between structural mode and tag mode will be the delay of the tag 'Delay $_{tag}$' and can be used for the encoding. It is clear from the figure that the delays are independent of each other and will change only by a change in the length of the C-section. In all other cases it remains the same.

(a)   (b)
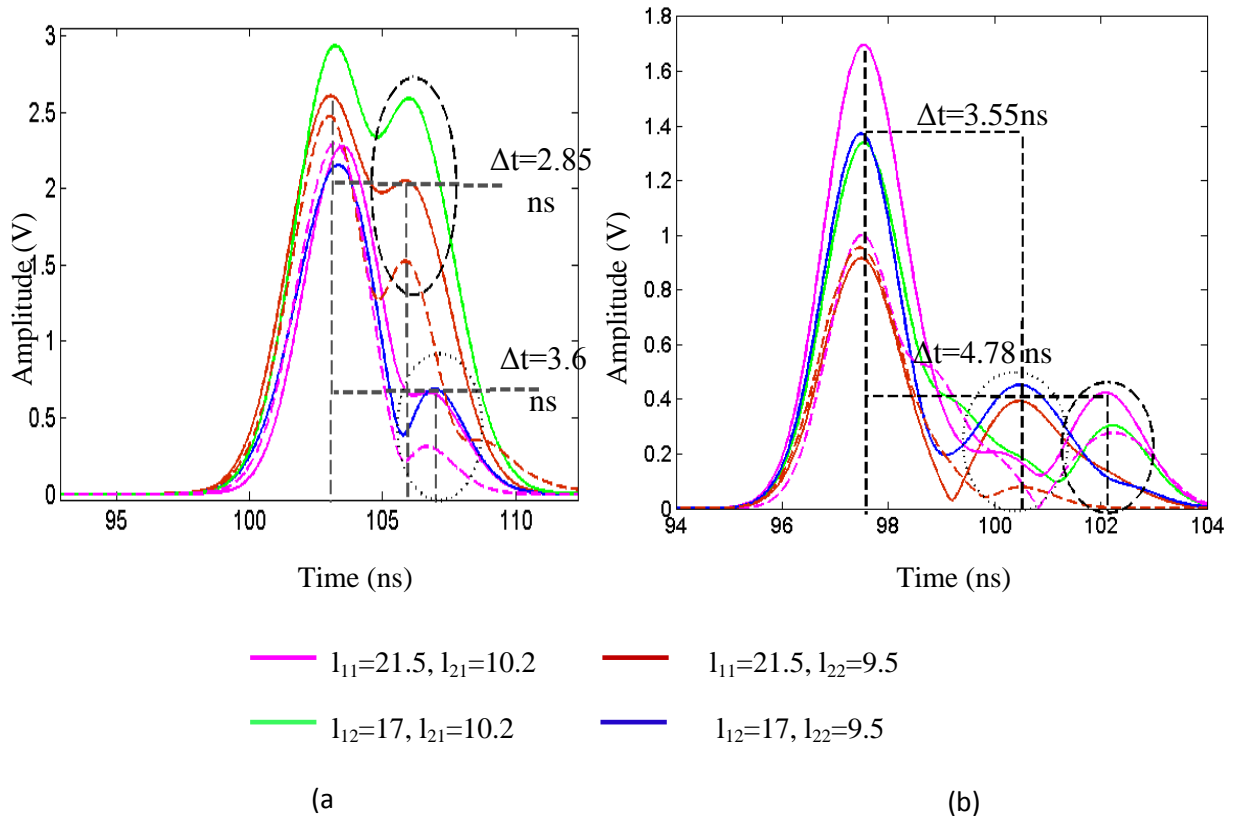
Fig.4. 9 : Measured delays for chipless tag with two groups of C-section; a) at 2.45 GHz, b) 5.8 GHz. Dashed line represents the response obtained from the commercial radar Novelda. Solid lines represent measurement using DSO and pulse generator. All units are in mm.

Table 4. 2 gives the calculated, simulated and measured delays obtained along with the delay produced by the UWB antennas at 2.45 GHz and 5.8 GHz. In this case the calculated delay is the sum of delay produced by cross-polarized antennas and C-sections at. 2.45 GHz and 5.8 GHz respectively in simulation, by using the equation (16) explained in chapter 3.

Measurement was also done using commercially available UWB radar Novelda (NVA6100) [4]. The dashed lines in Fig.4. 9 represent the results obtained for one of the each

combination. As shown in figure, there is a good agreement with the results obtained using a Digital Oscilloscope and impulse generator. As already explained, the results produced by the radar have a less amplitude, which may be due to the poor dynamic range of the radar compared to the Oscilloscope. The maximum amplitude produced by Picosecond pulse generator is 2 V into a 50 Ω load giving a maximum instantaneous power of 19 dBm and that of Novelda is of the order of 200 mV (6 dBm).

Table 4. 2 : Chipless tag (tag with antennas and C-section) : Calculated , simulated, and measured delays obtained along with the percentage error.

$$\text{Delay}_{VA2.45GHz}+\text{Delay}_{HA2.45GHz}= 0.68 \text{ ns} + 0.53 \text{ ns} =1.21\text{ns}$$

l_{11} (mm)	l_{21} (mm)	GD of C-secion Sim. (ns)	Calc. Δt (ns) Sim-ulation	Sim. Δt (ns)	Meas. Δt (ns) DSO	Prcentage Error between simulated & measured (DSO)	Meas. Δt (ns) Novelda radar	Prcentage Error between simulated & measured (Novelda)	code
21.5	10.2	2.24	3.45	3.65	3.5	4.2	3.7	1.36	01
21.5	9.5	2.18	3.39	3.6	3.58	0.5	3.65	1.38	00
17	10.2	1.44	2.65	2.89	2.85	1.38	2.95	2.07	11
17	9.5	1.33	2.54	2.85	2.8	1.7	2.91	2.1	10

$$\text{Delay}_{VA5.8GHz}+\text{Delay}_{HA5.8GHz}= 0.64 \text{ ns} + 0.47 \text{ ns} =1.11\text{ns}$$

21.5	10.2	2.97	4.08	4.7	4.78	1.7	4.77	1.48	01
21.5	9.5	2.56	3.67	3.75	3.55	5.3	3.55	5.3	00
17	10.2	2.83	3.94	4.6	4.55	1.08	4.77	3.6	11
17	9.5	2.65	3.76	3.65	3.48	4.65	3.49	4.38	10

The Federal Communications Commission (FCC) defines a power spectral density (PSD) of -41.3 dBm/MHz for the UWB band (3.1 GHz-10.6 GHz) [13]. If a CW signal is sent, it has to be very weak. But the possible way could be to develop an impulse radio based approach. In this case, a monocycle pulse of width lower than 100 ps is sent by the reader, but with a very low duty cycle. The minimum is 1 pulse/s (i.e., a duty cycle of 0.01%). European Telecommunication Standard Institute (ETSI) also allows the same PSD/MHz for the UWB band (3.1 GHz-4.8 GHz and 6 GHz-9 GHz). For ISM bands (2.4 GHz-2.4835 GHz), ETSI allows 10 mW (10 dBm) of e.i.r.p. (effective isotropic radiated power) for generic use. Thus, the allowed emission power is more in the case of ISM bands.

4.8   CONCLUSION & PERSPECTIVES

A novel encoding for chipless RFID based on temporal multi-frequency is proposed in this chapter. The proposed tag can operate in ISM bands which permits the emission of more power making it suitable for applications where read-range has an importance. A good reading distance of 1.5 m is obtained with a UWB compatible pulse. The accordance of the results in the real environment using commercial radar proves its importance in practical applications. This technique also proves the robustness of phase and provides good results without a calibration tag. The robustness of the phase is the ability of phase to remain same in all environmental conditions. It has been proved experimentally in [14] that the phase information is more resilient to noise and can be read from a greater distance when compared to the amplitude information of the frequency signature. The multi frequency approach in

time domain provides a new way of increasing coding capacity with a significant amount of delay. However, for the tags presented in this chapter do not have a higher order number of bits. In order to prove the concept, only 4 combinations (hence 2 bits) are explained in this chapter. If we use 8 variations, as we explained in the preceding chapter, at each frequency, multi-frequency approach will permits coding of 6 bits. The succeeding chapter will explain the case where more number of delay variations will be considered. The size of the tag is more important now. This can be reduced by considering a more compact antenna, as the global size is due to the antenna sizes. Also techniques can be used to improve the amplitude of tag modes so that circularly polarized antennas can be used instead of the cross polarized one. Utilization of multi-layer design is also another solution. This will in turn increases the capacity of coding since more number of delay levels can be included instead of four as in the existing one. Because the delay peaks will be more selective in frequency for a multi-layer design. The number of C section groups can be increased to increase the capacity of coding. In this case, the structure should be more selective in frequency. As already explained multi-layer C-sections is a possible solution for this. Thus, this chapter proves the use of temporal multi frequency encoding in chipless RFID applications. Instead of two groups of C-section, cascading more number of groups of C-sections in a selective manner is also another way of increasing coding capacity. These are the preliminary results obtained and the tag can be reproduced in a more efficient way. The cost of the tags is more important now. However, use of flexible circuits like paper or PE can reduce the cost significantly. As already explained, the coding capacity can be increased by the use of multi-layer structure which will be explained in the next chapter.

REFERENCES

[1] C. Mandel, B. Kubina, M. schubler, and R. Jakoby, "Group Delay Modulation with Meta-material Inspired Coding Particles for Passive Chipless RFID, IEEE International Conference on RFID-Technologies and Applications, Nice, France, November 2012.

[2] S. Gupta, A. Parsa, E. Perret, R.V. Snyder, R.J. Wenzel, and C. Caloz, "Group delay engineered non-commensurate transmission line all-pass network for analog signal processing," IEEE Transactions on Microwave Theory and Techniques, September, 2010, vol. 58, issue. 9, pp. 2392-2407.

[3] S. Gupta, B. Nikfal, and C.Caloz, "Chipless RFID System Based on Group Delay Engineered Dispersive Delay Structures", Antennas and Wireless Propagation Letters, IEEE, vol. 10, pp. 1366-1368, 2011.

[4] Novelda Nanoscale Impulse Radar (2013 January) [Online] Available : https://www.novelda.no/

[5] A.Vena, E.Perret, and S. Tedjini, "Design of Compact and Auto Compensated Single Layer Chipless RFID Tag", IEEE Transactions on Microwave Theory and Techniques, vol. 60, No 9, pp. 2913 – 2924, 2012.

[6] R. Nair, E. Perret, S. Tedjini,"Chipless RFID based on Group Delay encoding" ,IEEE International Conference on RFID technologies and Applications(RFID-TA),September 2011,Barcelona,Spain,pp. 214-218.

[7] S. Hu, Y. Zhou, C. Law, and W. Dou, "Study of a Uniplanar Monopole Antenna for Passive Chipless UWB-RFID Localization System", IEEE Transactions on Antennas and Propagation, vol. 58, No 2, pp. 271-278, 2010.

[8] R.K. Settaluri et al. "Design of Compact Multi-level folded line RF couplers", IEEE Transactions on Microwave Theory and Techniques, Vol.47, No.12, December 1999, pp.2331-2339.

[9] A. Ramos, A. Lazaro, D. Girbau, and R. Villarino "Time domain measurement of time-coded UWB chipless RFID tags", Progress In Electromagnetic Research, vol. 116, pp. 313-331, 2011.

[10] R. Nair, E. Perret and S. Tedjini, "Temporal Multi-Frequency Encoding Technique for Chipless RFID Applications", IEEE MTT-S International Microwave Symposium IMS 2012, Montréal, Canada, June 17-22.

[11]   A. Vena, E. Perret, and S. Tedjini, "Novel compact RFID chipless tag," presented at the Proc. Progress in Electromagnetic Research Symp., Marrakesh, Morocco, Mar. 20–23, 2011.

[12]   A. Lazaro, A. Ramos, D. Girbau, and R. Villarino, "Chipless UWB RFID tag detection Using Continuous Wavelet Transform ", IEEE Antennas and Wireless Propagation Letter, vol.10, 2011, pp.520-523.

[13]   S. Härmä, V. P. Plessky, X. Li, and P. Hartogh, "Feasibility of ultrawideband SAWRFID tags meeting FCC rules," IEEE Trans. Ultrason., Ferroelect. Freq. Control, vol. 56, no. 4, Apr. 2009.

[14]   S. Preradovic, I. Balbin, N. C. Karmakar and GF. Swiegers, "Multireasonator based chipless RFID system for low cost item tracking," IEEE Trans. Microwave Theory & Tech, vol. 57, issue. 5, pp. 1411-1419, May, 2009.

CHAPTER FIVE
MULTI-LAYER C-SECTIONS AND DELAY BASED ID GENERATION USING FLEXIBLE SUBSTARTES

CHAPTER SIX
CHIPLESS RFID HUMIDITY SENSOR USING SILICON NANOWIRES

This chapter explains a novel temporal chipless RFID sensor tag for humidity sensing applications. The proposed tag is composed of C-sections and Ultra-Wide band antennas. Silicon nanowires have been manually deposited to the strips of the C-sections. Silicon nanowires change permittivity upon humidity absorption which in turn change the magnitude and phase of the reflected signal and hence group delay also. A prototype of the tag is tested and the results are validated. Further, the measurement with a chipless tag is incorporated. The measurement was conducted in real environment. A very good variation in the magnitude, phase, and group delay was observed as a function of relative humidity. A magnitude change of 30 dB and group delay variation of nearly 22.3 ns was observed near the fundamental frequency over a bandwidth of 40 MHz for a relative humidity variation of 60.2 %-88 %. Measurement was also conducted by increasing the ambient temperature. It was proved that an increase in ambient temperature causes a huge variation in the S21 magnitude, phase, and hence group delay.

CHIPLESS RFID HUMIDITY SENSOR USING SILICON NANOWIRES

6.1   INTRODUCTION

The demand for RFID enabled sensor has enhanced in the modern world especially in areas such as logistics, anti-counterfeiting, supply chain monitoring etc. [1]. However their need is limited due the cost of chip based RFID tags and their sensitivity and reproducibility. Chipless RFID sensor tags owing to their low cost have opened a new path for low cost wireless sensor tag applications. Also, unlike the approaches used in UHF RFID sensors where the chip is directly involved in capturing the quantity to be measured, the absence of the chip will allow to increase the sensitivity significantly. Indeed, the use of a low cost conventional UHF RFID chip can cause additional threshold. The same way as in conventional RFID, but more recently, the addition of "sensor" functionality in chipless RFID tags appeared in [2] using a delay line for identification and a thermistor for sensing. A more integrated wireless chipless sensor tag, without identification to detect ethylene gas can be found in [3]. The sensor is based on the use of a capacitor that is directly integrated to the tag. Thereafter, the same team also has added the ID in the chipless tag using a delay line [4]. However, in this case, the sensor function is simply reproduced by integrating a lumped element at the end of the delay line. To the author's knowledge, the first compact wireless chipless RFID sensor tag which validates the identifier and sensing the physical quantities is [5]. It also proves the possibility to realize the sensor tags without any localized CMS element or complex techniques of realization, instead using a deposition of silicon nanowires which are potentially printable.

On the other hand the idea of using nanomaterial as wireless sensor is not recent. [6-8] represent the first investigations that have been conducted in this area, here a proof of concept of the principle "theory" of the wireless sensor based on the use of nano materials can be found. However, it is noted that no practical implementation (wireless measurement of the variation of the physical parameter) is presented. Instead difficulties in the realization of remote measurements (sensitivity of the RF channel in relation to the tag environment) are underlined [6]. In addition, none of these articles consider associating an identifier in order to

obtain what we previously called tag-sensor. This is a critical application point of view while considering a network of sensors in a same area.

Humidity sensors based on SAW can be also seen in the literature [9-11]. The principle of these sensors is based on the change of velocity or attenuation of the surface acoustic wave caused by the change in electrical properties, elastic or dielectric of the propagation medium under the effect of humidity. Typically, the humidity sensors are formed by the association of two separate inter-digital transducers and a film of a material sensitive to humidity such as hygroscopic film of cellulose or nanomaterials. A chipless RFID tag combined with a SAW sensor for producing a wireless sensor can be seen in [11]. This sensor also incorporates chemical sensing which is achieved from the respective analyte compound that reacts reversibly and non-covalently with the recognition material and in this way directly changes the electronic properties of the respective device. However, the methods used for the realization of SAW devices rely on techniques developed in microtechnology, thus increasing the cost and complexity of manufacturing the sensor.

In this chapter we continue the approach that has been previously introduced in [5] but this time by applying it to time domain chipless tags. One interesting feature of time domain tags compared to frequency domain tags is their ability to operate in narrow frequency bands more precisely ISM bands [12-13]. ISM bands permits the use of more power level which in turn increases the read range in the order of some meters which is approximately three times larger than that of the tags that operates with UWB standards (as explained in the preceding chapter, with UWB band, a reading range of 50 cm is obtained, with ISM band a reading range of few meters is obtained as in the case of SAW).

This chapter explains a novel chipless RFID time domain humidity sensor tag using silicon nanowires which can produce ID and sensing function at a single frequency. The tag ID purely depends on the length of the proposed C-section. The sensing is achieved by depositing the nanowires on the strips of transmission line sections. Nanowires change their properties upon humidity absorption which in turn changes the magnitude and phase of the reflected signal from the tag and hence group delay. The proposed tag is composed of single group of C-sections (see Fig.6. 1). However, the coding capacity for the identification can be increased by using multi group of C-section [13]. The identification part is already explained in the previous chapters and hence this chapter is mostly oriented in the sensing part. First the results for the prototype measurement are explained. Measure was conducted for different temperatures. Furthermore, the backscattering real environment experimental results are

explained and the predictions are validated with the simulations using CST Microwave Studio. Thus, the obtained results prove the efficiency of silicon nanowires in humidity sensor for remote applications.

6.2   OPERATING PRINCIPLE

As shown in Fig.6. 1, the chipless sensor tag consists of cross polarized UWB antennas and cascaded commensurate C-sections. The C-section is capable of producing a group delay peak at each odd multiple of $\lambda_g/4$ of frequency; where λ_g is the guided wavelength; i.e. for a particular length l_i; where i=1,2,3,..n; as already explained in the preceding chapters, the frequency at which group delay peak is maximum is approximated by $F(l_i) = c/(4*(\varepsilon_{eff})^{1/2}l_i)$, where ε_{eff} is the effective permittivity of the microstrip line. The receiving antenna in the chipless tag receives the integration signal sent by the reader. The signal guided through the C-sections and the transmitting antenna at the other end will re-transmits the response of the tag to the reader with a specific delay. Consider 'n' tags with different lengths $l_1,l_2...l_n$ where l_n is the maximum length and one frequency $F(l_n)$ (the same tags explained in Chapter 3 can be considered). These 'n' tags will be able to produce different IDs with ID1=$\Delta t(l_1)$, ... , IDn= $\Delta t(l_n)$, where Δt is the amount of temporal shift of the signal component $F(l_n)$ while passing through the C-sections with lengths $l_1,l_2...l_n$. As shown in Fig.6. 1, these IDs will be different since each of them has a particular time slot depending on the length of the C-section. Suppose silicon nanowires have been deposited to the tag with length l_1. Nanowires change their characteristic upon humidity absorption and cause the shifting of group delay curve of the corresponding C-section within the allocated time delay slot as shown in Fig. 6.1.
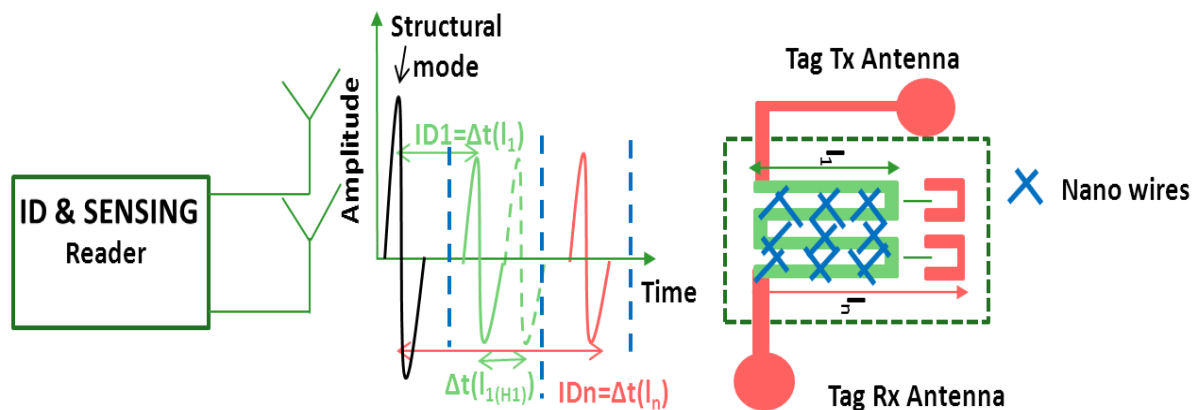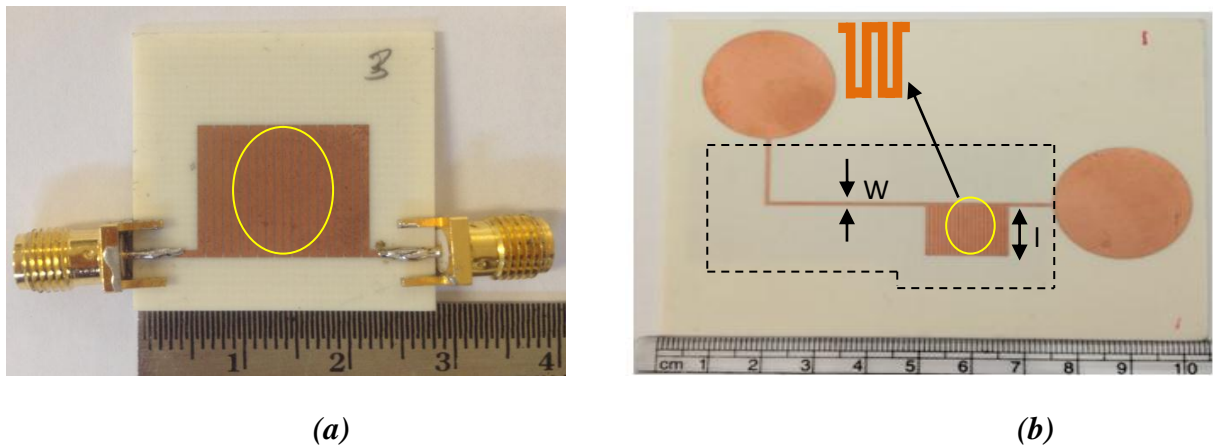

Fig.6. 1 : **Principle of identification and sensing.**

In this case, tag response without nanowires can be considered as the reference and any shift from this response due to nanowires can be considered for the sensing application. As indicated in the figure, this time shift will be a function of relative humidity, ie. $\Delta t(l_{1(H1)})$, where H denotes the relative humidity.

(a)   *(b)*

Fig.6. 2 : Fabricated chipless tag with the prototype. a) The prototype of the proposed chipless tag. b) Chipless tag with one group of 10 C-sections; bottom ground plane is marked as dashed lines. w=0.7 mm, l=14.9mm. The yellow color represents the zone for depositing nanowires.

Fig.6. 2(a) shows the structure of the tag without antennas (prototype). The tag with length of C-section as l=14.9 mm and tag dimension of 9.8x6.3 cm^2 is chosen as the device under test (DUT). For this work, the silicon nanowires have been developed by catalytic
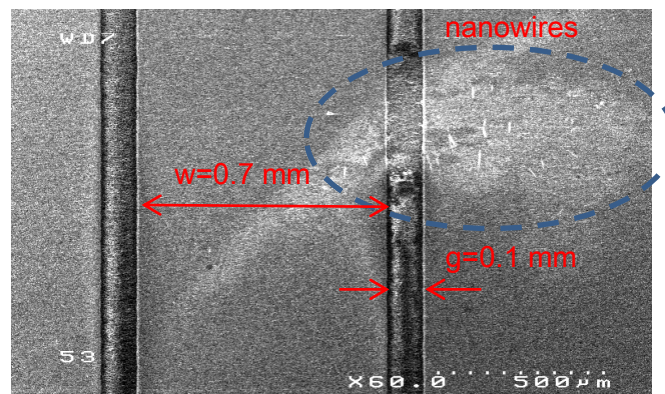

Fig.6. 3 : Microscopic image of silicon nanowires deposited between the strips of the C-sections. The white color represents nanowires.

chemical vapour deposition. The nanowires have been put in a solution of alcohol and a drop has been manually deposited on the strip of the C-section where the electric field is maximum, using a pipette. The alcohol will evaporates and the nanowires will remain fixed on the C-section. Since we are not aware of the amount of nanowires dissolved in alcohol, it is a difficult task to control the amount to be deposited. Pipette allows the deposition of nanowires as drop by drop and hence can understand that two drops means two times more the nanowires. But we cannot guarantee the distribution of nanowires. A microscopic image of typical silicon nanowires deposited in between the strips of the C-sections is presented in Fig. 6.3. It was found that the nanowires were not uniformly deposited.

6.3   SENSOR PROTOTYPE MEASUREMENT SET-UP

The measurement set up consists of a plastic box with water as shown in Fig.6. 4 [14]. A humidity-temperature meter was connected to the box. The probe of the humidity temperature meter was placed inside the box. The box is closed and the variation of relative humidity was measured and the data was saved automatically at each 10 seconds using a homemade interface program. This was done as in the same manner of previously explained RF measurements. It enables to visualize the tag response as a function of humidity. Once the box is closed the relative humidity will reach until 100%. Typically the humidity starts at 60%, which is assumed to be the humidity of the atmosphere inside the room. The measurement time is very important. The time is a function of the temperature of water. If the temperature is high, the measurement rapidly ended up with 100% of RH variation which causes difficulty in conducting the measurement for low RH variation, for example at 50%. If the temperature of the water is low, it is found that, we need to wait a long time to reach the RH variation at 100%. In this case, the measurement was obliged to stop before reaching 100% of RH variation. The measurement was done separately for the two different prototypes with and without nanowires. Variation of magnitude, phase and group delay was measured for the humidity sensor application. The measurement was performed in an air conditioned room with a temperature of 24°C and this temperature is constant throughout the measurement time.
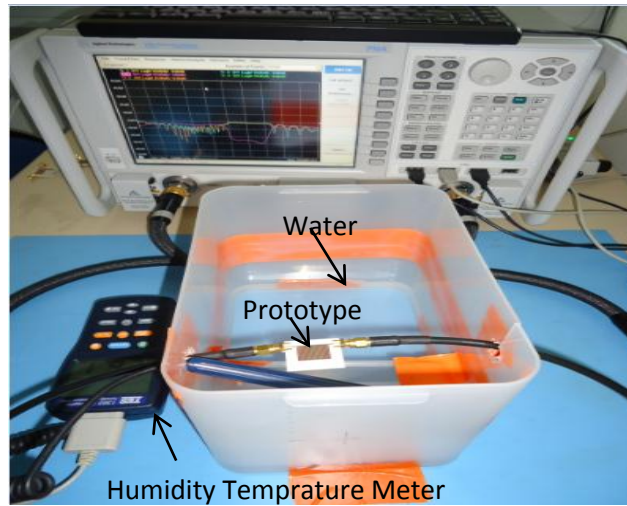
Fig.6. 4 : Measurement set-up for the sensor tag prototype.

A few drops of nanowires have been deposited on the metal strips of the prototype with length 14.9 mm and kept inside the closed plastic box. The two ports of the tag prototype were connected to the VNA. The variation of magnitude, phase, and group delay has been measured.

6.4   SENSOR PROTOTYPE: EXPIRIMENATL RESULTS

The S21 magnitude, phase, and group delay of the device has been measured for different

*(a)*   *(b)*
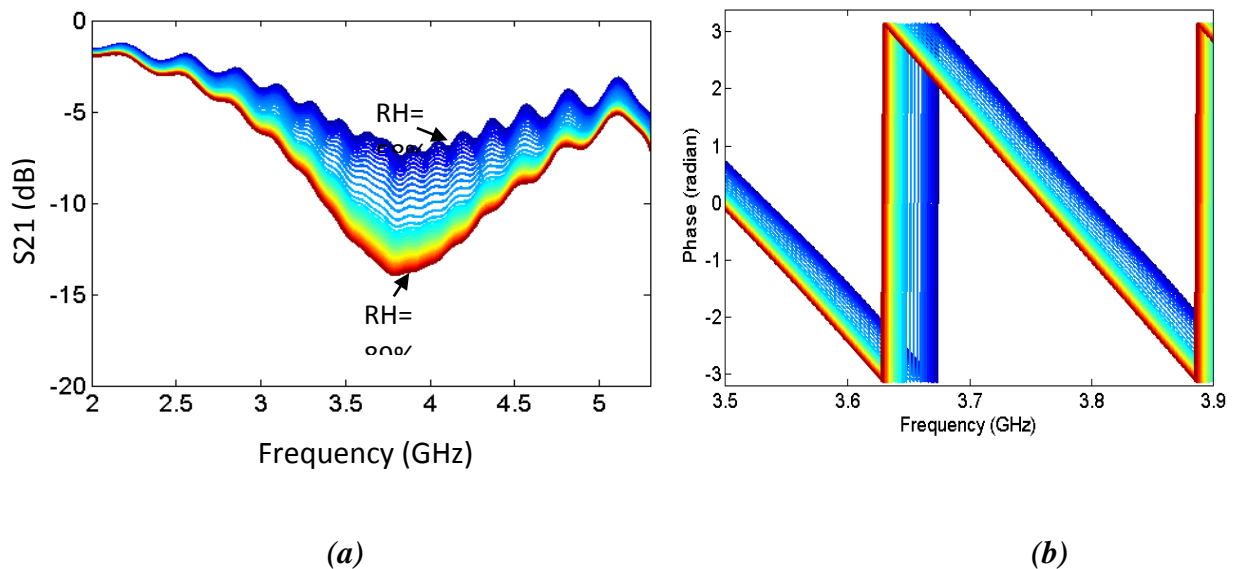
Fig.6. 5 : S21 magnitude and phase measured at fundamental frequency for the tag prototype (Fig.6. 2) with a relative humidity variation of 58%- 89% and an ambient temperature of $23°C$. a) S21 b) Phase.

ambient temperature conditions inside the plastic box. It should be noted that only the temperature variations inside the box is taken into account. However, the ambient temperature inside the measurement room, which is set to be 23-24°C, was always remains constant. 12 drops of nanowires have been deposited on the C-sections with length l=14.9 mm (shown in Fig.6. 2 (a)); which corresponds to a frequency $F(l_n)$=3.5 GHz; and kept inside the closed plastic box. Variations of S21 magnitude phase and group delay was observed at the fundamental frequency at 3.5 GHz over a bandwidth of 20 MHz. Fig.6. 5 (a) shows the S21 magnitude measured with a temperature inside the box of 23°C (room ambient temperature). 7 dB of magnitude change was observed in this case. Fig.6. 5 (b) shows the change in phase observed in the fundamental frequency for 58%-89% of RH variation.


(a) *(b)*
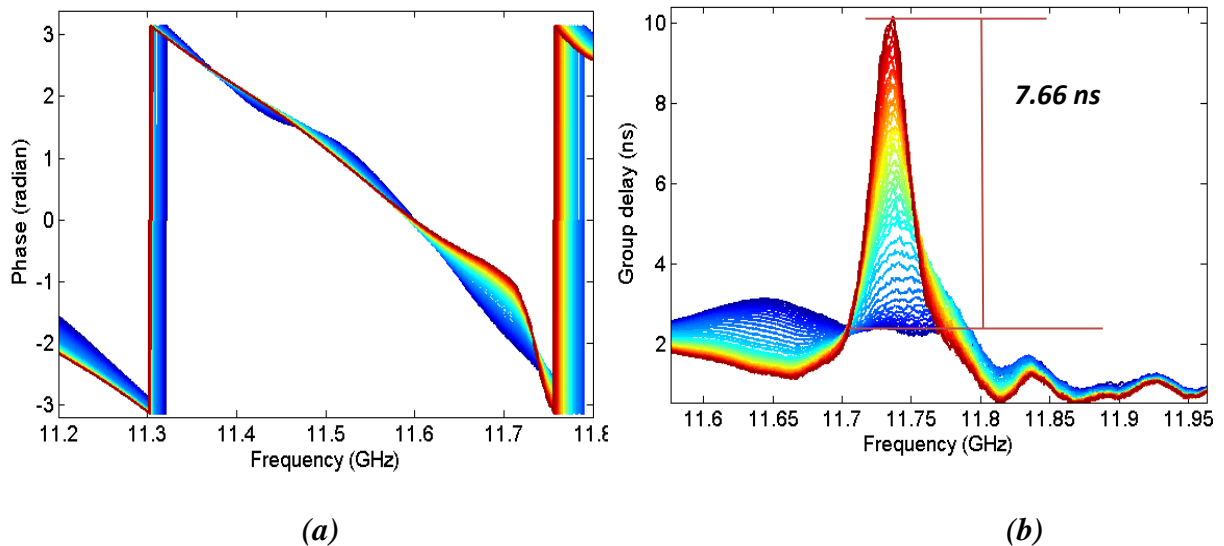
Fig.6. 6 : The phase and group delay variation observed at higher order harmonics for a humidity variation of 58%- 89% and an ambient temperature of 23°C. a) Phase, b) group delay.

The group delay was also extracted in this case. It was found that the group delay shows very less variation in the lower fundamental frequency. However, at higher order harmonics a group delay variation of 7.66 ns was observed. Fig.6. 6 (a) and (b) shows the phase and group delay respectively at second harmonics. It is clear that group delay shows a strong variation. Measurement was also conducted for tag prototype without nanowires. Negligible variation was observed for S21 magnitude and group delay (0.1 dB and 0.01 ns). Fig.6. 7 shows the S21 magnitude obtained for a humidity variation of 62%-92%.
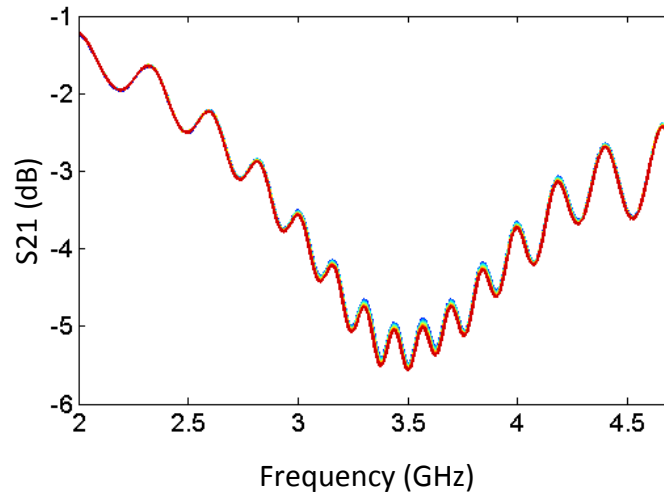
Fig.6. 7 : S21 magnitude obtained for the tag prototype without nanowires for a humidity variation of 62%- 92% and an ambient temperature of 23°C. The curves are almost superimposed one on the other.
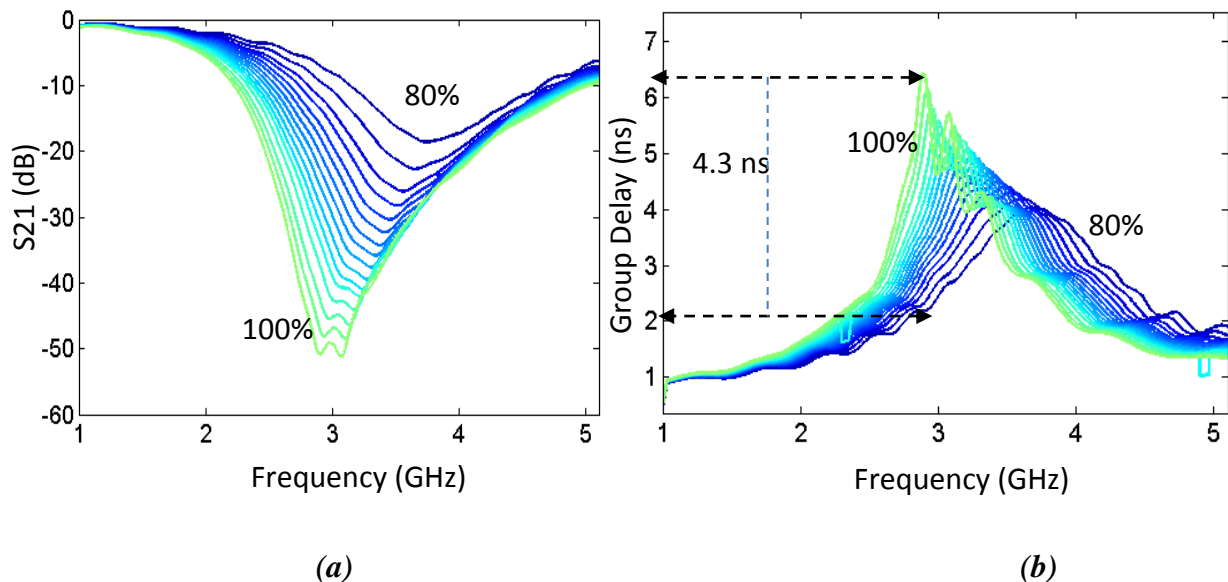
Now the ambient temperature inside the box was increased by adding some hot water into it. The physical conditions inside the box were observed. It was found that the temperature increases from $24°C$ to $29°C$. The presence of mist was observed inside the plastic box. The S21 magnitude was always measured using VNA. It was found that

(a)

(b)
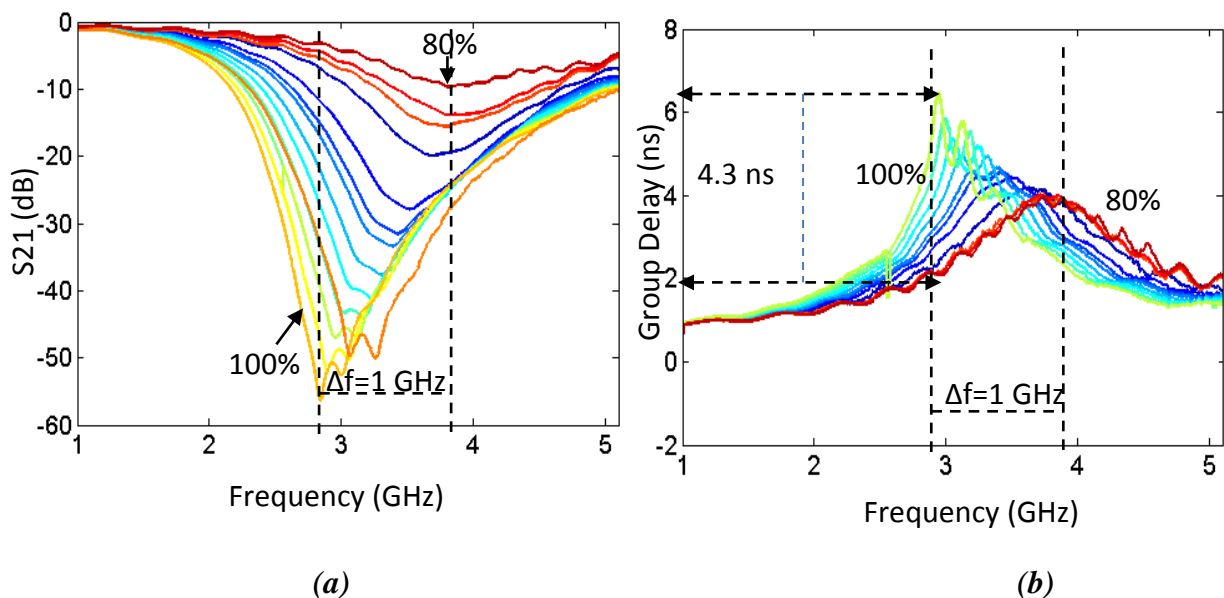
Fig.6. 8 : Measured S21 and group delay after increasing the ambient temperature inside the plastic box for a humidity variation of 80%-100% with a temperature range of 24°C-29°C. a) S21 magnitude, b) group delay.

increasing the temperature improves the S21 magnitude variation. It is due to the known fact that the rise in temperature increases the presence of water molecules inside the box and hence the amount of water molecules captured by the nanowires will also increase. From this, we observe an increase in the S21 magnitude. Fig. 6.8 (a) shows the S21 magnitude observed for a humidity variation of 80%-100% with a temperature variation of 24°C to 29°C. 47dB of magnitude variation was observed over a bandwidth of 1 GHz. Significant variations were observed in the phase and hence group delay also. These variations are much higher than previously observed 7 dB. In addition to this, the range of humidity is significantly reduced here. Fig.6. 8 (a) and (b) shows the variations observed in magnitude and group delay respectively.

If we compare with the existing chipless RFID humidity sensors [15] where a magnitude variation of 5 dB is reported for a bandwidth of 20 MHz, this is the maximum variation reported until now. It is clear from the figure that while humidity is increasing the S21 magnitude and group delay peaks shift to the lower frequency level. It is due to the fact that the nanowires change their permittivity upon water absorption which causes the curves shifting to the lower frequency zone. The repeatability has been tested within an interval of

(a)   (b)

Fig.6. 9 : Repeatability test conducted after 4 days. Measured S21 and group delay after increasing the ambient temperature inside the plastic box as 24°C-29°C for an RH variation of 80%-100%. a) S21 magnitude, b) group delay.

four days. It was observed that the S21 magnitude and group delay shows the same kind of behavior as in the previous case as shown in Fig.6.9 (a) and (b) respectively. In this case also, 47 dB of variation is observed for S21 magnitude over a bandwidth of 1 GHz. The group delay also shows significant variation (4.3 ns). Thus it is clear from the study that the temperature of water has a significant impact. When there is more water molecules in the water, nanowires will capture more water molecules and this will increase the rate of variation of magnitude phase or group delay.

Measurement was also done for the prototype without nanowires also. The same ambient atmosphere was re-created with an ambient temperature varies between 25-30°*C*. It was observed that the prototype gives 6 dB of variation in the fundamental frequency as shown in Fig.6.10. When the density of water molecules deposited on the prototype increases, it can cause a permittivity change and that may be the reason for the variation in magnitude. This measurement can be considered as the reference measurement and this variation is low compared to the variation produced by the presence of nanowires, which was 47 dB. This proves the role of nanowires as a good catalyst. Fig.6. 10 shows the S21 magnitude variation for the prototype without nanowires which is considered to be the reference measurement. In the all above explained cases, for better comparison, same replicas of prototypes have been used.
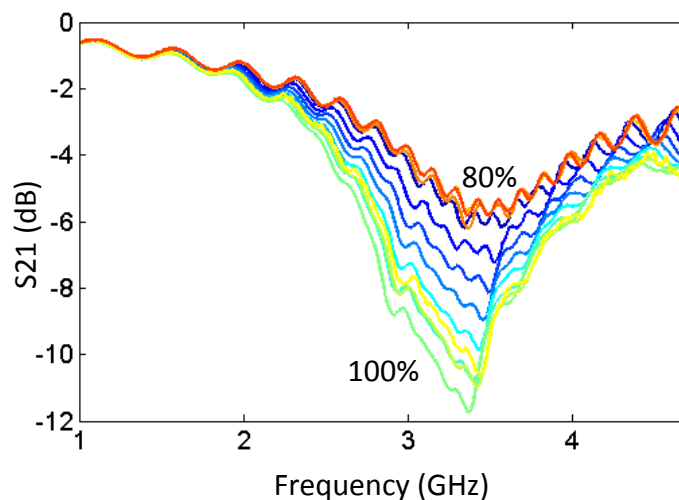
Fig.6. 10 : Measured S21 for prototype without nanowires after increasing the ambient temperature (25°C-30°C) inside the plastic box with an RH variation of 80%-100%.

It has been found that when temperature is increasing, the S21 magnitude, phase and hence group delay exhibits more variation. This is due to the fact that when the temperature is increasing; there will be more water molecules in the medium so that the nanowires can capture more number of water molecules than previously which results in a significant variation. Thus, for a given temperature, the change in humidity induces variation in S parameters. However, for different temperatures, they show a small percentage of error. This can be rectified by expressing the rate of change of variation in magnitude or group delay as a function of absolute humidity. Absolute humidity (AH) is related to the absolute amount of water molecules in air. Relative humidity, expressed as a percent, measures the current absolute humidity relative to the maximum for that air pressure and temperature. It means that, for two different temperatures for a given RH, the density of water molecules in air will be different. More the temperature is, more will be the density of water molecules are (the storing capacity of water molecules in air for high temperature will be high). When we take two different temperature variations, it is always better to express the S parameter as a function of AH. Thus, AH can be expressed as,

$$AH = \frac{y_e M_e}{(1 - y_e) M_a}$$

, where M_e and M_a is the molecular mass of the water (18 g/mols) and air (29g/mols) respectively and

$$y_e = (RH \times {}^{P_e}/_P)/100,$$

, where P is the standard atmospheric pressure (101325 Pa) and Pe is the saturation pressure of water depending in temperature and can be expressed as $P_e = e^{(23.1964 - ({}^{3816.44}/_{(T_k - 46.13)}))}$. Thus we see that AH can be expressed as a function of temperature T_k expressed in Kelvin.
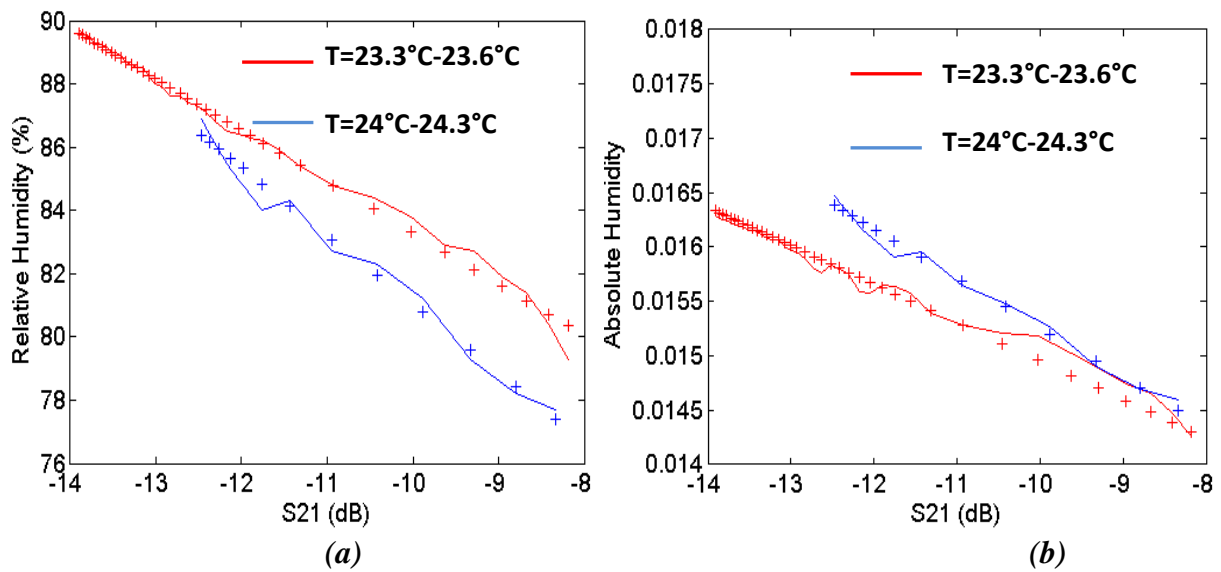
Fig.6. 11 : Rate of change of S21 magnitude in dB for two different temperatures as a function of a) relative humidity, b) absolute humidity. The cross curves represents the curves obtained using curve fitting method with the expression AH or RH=a*S21$_{dB}$+b, where a & b are the constants obtained from curve fitting method.
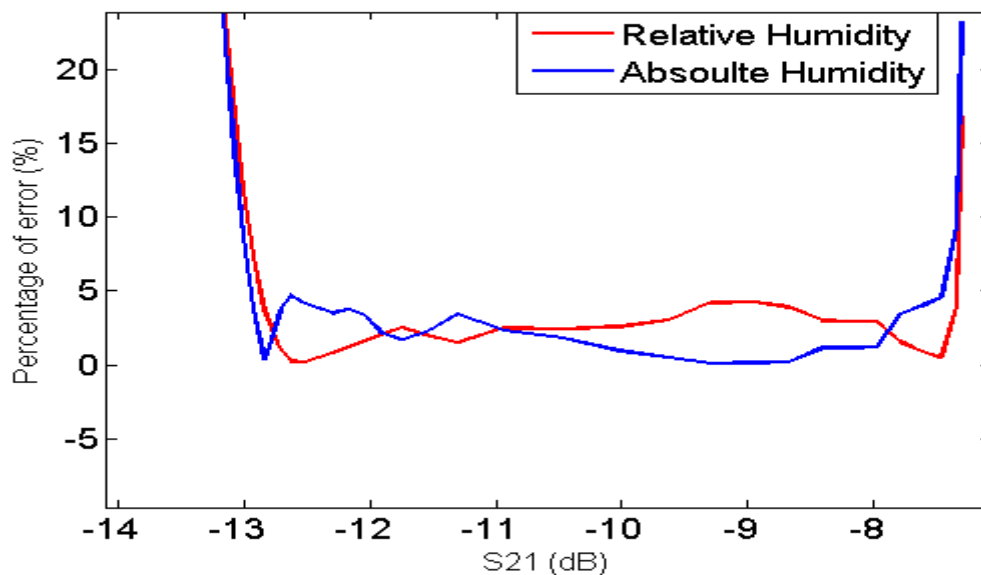
Fig.6. 12 : Percentage of error calculated for the two different temperatures (Fig.6.11) for relative and absoulte humidity .

Fig.6. 11 (a) and (b) shows the rate of change of S21 magnitude in dB for different temperatures as a function of relative and absolute humidity respectively. Curve fitting has

been done in order to find the analytical expression between S21 in dB and relative humidity or absolute humidity. It has been found that S21 is linearly proportional to relative humidity and absolute humidity as per the following equation,

RH or AH=a*(S21)$_{dB}$+b; where a and b are constants which have been calculated using curve fitting in MATLAB. This study has been carried out for a very small range of humidity (10%) and hence it results in a linear variation. However, for large range of relative humidity, the variation was found to be inversely proportional as we will see in the next section.

Fig. 6.12 shows the percentage of error calculated as a function of S21 for relative humidity and absolute humidity. The percentage of error is less for AH. However, we cannot end up with such a conclusion since the two temperatures are too close to each other. A good way to clearly obtain an idea is to repeat the measurements for different temperatures whose values are far from each other. In order to obtain this, the measurement time can be increased and hence a value of RH more than 90% can be obtained. This measurement can be compared with another measurement which has a higher value of temperature. In short, from the obtained results we can conclude that while considering two different temperatures, it is always better to express the S parameters as a function of AH. More precisely, we are not able to say whether the observed variation is due to variation in AH. However, it is clear that the measurement is a function of temperature and therefore not only be related to the change in RH. However, if we know the temperature, and if the sensor is calibrated, it is possible to use it to measure RH.The next section explains the backscattering sensor measurement conducted for the chipless tag shown in Fig.6. 2 (b).

6.5   WIRELESS SENSOR MEASUREMENT SET-UP

Fig.6. 13 shows the measurement set-up used for wireless sensor tag. A dual polarized horn antenna which can operate in 2-32 GHz with an average gain of 17 dBi, has been used as the reader antenna and each port of the reader antennas was connected to the performance Network Analyzer (PNA N5222A).
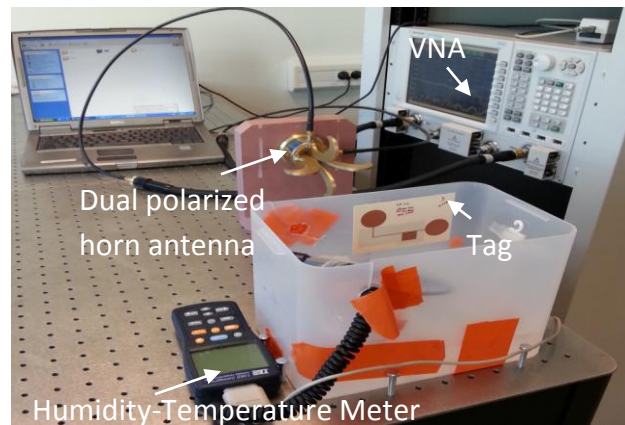
**Fig.6. 13 : Measurement set-up for sensor tag application.**

As shown in the figure, the tag was kept in a plastic box which contains water. The humidity inside the box was varying upon closing. The same above explained humidity-temperature meter is used to monitor real time humidity inside the box. The whole set-up was kept at 30 cm from the reader antennas and 10 dBm power was used to interrogate the tag. The measurement was performed in a real environment with lot of interference objects such as PC, cables, wall, metallic box etc. At each 10 seconds, the response of the tag, the humidity and the temperature was saved using a homemade interface program in MATLAB. The measurement was performed separately for both tags with and without nanowires.

The complex S_{21} has been measured using this configuration. An empty room measurement was also performed. This was to avoid all the unwanted reflections from the nearby objects. The empty response shows a significant magnitude as the tag response. Further, measurement with a reference tag was also performed. Two cross polarized tag antennas connected to each other was used as a reference tag (i.e. tag without C-sections group). The empty response was subtracted from all further chipless tag measurement and a calibration process explained in [16] has been followed.

6.6   RESULTS AND DISCUSSIONS

The backscattered response of the tag was measured using the horn antenna which is connected to the two ports of the PNA. Variations of magnitude (we can call it as S21), and phase of the reflected signal from the tag and hence group delay were observed over certain band of frequencies. However, near the fundamental frequency at 3.7 GHz, strong

variations were found.
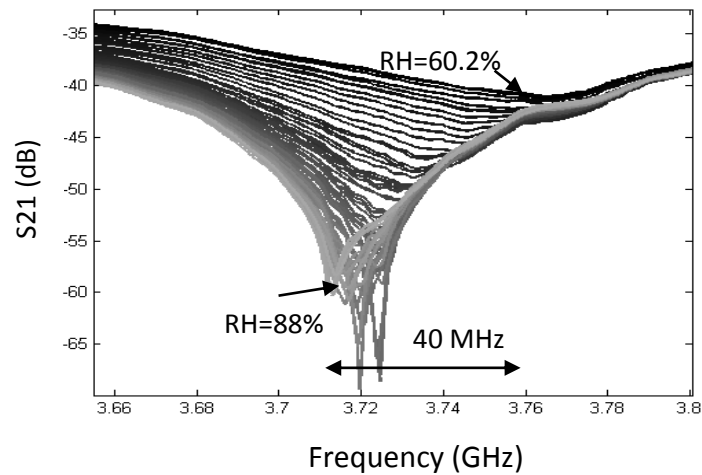
Fig.6. 14 : S21 magnitude of the sensor tag (as shown in Fig.6. 2(b)) for a relative humidity variation of 60.2%-88% for an ambient temperature of 23°C.

Fig.6.14 shows the S21 magnitude obtained for a humidity variation of 60.2%-88% for an ambient temperature of 23°C. The S21 magnitude shows a clear variation near the fundamental frequency relative to the humidity change. A variation of 30 dB was observed. It is clear from the figure that, while increasing the humidity variation, the S21 is shifting to the lower frequency region. This can be explained by the fact that the nanowires changes permittivity while absorbing water.

The changes are inversely proportional as shown in Fig.6. 15 (a). Using curve fitting method, the analytical expression between RH and the S21 magnitude in the fundamental frequency for a temperature of 23°C has been found as,

$$RH= a/S21(dB) + b$$

where a=2.918e+3, b=145 are constants which are calculated using the curve fitting method. From the figure we can see that this equation is valid for range of humidity between 65%-86%. Again, we observed that when S21 is increasing, RH is decreasing which corresponds to the already stated expression, $RH=a*(S21_{dB})+b$ with a<0 (for 10% RH range). The expression obtained for a high range of RH is not linear, instead is inversely proportional.

<center>(a)</center> <center>(b)</center>
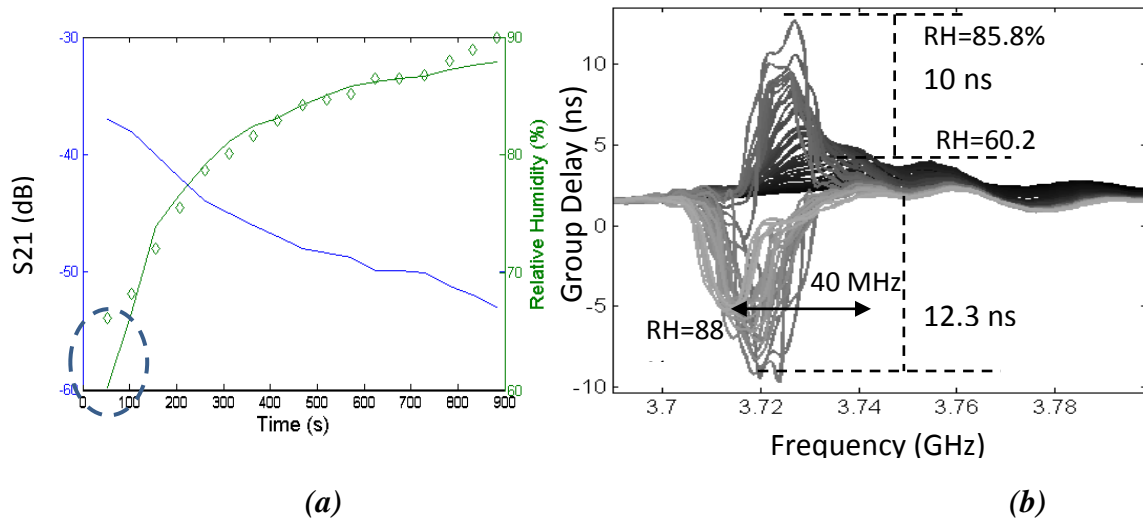
Fig.6. 15 : S21 magnitude and group delay variation during the backscattering measurement of the chipless sensor tag. a) S21 and relative humidity variation as a function of time. The green curve represented using diamonds is in accordance with the relation RH= a/S21 (dB) + b ; where a=2.918e+3, b=145. b) Group delay variation of the sensor tag near fundamental frequency for a relative humidity variation of 60.2%-88%.

Fig.6. 15 (b) depicts group delay variation with respect to a change in relative humidity. As shown in the figure, a group delay variation of 13 ns was observed in the positive real axis. A negative group delay of 10 ns was observed after reaching certain humidity range which can be attributed to the presence of absorption in an already highly dispersive structure. In this limited frequency band, the group velocity no longer represents the velocity of a signal or of energy transport and ceases to have a clear physical meaning [16]. However, it is still possible to retrieve this information which is directly related to the humidity. The group delay peak is minimum for a minimum value of the relative humidity of 62.5%. The delay peak increases with respect to humidity and reaches the maximum value. This is due to the known fact that, a high permittivity causes the signal traveling through a medium to be delayed (with a small group velocity) which in turn increases the group delay. This high permittivity may be due to the presence nanowires which increases permittivity upon humidity absorption. In order to interpret the variations in terms of change in permittivity or loss, a simulation study was conducted. A thin dielectric material was added on the top of the C-section as nanowires, with a thickness of 10 μm as shown in Fig.6. 16. The

impact of change in permittivity ε$_r$ and losses tanδ on the group delay values were observed. Each time, these two values were varied by taking the aspect that nanowires change their permittivity and losses upon humidity absorption. However, this simulation cannot take into account of the thickness of the nanowires and the concentration of nanowires in the deposition zone. This simulation was conducted just to give an idea about the evolution of group delay as function of permittivity and losses.
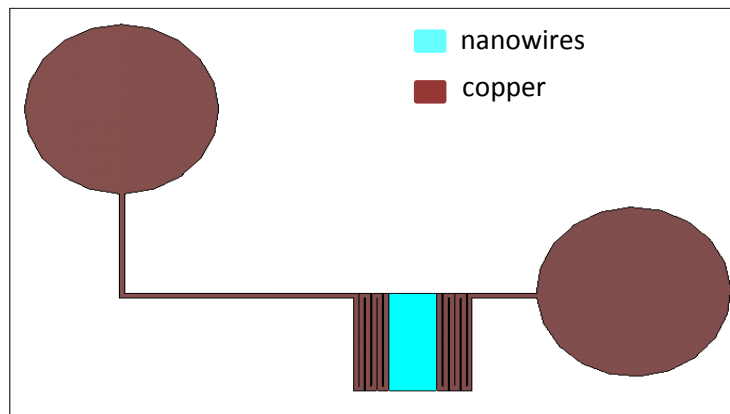

Fig.6. 16 : The simulated sensor tag model in CST in order to explain the observed evolution of group delay as a function of permittivity and loss tangent.

As shown in Fig.6. 17, same kind of behavior as in the case of measurement was observed. In the simulation the permittivity has been varied from 1 to12 and loss tangent ranges between 0.01-0.4. It was found that group delay tends to its negative value while the loss tangent is increasing. It proves the already stated fact that negative group delay arises with highly dispersive medium followed by absorption. It is also clear that a change in permittivity will shift the group delay curve. Since it is not possible to take into account of the exact geometry of nanowires, the magnitude of the group delay varies from that of measurement. This is a simple model to explain the accumulation of water molecules in the tag surface and the change in permittivity of the nanowires upon water molecules absorption. However, this model study was enough to explain the behavior observed in the measurement.
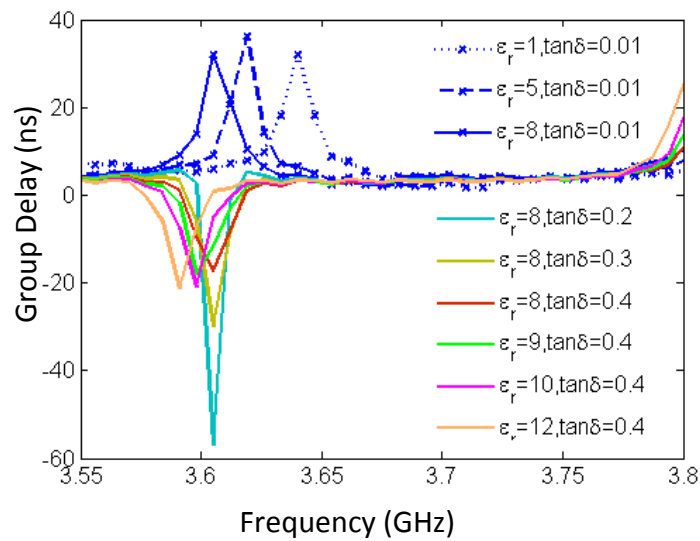
Fig.6. 17 : **Evolution of group delay as a function of permittivity and loss tangent in simulation study (see Fig.6. 16).**

Now coming to the measurement, measurement was carried out without nanowires also. No significant variation was observed for S21 magnitude, phase, and hence group delay (1.44 dB on the S21 magnitude and 0.7 ns on the group delay). Fig.6. 18 (a) and (b) shows the variation of magnitude and group delay respectively for an RH variation of 58%-88%. This measurement was conducted for the same tag shown in Fig.6. 2 (b) with l=14.9 before depositing the nanowires.

(a)   *(b)*
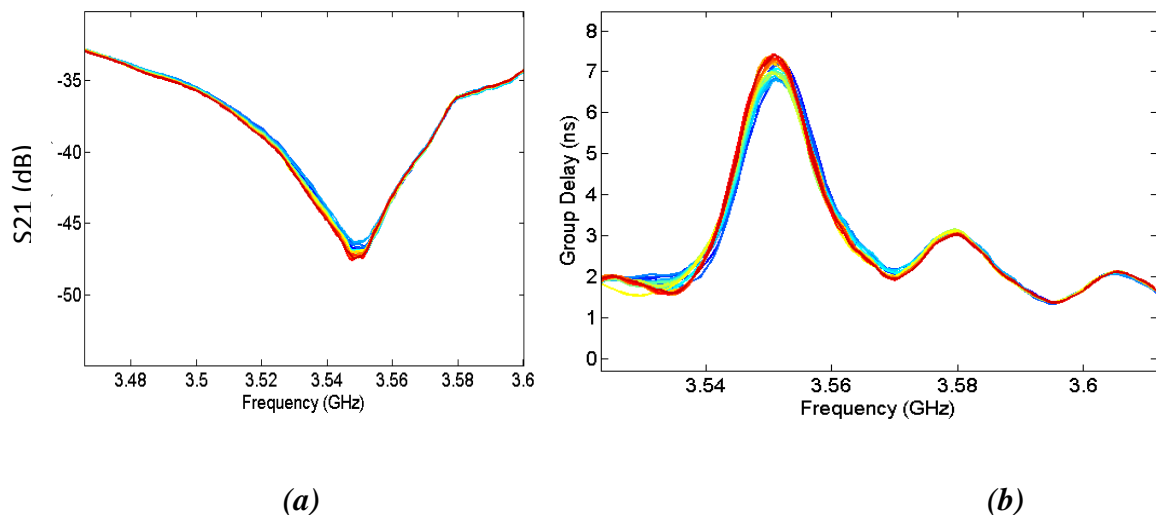
Fig.6. 18 : Results obtained for measurement for tag without nanowires for an RH variation of 58%-88% for an ambient temperature of 23°C. a) S21, b) group delay.

6.7   CONCLUSION & PERSPECTIVES

Few investigations regarding the use of nanowires for wireless humidity sensor application which is completely autonomous and potentially printable is explained in this chapter. Interesting preliminary measurement results were obtained. Contrary to the early reported works, the nanowires shows a measurable variation in S21 magnitude, phase, and hence group delay curves. This proves the potential of chipless tags in sensor applications. It has been found that when temperature is increasing, the S21 magnitude, phase and hence group delay exhibits more variation. This is due to the fact that when the temperature is increasing; there will be more water molecules in the medium so that the nanowires can capture more number of water molecules than previously which results in a significant variation. Thus, for a given temperature, the change in humidity induces variations in the S parameters and the magnitude of the reflected signal from the tag, in dB, will be inversely proportional to the rate of change of humidity. A magnitude change of 30 dB and group delay variation of nearly 22.3 ns was observed near the fundamental frequency over a bandwidth of 40 MHz for a relative humidity variation of 60.2 %-88 %. In order to avoid the problem in difference in rate of variation for different temperatures, it is advised to express the rate as a function of absolute humidity since it also takes into account of the temperature variations. However, so far this conclusion is not yet fully validated. Repeating the measurements with two distinct temperatures may prove this. The amount of nanowires to be deposited and also the positions of transmission line strips where nanowires need to be deposited need to be determined. Further, the repeatability of the measurement also has to be determined. It is found that the evolution of S21 magnitude and group delay is a function of humidity as well as the ambient temperature. Hence the backscattering measurement tests need to be conducted with different temperatures also. The measurement has to be done in the exterior environment also. These aspects can be considered as the future works. The tags need to be printed in paper so that the nanowires can be deposited using inkjet printing making the whole system printable.

REFERENCES

1. A.Rida, L. Yang, and M. Tentzeris, RFID-Enabled Sensor Design and Applications: Artech House, ISBN 13: 978-1-60783-981-1, 2010.

2. S. Peradovic and N. C. karmakar, "Chipless RFID tag with Integrated Sensor," in Proc. of IEEE International Conference in Sensors, 2010, pp. 1277-1281.

3. M. Balachandran, S. Shrestha, M. Agarwal, Y. Lvov, and K. Varahramyan, "SnO2 capacitive sensor integrated with microstrip patch antenna for passive wireless detection of ethylene gas," Electronics Letters, vol. 44, pp. 464-466, 2008.

4. S. Shrestha, M. Balachandran, M. Agarwal, V. V. Phoha, and K. Varahramyan, "A Chipless RFID Sensor System for Cyber Centric Monitoring Applications," IEEE Transactions on Microwave Theory and Techniques, vol. 57, pp. 1303 - 1309, may 2009.

5. A.Vena, E. Perret, S. Tedjini, D. Kaddour, A. Potie, and T. Baron, "A Compact Chipless RFID Tag with Environment Sensing Capability," IEEE MTT-S IMS 2012, 2012.

6. M. P. McGrath and A. Pham, "Carbon nanotube based microwave resonator gas sensors," International Journal of High Speed Electronics and Systems, vol. 16, pp. 913-935, Dec. 2006.

7. H. Yoon, J. Xie, J. K. Abraham, V. K. Varadan, and P. B. Ruffin, "Passive wireless sensors using electrical transition of carbon nanotube junctions in polymer matrix," Smart materials and structures, vol. 15, pp. S14-S20, 2005.

8. Y. Li, Z. Rongwei, D. Staiculescu, C. P. Wong, and M. M. Tentzeris, "A Novel Conformal RFID-Enabled Module Utilizing Inkjet-Printed Antennas and Carbon Nanotubes for Gas-Detection Applications," Antennas and Wireless Propagation Letters, IEEE, vol. 8, pp. 653-656, 2009.

9. Nomura, Oofuchi, Yasuda, and Futukawa," SAW Humidity Sensor Using Dielectric Hygroscopic Polymer Film, ULTRASONICS SYMPOSIUM, 1994.

10. Sheng, Dajing and Yuquan, "A surface acoustic wave humidity sensor with high sensitivity based on electrospun MWCNT/Nafion nanofiber films", Nanotechnology, 2011.

11. Lieberzeit, Palfinger, L. Dickert, and Fischerauer, "SAW RFID-Tags for Mass-Sensitive Detection of Humidity and Vapors", Sensors, 2009

12. C. S. Hartmann, "A global SAW ID tag with large data capacity," in Proc. IEEE Ultrasonics Symp, Munich, Germany, 2002, pp. 65-69 vol. 1.

13. R. Nair, E. Perret, and S. Tedjini, "Temporal Multi-Frequency Encoding Technique for Chipless RFID Applications," IEEE MTT-S International Microwave Symposium (IMS), 2012.

14. R. Nair, E. Perret, and S. Tedjini, "A Humidity Sensor for Passive Chipless RFID Applications," in IEEE International Conference on RFID-Technology and Applications, 5-7 Nov. 2012, Nice, France, 2012.

15. Amin, E.M.; Karmakar, N.C. "Development of a low cost printable humidity sensor for chipless RFID technology", IEEE Intrenationa Conference on RFID Technologies and Applications, Nice, France, November, 2012.

16. A.Vena, E. Perret, and S. Tedjini, "Chipless RFID tag using hybrid coding technique," Microwave Theory and Techniques, IEEE Transactions on, vol. 59, pp. 3356-3364, 2011.

17. L. Brillouin and A. Sommerfeld, Wave propagation and group velocity, vol. 960: Academic Press New York, 1960.

CONCLUSION & FUTURE WORKS

The conclusions drawn from the simulation and experimental studies carried out on temporal multi-frequency chipless RFID tag is explained in this chapter. A few suggestions for further investigations on this topic are also explained here.

CONCLUSION & FUTURE WORKS

- ## THESIS HIGHLIGHTS

A summary of the investigations performed on temporal multi-frequency chipless RFID tag is presented here. The chipless tags should be compatible with the FCC and ETSI regulations in terms of frequency and emission power. As already explained in the preceding chapters, two main categories of chipless tags can be seen in the literature; time domain tags and frequency domain tags. In frequency domain (spectral signature tags) the only solution to respect these standards while having a broad frequency band is to emit short pulses, i.e. using UWB standard (like in UWB radar). However, the allowed power level is very low in this case which leads to a low reading range of the order of 50 cm which make them compatible with short range applications. Nevertheless, the frequency signature tags allow a better coding capacity. In contrast, time domain tags can operate in narrow bands. For the applications where the power level is more important, the solution is to use ISM bands. Since ISM bands can use more power, it can increase the reading range as in the case of SAW tags. However, in this case the frequency band is very limited, but it remains compatible with the use of a temporal approach. Time domain tags allow a poor coding capacity since it operate in narrow frequency bands. Thus this thesis, for the first time, combines certain advantage of time domain tags and frequency domain tags. As a result, a novel temporal multi-frequency tag has been developed. Time domain tags were less studied in the literature since it can produce only few bits in terms of coding capacity. This problem is solved in this thesis by allowing multi-frequency bands in time domain. In the case of TDR based tags, the delay is produced by using a linear or meandered transmission line which allows information encoding at a single frequency. In contrast, the proposed tag uses transmission line sections coupled at alternative ends; which is also known as C-sections; which is able to produce group delay peaks at a particular frequency as a function of the length. Thus, the C-sections with different lengths will be able to produce different peaks at frequency and which will be independent on each other also. The dispersive character of the C-sections is exploited for this purpose. Dispersive character allows different spectral components to be arranged in different time. This feature is utilized for the coding of information. Information can be encoded at different frequencies. Thus it allows the augmentation of coding capacity compared to the existing TDR based tags.

This thesis also proposes a multi-layer structure. The proposed multi-layer design offers broadside coupling between each C-sections which enables a significant amount of delay with highly narrowband delay peaks. These two features allow increasing the coding capacity in time domain tags. The proposed time domain multi-layer tag with single group of C-sections can offer a coding capacity of 6 bits and that of multi-group of C-sections can offer a coding capacity of 12 bits in the two ISM bands with an acceptable dimension. The proposed design also provides a coding capacity of 43 bits, with a 22 MHz of frequency resolution, in the UWB band. This is a significant amount of bits in comparison to the existing time domain tags which offer a highest coding capacity of 8 bits. This is comparable with the EAN 13 barcode which has a coding capacity of 41 bits.

As a perspective of the time domain tags, a humidity sensor tag is also proposed. Silicon nanowires are used for this purpose. Silicon nanowires are manually deposited on the strips of the C-sections. Silicon nanowires change permittivity upon humidity absorption which in turn changes the magnitude and phase, and hence the group delay of the reflected signal. The experimental validation of the proposed wireless sensor tag is also demonstrated.

The following part explains the summary of each chapter.

Microstrip Single Group of C-Sections and Delay Based ID Generation

A time domain chipless tag using single group of microstrip C-sections is explained here. A comparison of delay produced by linear transmission line, meander transmission line, and C-sections are also given. The design of prototype of the tag and further the transformation of the prototype into a chipless tag by adding cross polarized antennas at the two port of the prototype is also explained. The proposed idea is validated using simulation and measurement results.

Microstrip Multi-Group of C-Sections and Delay Based ID Generation

This chapter explains the possibility of increasing the coding capacity using multi-group of C-sections. Two different C-section groups are cascaded which allows two group delay peaks at two different frequencies. The frequency dispersive characteristics of transmission line are utilized for this purpose. As an example, 2 bit coding is explained. The design of tag prototype by cascading two C-section groups is explained. Further, as in the

preceding chapter, transformation of tag prototype into chipless tag is also demonstrated. The proposed tag is validated with measurements using Digital Oscilloscope and pulse generator and also with commercially available UWB radar.

Multi-Layer C-Sections and Delay Based Id Generation Using Flexible Substrates

A novel multi-layer design using flexible substrates is presented here. The proposed design is obtained by sandwiching the folded flexible substrate in between the base and top substrates. Pyralux AP and white PET are used as the flexible substrate and Rogers R4003 is used as the base and top substrate. The broad side coupling enables a significant amount of delay with highly selective delay peaks and hence a significant increase in coding capacity. A coding capacity of 5.78 bits is possible with multi-layer single group of C-sections and 12.05bits are possible with multi-group of C-sections, within the unlicensed ISM bands at 2.45 GHz and 5.8 GHz. Moreover, with UWB regulation, it offers a coding capacity of 43.27 bits with a 22 MHz of frequency resolution.

Chipless RFID Humidity Sensor Using Silicon Nanowires

An application of the proposed chipless tag as a humidity sensor tag can be seen here. The proposed sensor tag is based on silicon nanowires. Silicon nanowires have been manually deposited on the strips of the C-section. The nanowires vary permittivity and losses upon humidity absorption which in turn changes the backscattering characteristics of the tag. In the first section, the measurement using a tag prototype can be seen. Influence of change in ambient temperature is also tested here. A change in the magnitude of S21, phase and group delay has been measured here. Further, the real environment backscattering measurement of the chipless tag sensor is also done. The variation of magnitude, phase and group delay of the reflected signal have been observed.

- ## FUTURE WORKS

The thesis proposes an idea of increasing the coding capacity in time domain chipless RFID tags. To do so, a temporal multi-frequency tag is proposed. So far, the measurement using the multi-layer structure is not yet completed. It currently faces the problem of presence

of air and also lack of techniques to affix the flexible layers together. A highly professional industrial packing can be used for this purpose and the measurement can be continued. Moreover, the proposed technique can also be used for other RF devices like filters and antennas for miniaturizing the structure. Work can be continued in this area also. Again, the proposed prototype should be transformed into a chipless tag by adding the tag antennas. Measurement has to be repeated in this case also. So far, the tag size is more important. Two tag antennas can be replaced with a single tag antenna which in turn will reduce the tag dimension. Some of the preliminary results of humidity sensor are proposed in the thesis. Measurement needs to be conducted in the humidity sensing application also. The influence of change in ambient temperature in the real environment performance of tag has to be monitored. Moreover, measurement can be performed outside the building with lot of interfering objects, in order to monitor the atmospheric humidity level.

APPENDIX I
METHODOLOGY

The simulation and experimental methodology utilized for the analysis of the respective chipless tags are explained here. CST microwave Studio is used to perform the parametric analysis of the designs. Photolithographic process is used to develop each chipless tag. Vector Network Analyzer and Agilent Digital Oscilloscope are used to do the tag characterization.

METHODOLOGY

## TECHNIQUES USED FOR DESIGN AND OPTIMIZATION OF VARIOUS CHIPLESS RFID TAGS

A short description of the software used for the design and optimization of various chipless RFID tags is explained. CST Microwave Studio is used as the design platform for all the tags presented in this thesis. The fabrication method and measurement technique is also presented.

CST MICROWAVE STUDIO

CST Microwave Studio is the specialist tool for the 3D EM simulation of high frequency components [1]. It enables the fast and accurate analysis of high frequency devices such as antennas, filters, couplers, planar and multi-layer structures. In spite of the time domain and frequency domain solvers, CST offers further different solver modules such as fast resonant solver option for highly resonant circuits, multi-layer solver option etc. A key feature of CST Microwave Studio is the *Method on Demand ^{TM}* approach which gives the choice of simulator or mesh type that is best suited to a particular problem. With CST, engineers can extract parasitic parameters (S, Y and Z) and visualize 3D electromagnetic fields.

Since the tag design is based on time domain, it is important to use the time domain representation of the signals. CST offers transient solver which results in getting the results in time domain itself, hence allows coding the information in time domain. Moreover, it is also possible to use user defined time domain excitation signals so that we can impose the excitation signal used in practice. CST also provides results in frequency domain also which we have used for the group delay calculation when the tag acts as a two port network (tag without antennas). Thus, transient solver is utilized for the design and optimization of chipless tags throughout this thesis. It is using a hexahedral grid, which can obtain the entire broadband frequency behavior of the simulated device from only one calculation run (in contrast to the frequency step approach of many other simulators). This solver is remarkably efficient for most high frequency applications such as connectors, transmission lines, filters,

antennas, amongst others. The optimization tool available in CST is very useful for antenna designers to optimize the antenna parameters very accurately. E, H and J simulation value representation gives a good insight into the problem under simulation.
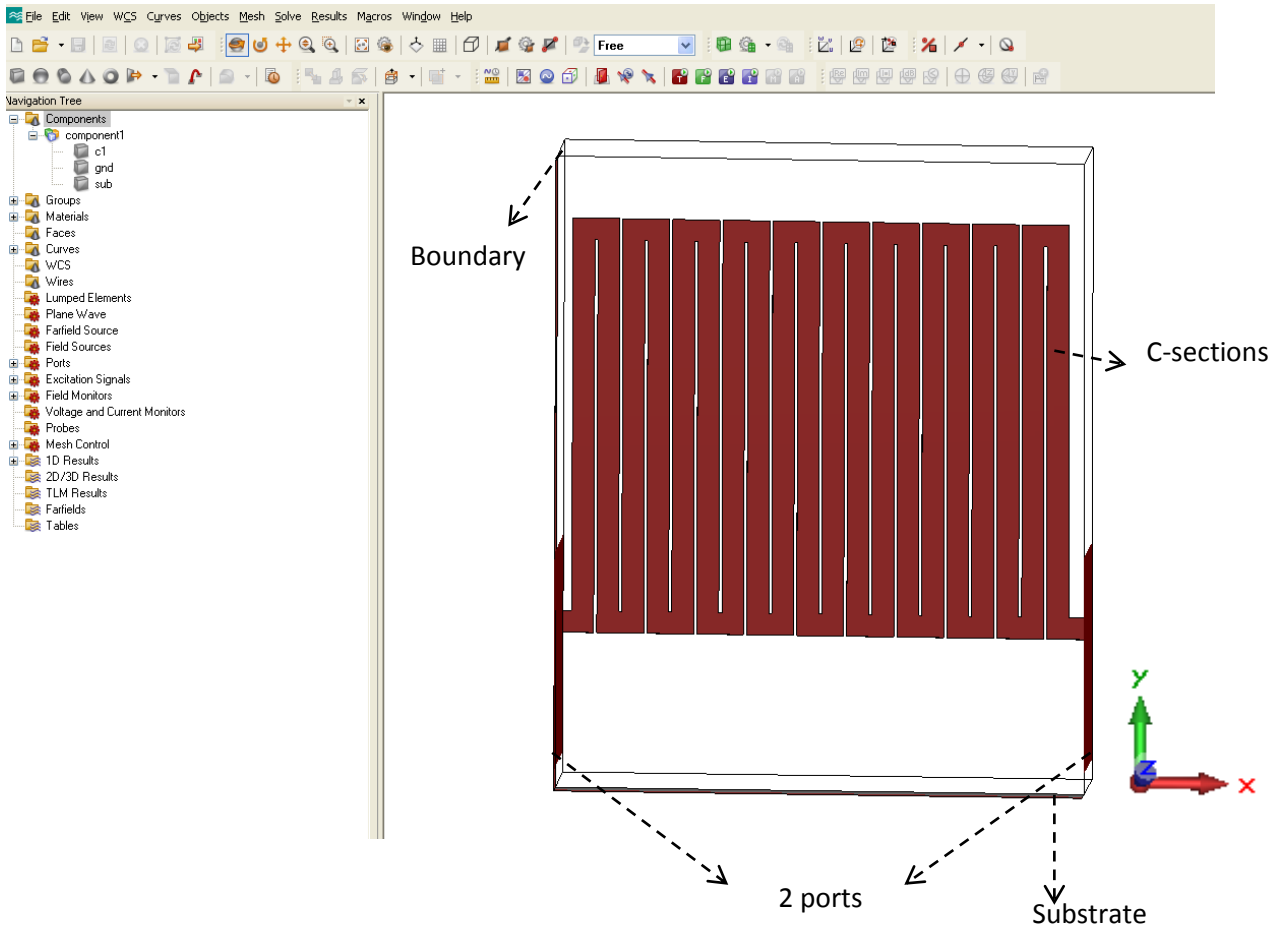
*Fig. A.1: Modelled structure in CST*

The first step in simulating a structure in CST involves determining the most appropriate template for the corresponding design. CST allows automatically assignment of the boundary conditions by selecting the appropriate template. PEC and open boundary conditions are used throughout this thesis. The next step is to determine the units for frequency and structure dimensions and further draw the intended architecture using the drawing tools available in the software as shown in Fig. A.1.

The designed structure is excited using the suitable port excitation schemes. Now the simulation engine can be invoked by giving the suitable frequency of operation. Finally the simulations results such as the scattering parameters (Fig. A.2), port impedance information, animated electric and magnetic fields, current pattern, radiation pattern etc. is displayed.
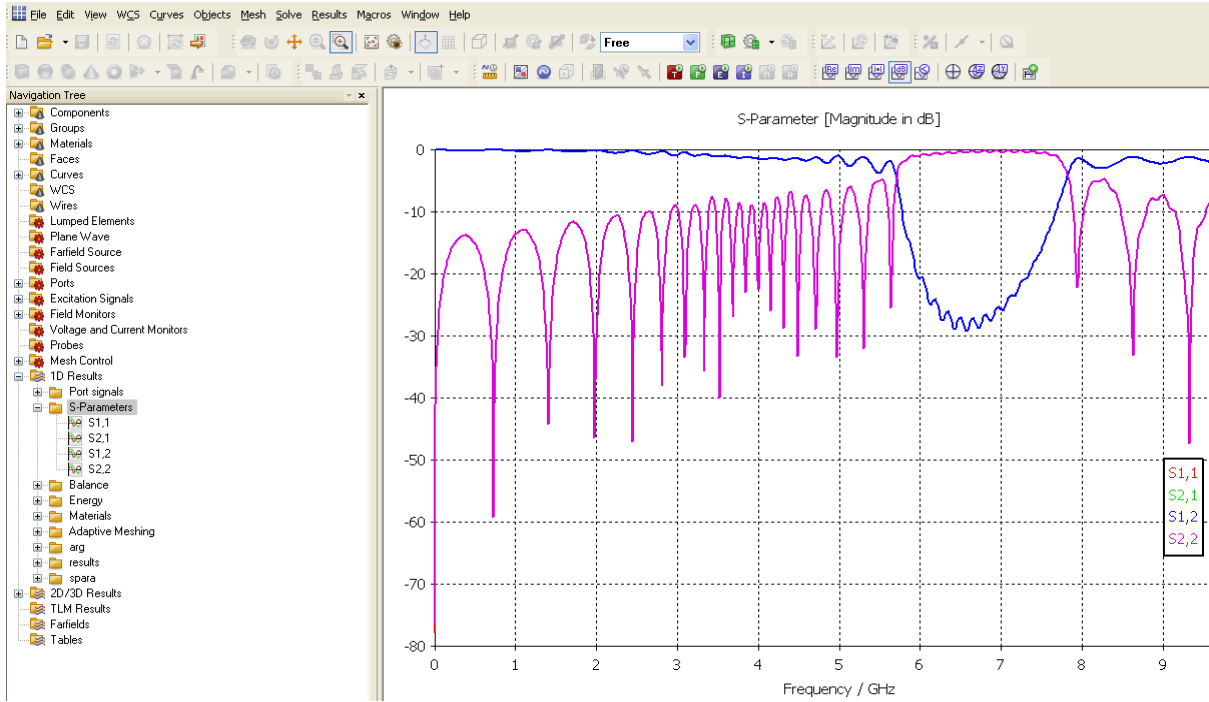
Fig. A.2: S-parameter plot of the simulated structure.

Another special feature of CST which can exploited to design the chipless tags is the excitation using plane waves and collecting the backscattering information such as RCS or time domain signals by placing appropriate probes at a particular distance. The visualization of signal information in time domain gives deep insight into the problem. Fig. A.3 (a) and (b) shows the excitation using plane wave and placement of different probes at a particular distance.

(a)   *(b)*
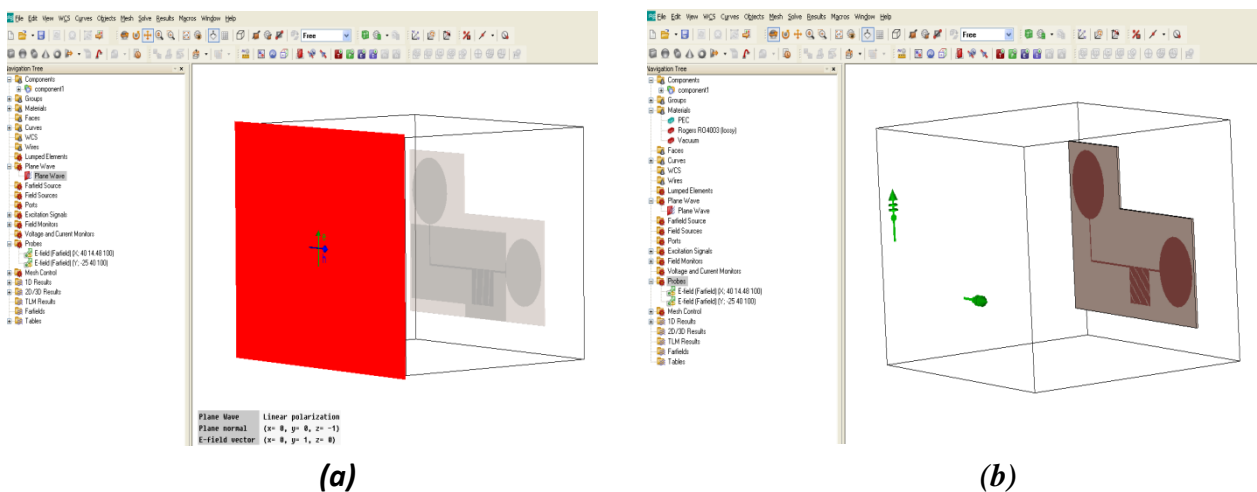
Fig. A.3: Plane wave and probe assignment in CST. a) Plane wave assignment, b) probe assignment.

CST allows the user to define the excitation signal. Fig.A.4 (a) shows such an excitation signal. It is a Gaussian modulated signal at a carrier frequency of 3.5 GHz. Fig. A.4 (b) shows the corresponding time domain results of the back scattered signal. CST took the FFT of the time domain signal and will produce the corresponding response in frequency domain also.

(a)   *(b)*
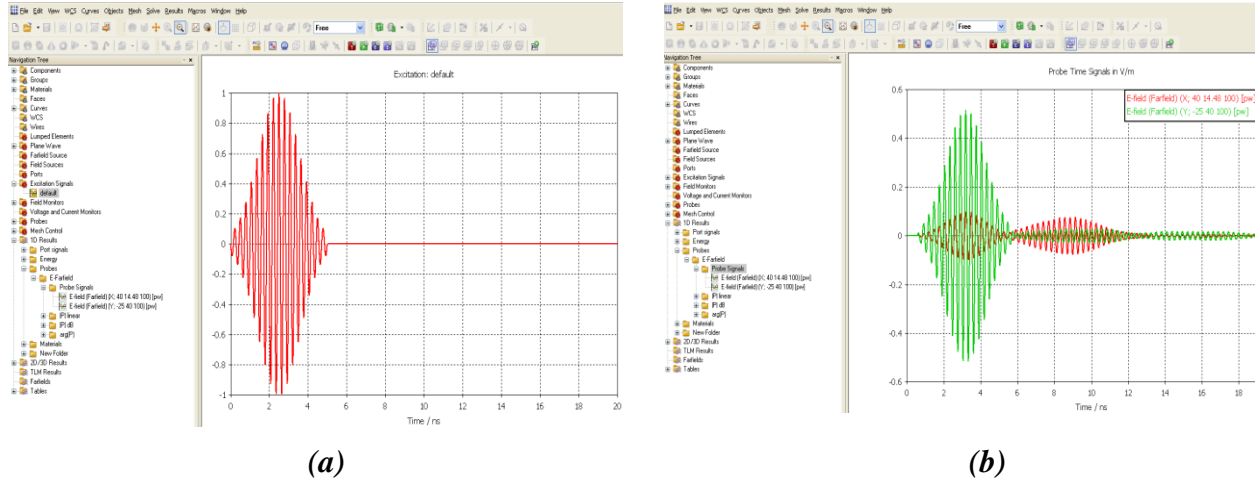
Fig.A.4: The user defined excitation signal and the corresponding back scattered response. a) Excitation signal b) Back scattered signal collected by the far-field probe placed at a particular distance.

Advanced version of CST provides multi-layer solver and fast resonant solver in frequency domain which gives a fast solution for the highly resonant multi-layer structures.

TAG FABRICATION

The optimized tags are fabricated using photolithographic process and also using digital printing technique (inkjet printing) [2-3]. The standard deposit thickness by inkjet is 1-5 µm. Photolithography is a chemical process by which the unwanted metal regions of the metal layers are removed so that the intended design is obtained [4]. Depends on the design of tags, single or double sided substrate is used. The tags can also be printed on paper substrate. Different tags were fabricated on four different types of substrates. In the beginning of the thesis FR-4 was used. Later, designs were developed on Rogers R4003 because of its low tangent loss (tanδ=0.0027) which enhances the backscattering properties of the tag. FR-4 has a permittivity of 4.4 and that of Rogers is 3.55. Both of them have a thickness of 0.8 mm. It was found that the high tangent loss of FR-4 (tanδ=0.025) deteriorates the tag mode amplitude. However, Rogers is costlier than FR-4. For developing multi-layer structures,

Kapton and PET are used because of its low thickness and tangent loss (thickness h=50 microns and tanδ=0.005). Kapton has a permittivity of 3.25 and that of PET is 3.4. In this case the mode of fabrication is different; it is not the classical etching process, but the inkjet printing technique. The geometry of the different tags are given below which is designed for 82 Ω impedance. The reason why 82 Ω is chosen is explained in chapter 3.

a) Planar Tag containing single group of C-sections

These kinds of tags always contain a ground plane. It has microstrip design. In the following representations, for better view, the dielectric layer and ground plane are omitted results just the copper trace representations.

Geometry of the planar tag containing single group of C-sections is shown in Fig. A.5.

l is the length of the C-section

w is the width of the C-section

g is the gap of the C-section

w' is the gap width of the C-section

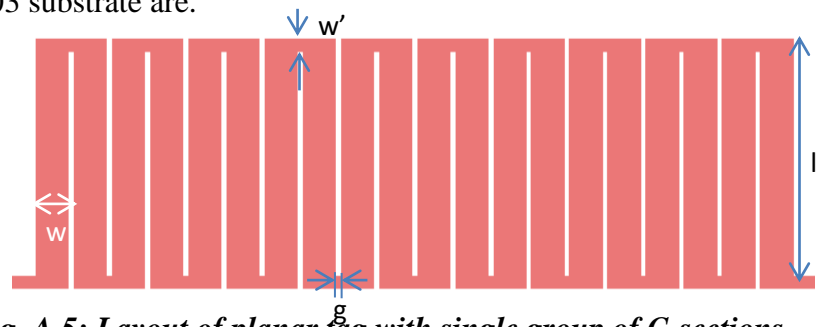Tag dimensions in Rogers R4003 substrate are.

w=0.7 mm

g=0.1 mm

w'=0.7 mm

l=14.9 mm

Fig. A.5: Layout of planar tag with single group of C-sections.

b) Planar Tag containing multi-group of C-sections

Geometry of the planar tag containing multi-group of C-sections is shown in Fig. A.6.

In this case g' is the gap between two groups.

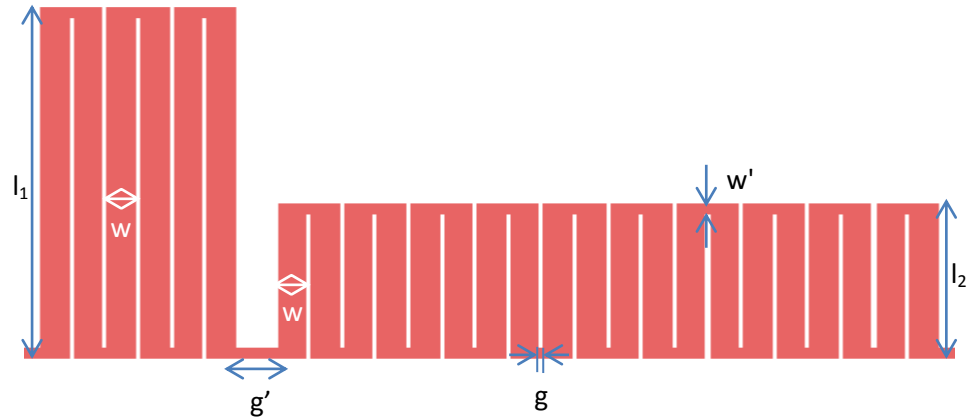Rest all parameters remains the same. Tag dimensions in Rogers R4003 substrate are.

w=0.7 mm

g=0.1 mm

w'=0.7 mm

g'=1 mm

l_1=21.5 mm

l_2=9.5 mm

Fig. A.6: Layout of planar tag with multi- group of C-sections.

c) Multi-layer Tags

Multi-layer tags are printed on flexible substrates (Kapton and PET). Further, the flexible substrate is sandwiched between a top and base substrate. The base substrate always contains a ground plane but the top substrate will not have a ground plane. It is used just to affix the flexible substrate with the base substrate. The following part represents the outline of the folded C-section.

TAG MEASUREMENT

The digital Oscilloscope DSO 91204A, Impulse generator Picosecond Pulse Labs-Model 3500, Vector Network Analyzer (VNA) Agilent 8720D and Performance Network Analyzer (PNA) N5222A is used for the measurement. A Short description of this equipment is presented in this section. Measurement with oscilloscope and a pulse generator resembles with a practical reader measurement.

A **digital storage oscilloscope** is an oscilloscope which stores and analyses the signal digitally rather than using analogue techniques. It is now the most common type of oscilloscope in use because of the advanced trigger, storage, display and measurement features which it typically provides. The input analogue signal is sampled and then converted into a digital record of the amplitude of the signal at each sample time. The sampling frequency should be not less than the Nyquist rate to avoid aliasing. The Oscilloscope DSO

91204A is capable of producing 40 GSa/s. DSO 91204A has 12 GHz bandwidth and four analogue channels. It has an analog bandwidth of 12 GHz. Its analog to digital converter has a resolution of 8 bits to a signal at zero frequency. But increasing the frequency to a few GHz, the effective resolution decreases to 4.5 bits because bits are found drowned in the noise. To artificially increase the number of bits and optimize sensitivity, an averaging operation using repeated measures can be performed. And with 64 records the number of bits of the analog / digital converter changes from 4.5 to 6 bits for a full scale of 40 mV. This gives sensitivity of the order of power -50 dBm (see [5]. Fig. A.7 shows the measurement set-up used for the back scattered time domain measurement.
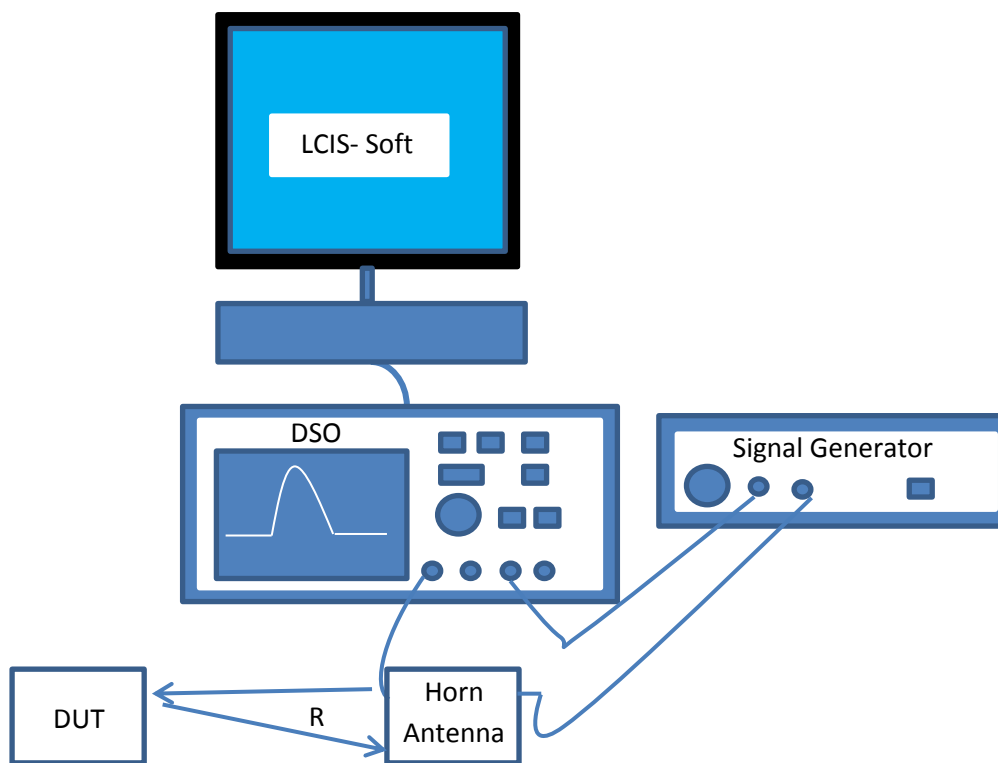
Fig.A.7: The back scattering measurement set-up using DSO 91204A.

As shown in the figure, the entire system is piloted by homemade software. The signal generator is connected to the one port of the double polarized horn antenna. The horn antenna receives the back scattered signal produced by the tag which is kept at a distance R from the horn antenna. The other end of the horn antenna is connected to the digital oscilloscope which is controlled by the PC and does the necessary post processing for the received signal in time domain. The dual polarized horn antenna used can operate in 2-32 GHz with an average gain

of 17 dBi. Single polarized antennas were also used in another instance which can operate within 700 MHz-18 GHz with a gain of 12 dBi. The pulse generator Picosecond 10060A that was used is able to send a Gaussian pulse of 110 ps of width, with maximum amplitude of 2 V into a 50 Ω load. That gives a maximum instantaneous power of 19 dBm. The same experimental set-up explained in [5] is used in this thesis also.

The frequency domain tags possess a high complexity calibration technique in order to recover the tag information. In all frequency domain tags, three measurements are needed; an empty measurement, measurement with a reference object and the measurement of the tag. This reference allows removing all the static noise due to the environment. All tag measurements are subtracted from empty measurement and divided by the reference measurement [5][6]. Finally the RCS can be calculated using the equation; $\sigma^{tag} = \left[\dfrac{S_{21}^{tag} - S_{21}^{isolation}}{S_{21}^{ref} - S_{21}^{isolation}}\right]^2 . \sigma^{ref}$, where σ^{tag} is the complex RCS value of the tag, σ^{ref} is the complex RCS value of the metallic rectangular plate obtained using an analytical formula and S_{21} are the three measured complex values obtained using bi-static configuration.

Vector Network Analyzer (VNA) Agilent 8720D and **Performance Network Analyzer** (PNA) N5222A were used to measure the scattering parameter characteristics. These analyzers can be used to measure the magnitude, phase and group delay of the two port networks. These analyzers are also capable of displaying a network's time domain response to an impulse or a step waveform by computing the inverse Fourier transform of the frequency domain response.

VNA 8720D is able to measure in a range of 50MHz-20 GHz [7]. The dynamic range of this analyzer is 105 dB. PNA N5222A is capable of doing measurement in a range of 10MHz-26.5GHz [8]. Its receiver dynamic range is 135 dB with an IF bandwidth of 15MHz. The Agilent PNA is used to test a wide variety of passive and active devices such as filters, duplexers, amplifiers and frequency converters. The high-performance characteristics of the PNA make it an ideal solution for these types of component characterizations as well as millimeter-wave, signal integrity and materials measurements.

Calibration has to be done in the two-port measurements (tag without antenna), before connecting the device under test. The vector network analyzer can be calibrated for full two ports by connecting the standard short, open and thru loads suitably whereas PNA provides

electronic calibration facility using a load which allows to perform a full 2-port or 4-port calibration. The two port device can be connected to the ports of the VNA/PNA. The magnitude and phase of S11, S22 and S21 are measured and stored in ASCII format.S11 and S22 indicate the return loss at the two ports of the DUT and S21 indicate the insertion loss (transmission characteristics) of the DUT from which the resonant frequency and the bandwidth are calculated. The DUT used is a two port tag prototype throughout this thesis.

REFERENCES

1   CST-Computer Simulation Technology [Online] Available at: http://www.cst.com/Content/Products/CST_S2/Overview.aspx

2   Rapid Low Cost Digital Flex [Online] Available at: http://inkjetflex.com

3   A. Vena, E. Perret, S. Tedjini, E.P.T. Guy, A. Delattre, F. Garet, and Y. Boutant, "Design of chipless tags printed on paper using flexography", Accepted for publication in IEEE Transactions on Antennas and Propagation.

4   Photolithography [Online] Available at: http://www.ece.gatech.edu/research/labs/vc/theory/photolith.html accessed on October 30 2012.

5   A. Vena, "PhD Dissertation, Contribution au développement de la technologie RFID sans puce à haute capacité de codage", Grenoble Institute of Technology, LCIS Lab, June 2012.

6   W. Wiesbeck and D. Kähny, "Single reference, three target calibration and error correction for monostatic, polarimetric free space measurements," *Proc. IEEE*, vol. 79, no. 10, pp. 1551–1558, Oct. 1991.

7   8720 D- Microwave vector Network Analyzer [Online] Available at: http://www.home.agilent.com/en/pd-1000002255%3Aepsg%3Apro-pn-8720D/microwave-vector-network-analyzer?&cc=FR&lc=fre

8   N5222A-PNA Microwave Network Analyzer [Online] Available at: http://www.home.agilent.com/en/pd-2001963-pn-N5222A/pna-microwave-network-analyzer?&cc=FR&lc=fre

APPENDIX II
EQUATIONS

Some of the equations for dispersion and a microstrip coupler can be seen here.

DISPERSION

Dispersion is a phenomenon in which the phase velocity is a function of frequency or alternatively the group velocity depends on the frequency. There is dispersion in microstrip so that the effective dielectric constant ε_{re} is a function of frequency and can in general be defined as the frequency dependent effective dielectric constant ε_{re} (f)[1]. To take into account of the effect of dispersion, the formula for ε_{re} (f) reported in eq. (1) and (3) in chapter three can be rewritten as,

$$\varepsilon_{re}\ (f)= \varepsilon_r - \frac{\varepsilon_r - \varepsilon_{re}}{1+(\frac{f}{f_{50}})^m}$$

where,

$$f_{50} = \frac{f_{TM0}}{0.75+(0.75-0.332\varepsilon_r^{-1.73})W/h}$$

$$f_{TM0} = \frac{c}{2\pi h \sqrt{\varepsilon_r - \varepsilon_{re}}} tan^{-1}(\varepsilon_r \sqrt{\frac{\varepsilon_{re}-1}{\varepsilon_r - \varepsilon_{re}}})$$

$$m= m_0\ m_c \leq 2.32$$

$$m_0 = 1 + \frac{1}{1+\sqrt{W/h}} + 0.32(\frac{1}{1+\sqrt{W/h}})^3$$

$$m_c = \{1+\frac{1.4}{1+W/h}\{0.15 - 0.235 \exp\left(\frac{-0.45f}{f_{50}}\right)\}\ \text{for W/h}\leq 1$$

$$1 \qquad\qquad \text{for W/h}\geq 1$$

Where c is the velocity of light in free space and whenever the product $m_0\, m_c$ is greater than 2.32 the parameter m is chosen equal to 2.32.

The dispersion model shows that the ε_{re} (f) increases with frequency and ε_{re} (f)$\rightarrow \varepsilon_r$ as f$\rightarrow \infty$.

The effect of dispersion in the characteristics impedance can be estimated by

$$Z_0(f)=Z_c\frac{\varepsilon_{re}\ (f)-1}{\varepsilon_{re}-1}\sqrt{\frac{\varepsilon_{re}}{\varepsilon_{re}\ (f)}}$$

where Z_c is the quasi static value of the characteristic impedance. This equation can be used in the case of C-section, in order to calculate the characteristic equation.

EVEN AND ODD MODE IMPEDANCE FOR A COUPLER

The even and odd mode characteristic impedance in eq. (14) in chapter three can be explained as follows [2],

$$Z_{0e}=Z_0\sqrt{\frac{\varepsilon_{re}(0)}{\varepsilon_{ree}(0)}}\ \frac{1}{(1-(\frac{Z_0(0)}{377})(\varepsilon_{re}(0))^{0.5}Q_4)}\qquad (15)$$

, where $Q_4=\left(\frac{2Q_1}{Q_2}\right)e^{-g}u^{Q_3}+(2-e^{-g}u^{-Q_3})^{-1}$

With $Q_1=0.8695u^{0.194}$

$Q_2=1+0.7519g+0.189g^{2.31}$

$Q_3=0.1975+(16.6+(8.4/g)^6)^{-0.387}+\ln(g^{10}/(1+(g/3.4)^{10})/241)$

$\varepsilon_{re}(0)$ denotes the effective dielectric constant of a single microstrip of width W.

$\varepsilon_{ree}(0)=0.5(\varepsilon_r+1)+0.5(\varepsilon_r-1)(1+\frac{10}{v})^{-a_e(v)b_e(\varepsilon_r)}$

, where $v=u(20+g^2)+ge^{-g}$

$$a_e(v) = 1 + \ln(\frac{v^4 + \left(\frac{v}{52}\right)^2}{(v^4 + 0.432))/49} + \ln(1 + \frac{\frac{v}{18.1}}{18.7}^3)$$

$$b_e(\varepsilon_r) = 0.564((\varepsilon_r - 0.9)/(\varepsilon_r + 3))^{0.053}$$

And u=W/h, g=S/h.

Similarly the quasi static odd-mode characteristic impedance of coupled microstrip line is expressed by

$$Z_{0o} = Z_0 \sqrt{\frac{\varepsilon_{re}(0)}{\varepsilon_{ree}(0)}} \frac{1}{(1 - (\frac{Z_0(0)}{377})(\varepsilon_{re}(0))^{0.5}Q_{10})} \qquad (19)$$

With,
$$Q_{10} = Q_2^{-1}(Q_2 Q_4 - Q_5 e^{\ln(u)} Q_6 u^{-Q^9}))$$

$$Q_9 = \ln(Q_7)(Q_8 + \frac{1}{16.5})$$

$$Q_8 = e^{(-6.5 - 0.95\ln(g) - \left(\frac{g}{0.15}\right)^5)}$$

$$Q_7 = (10 + 190g^2)/(1 + 82.3g^3)$$

$$Q_6 = 0.2305 + \ln(\frac{g^{10}}{1 + \left(\frac{g}{5.8}\right)^{10}}))/281.3 + \ln(1 + 0.598g^{1.154})/5.1$$

$$Q_5 = 1.794 + 1.14\ln(1 + \frac{0.638}{g + 0.517g^{2.43}}))$$

REFERENCES

1. J. Hong and M. Lancaster, "Microstrip Filters for RF/Microwave Applications", A WILEY-Interscience Publication, ISBNs: 0-471-38877-7 (Hardback); 0-471-22161-9 (Electronic), 2001.
2. R. K. Mongia, I. J. Bahl, P. Bhartia, and J. Hong, *RF and Microwave Coupled-Line Circuits*, 2nd ed. Norwood, MA: Artech House, 2007.

Contribution au Développement des Tags Chipless et des Capteurs à Codage dans le Domaine Temporel

Mots-clés: tag sans puce, chipless RFID, mesures dans le domaine temporel, C-sections, antennes UWB, nanofils de silicium, capteurs sans fil, capteur d'humidité, structures multi-couches.

Résumé: La RFID sans puce en raison de tu très faible coût des tags a ouvert une nouvelle voie pour les systèmes d'identification. Les étiquettes RFID sans puce fonctionnant dans le domaine fréquentiel ont l'avantage d'être compatibles avec de grandes distances de lecture, de l'ordre de quelques mètres, et de pouvoir fonctionner dans les bandes de fréquence ISM. Cependant, les tags de ce type développés jusqu'à lors n'offraient qu'une faible capacité de codage. Cette thèse propose une nouvelle méthode pour augmenter la capacité de codage des tags fonctionnant dans le domaine temporel en utilisant des C-sections, c'est-à-dire des lignes de transmission repliées de manière à avoir des zones fortement couplées ce qui leur donne un caractère dispersif. Une autre approche basée sur un tag multi-couches a également été introduite de façon à augmenter considérablement la capacité de codage. Pour terminer, la preuve de concept d'un tag-capteur d'humidité basé sur l'utilisation de nanofils de silicium est également présenté.

Contribution to the Development of Time Domain Chipless Tags and Sensors

Keywords: Chipless tags, time domain measurement, C-sections, UWB antennas, structural mode, humidity sensor, nanowires, chipless RFID sensor, multi-layer.

Abstract: Chipless RFID owing to their low cost has opened a new way to the identifications systems. Time domain chipless RFID tags have significance because of their large read range, of the order of few meters, and their ability to operate in the unlicensed bands with allowed emission power. However, there were not a lot of work in this area and the existing time domain tags offers poor coding capacity. This thesis provides a new method to increase the coding capacity of time domain tags by using highly dispersive coupled transmission line sections (also known as C-sections). It also explains a multi-layer design with which the coding capacity of the time domain tags can be increased considerably. As a perspective of the thesis, a humidity sensor tag using silicon nanowires is also explained.

Laboratoire de Conception et d'Intégration des Systèmes (LCIS)- Grenoble-INP

50, rue Barthélémy de Laffemas, 26902 Valence Cedex 9, France